AD-A050 025 NAVAL POSTGRADUATE SCHOOL MONTEREY CALIF F/G 20/4
UNSTEADY SURFACE PRESSURE AND NEAR-WAKE HOTWIRE MEASUREMENTS OF--ETC(U)
SEP 77 K A KAIL

UNCLASSIFIED NL

1 OF 2
AD A050025

NAVAL POSTGRADUATE SCHOOL

Monterey, California

THESIS

UNSTEADY SURFACE PRESSURE
AND NEAR-WAKE HOTWIRE MEASUREMENTS
OF A CIRCULATION CONTROL AIRFOIL

by

Karl Aurel Kail, IV

September 1977

Thesis Advisor: J.A. Miller

UNCLASSIFIED

SECURITY CLASSIFICATION OF THIS PAGE (When Data Entered)

REPORT DOCUMENTATION PAGE

READ INSTRUCTIONS BEFORE COMPLETING FORM

1. REPORT NUMBER

2. GOVT ACCESSION NO.

3. RECIPIENT'S CATALOG NUMBER

9

4. TITLE (and Subtitle)

6

Unsteady Surface Pressure and Near-Wake Hotwire Measurements of a Circulation Control Airfoil.

5. TYPE OF REPORT & PERIOD COVERED

Engineer's Thesis

September 1977

6. PERFORMING ORG. REPORT NUMBER

7. AUTHOR(s)

10

Karl Aurel Kail, IV

8. CONTRACT OR GRANT NUMBER(s)

9. PERFORMING ORGANIZATION NAME AND ADDRESS

Naval Postgraduate School
Monterey, California 93940

10. PROGRAM ELEMENT, PROJECT, TASK AREA & WORK UNIT NUMBERS

11. CONTROLLING OFFICE NAME AND ADDRESS

Naval Postgraduate School
Monterey, California 93940

12. REPORT DATE

11

Sep[redacted]77

13. NUMBER OF PAGES

141

14. MONITORING AGENCY NAME & ADDRESS (if different from Controlling Office)

12 141p.

15. SECURITY CLASS. (of this report)

Unclassified

15a. DECLASSIFICATION/DOWNGRADING SCHEDULE

16. DISTRIBUTION STATEMENT (of this Report)

Approved for public release; distribution unlimited.

17. DISTRIBUTION STATEMENT (of the abstract entered in Block 20, if different from Report)

18. SUPPLEMENTARY NOTES

19. KEY WORDS (Continue on reverse side if necessary and identify by block number)

Circulation Control Airfoil

20. ABSTRACT (Continue on reverse side if necessary and identify by block number)

The large lift coefficient changes attainable with Circulation Control Airfoils through small changes in boundary layer blowing suggest rotary wing cyclic control can be obtained through modulation of the blowing. Static pressure distributions were obtained to assess the unsteady behavior of a Circulation Control Rotor in a two-dimensional flow. A constant-radius hotwire wake traversing mechanism was constructed to augment the over

DD FORM 1473, 1 JAN 73 — EDITION OF 1 NOV 65 IS OBSOLETE

S/N 0102-014-6601

UNCLASSIFIED

SECURITY CLASSIFICATION OF THIS PAGE (When Data Entered)

251 450

1B

(20. ABSTRACT Continued)

pressure data and to study the flow phenomena occurring in the region of Coanda jet separation. Through correlation of turbulence intensity data with pressure data, it was discovered that the point of Coanda jet separation could be located using the hotwire. The objective of these tests was accordingly expanded to include correlation of the location of separation with flow parameter variation.

Although steady flow, steady blowing tests results were favorable, the unsteady blowing test was restricted in scope because of an inability of the injection air compressor to provide an adequate flow, and because the real-time acquisition system was not completed in time for these tests. From mean value and RMS data obtained during oscillatory blowing, no increase in average lift augmentation above that produced in equivalent steady blowing was discernible.

Approved for public release; distribution unlimited.

Unsteady Surface Pressure and Near-Wake Hotwire Measurements of a Circulation Control Airfoil

by

Karl Aurel Kail, IV
Lieutenant, United States Navy
B.S., University of Colorado, 1967

Submitted in partial fulfillment of the
requirements for the degree of

AERONAUTICAL ENGINEER

from the

NAVAL POSTGRADUATE SCHOOL
September 1977

Author ______________________

Approved by: ______________________
Thesis Advisor

____
Second Reader

____
Chairman, Department of Aeronautics

____
Dean of Science and Engineering

ABSTRACT

The large lift coefficient changes attainable with Circulation Control Airfoils through small changes in boundary layer blowing suggest rotary wing cyclic control can be obtained through modulation of the blowing. Static pressure distributions were obtained to assess the unsteady behavior of a Circulation Control Rotor in a two-dimensional flow. A constant-radius hotwire wake traversing mechanism was constructed to augment the pressure data and to study the flow phenomena occurring in the region of Coanda jet separation. Through correlation of turbulence intensity data with the pressure data, it was discovered that the point of Coanda jet separation could be located using the hotwire. The objective of these tests was accordingly expanded to include correlation of the location of separation with flow parameter variation.

Although steady flow, steady blowing tests results were favorable, the unsteady blowing test was restricted in scope because of an inability of the injection air compressor to provide an adequate flow, and because the real-time acquisition system was not completed in time for these tests. From mean value and RMS data obtained during oscillatory blowing, no increase in average lift augmentation above that produced in equivalent steady blowing was discernible.

TABLE OF CONTENTS

LIST OF TABLES

LIST OF FIGURES

LIST OF SYMBOLS AND ABBREVIATIONS

atm	Atmosphere
C	Chord length
CC	Circulation Control
C_D	Drag coefficient, $D/(qS)$
C_L	Lift coefficient, $L/(qS)$
C_M	Pitching moment coefficient, $M/(qSC)$
CMU	C_μ
C_p	Pressure coefficient, $(p - p_o)/q$
C_μ	Blowing (momentum) coefficient, $\dot{m}V_j/(qS)$
D	Drag
e	Voltage
f	Frequency, Hz
$\|G(\omega)\|$	Dynamic gain, p_o/p_i
k	Specific heat ratio
L	Lift
M	Molecular weight
$\dot{m}$	Mass flow rate
P	Pressure (see subscripts)
PR	Pressure ratio, P_j/P_i
q	Wind tunnel dynamic pressure, $\frac{1}{2}\rho V_\infty^2$
R	Universal gas constant
S	Airfoil planform surface area
V	Velocity
X/C	Nondimensional distance from leading edge
Y/C	Nondimensional distance from chord line

LIST OF SYMBOLS AND ABBREVIATIONS (Continued)

α	Angle of attack, degrees (ALPHA)
$\varepsilon(X)$	Amplification ratio of the variable X, $\sqrt{\left(\frac{X_{RMS}}{\overline{X}}\right)^2_{OSCILLATING} - \left(\frac{X_{RMS}}{\overline{X}}\right)^2_{STEADY}}$
ρ	Density
τ	Shear stress
ω	Angular frequency, $2\pi f$, sec^{-1}
ϕ	Phase angle

Subscripts

N	Normal
C	Chord
l	Lower
u	Upper
f	Front
r	Rear
i	Plenum value
j	Jet
g	Geometric
s	Steady
T	Total
o	Static

Superscripts

bar	Mean value
prime	Perturbation quantity

ACKNOWLEDGMENT

The author wishes to express his appreciation to Dr. James A. Miller and Dr. Louis V. Schmidt for their guidance and assistance during this investigation. Recognition is also due to Messrs. Ted B. Dunton, Glen Middleton, Don Harvey, Ron Ramaker and Stan Johnson for their technical assistance in the construction of the wake traversing mechanism and repair of the airfoil, to Mr. John Moulton for his assistance in conducting the tests, and to Mr. Robert A. Besel for his assistance throughout the project and in the completion of this paper.

I. INTRODUCTION

A. GENERAL DISCUSSION

Although jet flaps have been thoroughly investigated, it was not until 1959/1960 that Griswold [1] and Davidson [2] suggested that significant lift augmentation could be obtained through trailing edge blowing about bluff-edged airfoils. From their initial concepts, a distinct class known as Circulation Control Airfoils (CCA) has evolved, and is currently under extensive evaluation for possible application to V/STOL aircraft and helicopters.

Analytically, the flow field is perhaps the most complex studied, for neither slender body theory nor the Kutta condition apply. In fact it is the absence of the Kutta requirement which allows controlling the point of separation. This is effected by injection of a tangential turbulent jet of sufficient energy that it entrains flow from the upper portion of the boundary layer through the Coanda effect. The flow remains attached to the curved surface for distances, depending on the rate of injection, of the order of the trailing edge radius, substantially reducing the size of the wake. In addition to these analytical difficulties is the fact that helicopters and V/STOL aircraft typically operate in an unsteady flow environment posing additional complexity. Thus CCA aerodynamics embodies several complex topics, perhaps the most elusive of which is prediction of separation.

B. PREVIOUS EXPERIMENTAL INVESTIGATIONS

The initial experimental investigations with circulation control by tangential blowing were conducted on circular cylinders by Dunham [3] in 1967, whose work substantiated the high-lift concept. Unfortunately, the airfoil geometry employed was complicated by multiple slots and lacked the potential for high speed operation. Nevertheless, Cheeseman and Seed [4,5] and others suggested through design feasibility studies that the concept had promise. In 1967 Kind [6] completed the first experimental evaluation of an elliptical CC airfoil demonstrating control of lift through blowing.

Williams and Howe [7], Englar [8,9], and Harness [10] all demonstrated that camber adds to the CC capability of an ellipse. Included in this work was an evaluation of the effects of trailing edge shape, slot height, thickness to chord ratio and Reynolds number.

Investigations conducted by Oyler and Palmer [11] and Williams et al [12] with pulsed blowing over a blown flap and by Walters et al [13] with pulsed blowing on a cambered CC ellipse indicated additional lift augmentation could be obtained. For equal values of time averaged blowing coefficient the pulsed blowing produced higher trailing edge suction peaks and lift augmentation because of the instantaneous higher values of injection pressure and jet velocity which in turn produced greater flow entrainment and jet turning. This produced required lift coefficients at reduced

injection mass flow. Williams [12] indicated a mass flow reduction of as much as 50%. Both Oyler and Williams found optimum pulsing frequencies. Englar [14] in 1975 reported on pulsed blowing tests for a STOL wing section modified with a bluff rounded trailing edge. The pulsing valve produced a sinusoidal pressure variation of amplitude not greater than 15% of the mean for blowing coefficients, C_μ, of less than 0.14. He found the pulsing had little effect on lift augmentation, but assumed that the small trailing edge radius and the fact that the pulsing valve could not provide higher pressure variations were the major reasons for this result.

In 1974 Kaman Aerospace Corporation [15] and Lockheed Aircraft Corporation [16] completed detailed design feasibility studies of a helicopter with a Circulation Control Rotor (CCR). Subsequently a working model CCR was constructed and evaluated by Reader and Wilkerson [17] at the Naval Ship Research and Development Center. Included in the model was a throttling mechanism to enable rotor blade cyclic and collective control through modulated blowing from leading and trailing edge slots. Using sinusoidal pressure waves with amplitude ratios of the order of one, and various combinations of leading and trailing edge blowing, high lift-to-drag surface pressure distributions were obtained.

C. PREVIOUS ANALYTICAL INVESTIGATIONS

Analytically, CCA's have been modeled by Kind [18], Levinsky and Yeh [19] and Gibbs and Ness [20]. The accuracy of those analyses has depended primarily on how effectively the Coanda jet was modeled and separation determined. As noted by Kind [18], and Levinsky and Yeh [19], separation of a CCA occurs when the pressure coefficient on the trailing edge reaches a positive near-constant value just beyond the suction peak. Kind formulated his steady state solution using an empirical model based on the surface pressure distribution. But knowledge of the pressure distribution implies knowledge of the potential flow solution. Therefore, Gibbs and Ness, and Levinsky and Yeh formulated their steady state solutions using zero shear stress at the wall as the separation criteria. However, subsequently Englar [21] and Cebeci and Smith [22] found that the shear stress may only reach a minimum at separation and then increase again, never passing through zero. The range of validity of the zero wall stress criteria needs to be established and there is obviously a requirement to determine how to use minimum wall stress as a more general separation criterion.

In modeling the turbulent Coanda jet as a boundary layer in curvilinear coordinates, Gibbs and Ness [20] neglected body forces, and the streamwise derivatives $\frac{-R}{R+y}\frac{\partial \tau_{xx}}{\partial x}$ and $\frac{R}{R+y}\frac{\partial}{\partial x}(\bar{\rho}\,\overline{u'^2})$ from the x-momentum equation.

Assuming the height of the boundary layer was small compared with the reference length (distance from slot), they reduced the y-momentum equation to three terms:

$$-\bar{\rho}\,\frac{\overline{u'^2}}{R+y} + \frac{\partial \bar{p}}{\partial y} + \frac{\partial}{\partial y}(\bar{\rho}\;\overline{v'^2}) = 0$$

However, in regions of separation, the "boundary layer" thickness grows significantly and the fact that this modeling still yields a reasonable flow description seems to be a fortunate coincidence. There exists little experimental data to justify the assumptions. Sandborn and Liu [23] conducted one of the few contemporary experiments on turbulent separation in 1968. Even though the term $\frac{\partial}{\partial x}(\overline{u'^2})$ grows substantially near separation they observed that the convective term $\frac{\partial}{\partial y}(\overline{u'v'})$ eventually outgrows all other terms and dominates at separation. How small, constant radii of curvature affect the results was not clearly established.

D. OSCILLATORY FLOW RESEARCH

In general, problems of nonsteady flow have received far less attention than those of steady flow; in particular, there exists no unsteady blowing data of sufficient detail to permit formulation of a separation criteria. Nevertheless some perspective may be gained by examining recent studies on oscillatory boundary layers. Despard and Miller [24] measured the instantaneous velocity profiles in oscillatory laminar boundary layers subject to adverse pressure gradients,

and proposed that oscillatory separation occurred at the farthest upstream point at which there was "zero velocity" or reverse flow at some point in the velocity profile throughout the entire cycle of oscillation. They and Tsahalis and Telionis [25] agreed that the point of separation moves upstream from the steady state position, but the results of Tsahalis and Telionis seem to indicate that, at least for part of the cycle, the point of vanishing shear is downstream of the "separation" singularity.

Thus it appears that to accurately predict CCA aerodynamic properties and in particular, to permit modeling with oscillatory blowing, additional research concerning separation in a nonsteady turbulent Coanda jet is required.

E. PROBLEM STATEMENT

The primary purpose of the present investigation was to assess the feasibility of employing a CC airfoil with a modulated blowing coefficient of the form:

$$C_\mu(t) = \overline{C}_\mu(1 + \varepsilon \sin \omega t)$$

for values of ε of the order of unity.

A further objective was to correlate the location of separation with flow parameter variation so that reasonable engineering predictions of turbulent separation in steady and oscillatory Coanda jets might be made.

II. OUTLINE OF THE INVESTIGATION

A. APPROACH

The method of attack consisted of direct measurement of sectional aerodynamic characteristics by integration of surface pressure data from a typical example of a CC airfoil with steady blowing, and comparison with those obtained with modulated blowing. From an evaluation of near-wake velocity profiles, and correlation with surface pressure data, an engineering criterion for Coanda sheet separation point location was to be formulated.

B. INVESTIGATION PARAMETERS

The CC airfoil section chosen for investigation had a 21.4 percent thick modified elliptic profile with a 10.206 inch chord, a 0.0479 trailing edge radius to chord ratio, and 3 percent camber. The injection slot was 0.016 inches high and was located at 0.9551 X/C on the upper surface. Spanning the entire cross section of the Department of Aeronautics 2-by-2 foot oscillating flow wind tunnel, the model may be treated approximately as a two-dimensional airfoil.

To avoid compressibility effects and to remain outside the jet flap regime, the investigation was conducted at a tunnel q of approximately 10 psf with blowing coefficients, C_μ, of less than 0.1. The modulated blowing coefficient amplitude ratio ε, were to be varied from 0 to 0.7. Angle

of attack was to be varied to include values appropriate to the application of CC airfoils as helicopter rotor blades; i.e., from -5 to +8 degrees.

C. EXPERIMENTAL PROGRAM

The detailed investigation was to include:

1. Preliminary surface pressure measurements to calibrate the data acquisition system, and to determine the zero-lift angle of attack.
2. Pressure data acquisition system calibrations to determine the dynamic transfer function between the surface pressure taps on the airfoil and the signal produced by the pressure transducer.
3. A pressure and velocity survey of the wind tunnel test section in a steady and oscillating freestream without the model installed.
4. Determination of aerodynamic coefficients and near-wake velocity surveys with steady injection, steady freestream.
5. Determination of aerodynamic coefficients and near-wake velocity surveys with oscillatory blowing, steady freestream.
6. Determination of aerodynamic coefficients and near-wake velocity surveys with steady blowing, oscillatory freestream.

III. EXPERIMENTAL APPARATUS AND PROCEDURES

A. WIND TUNNEL

1. General Description

The experimental work was conducted in the low-speed, oscillating flow wind tunnel located in the Aeronautics Laboratories of the Naval Postgraduate School. Shown in Fig. 1, the open circuit wind tunnel has a 24-inch square by 223-inch long test section, an eight-foot square inlet and a 16:1 contraction ratio. Three high solidity screens located in the inlet section just upstream of the entrance nozzle help maintain freestream turbulence intensities to less than 1.0 percent for the velocities encountered in the present work.

The wind-tunnel drive consists of two Joy Axivane Fans in series, each of which has an internal, 100 horsepower, direct connected, 1750 rpm motor. The fan blades are internally adjustable through a pitch range of 25 to 55 degrees, providing a wide operating base. Two sets of variable inlet vanes, located immediately upstream of each fan, are externally operated to provide control of test section velocity. These vanes are of multileaf design, and preswirl the air in the direction of fan rotation to reduce fan capacity. The range of tunnel velocity is from 10 to 250 feet per second.

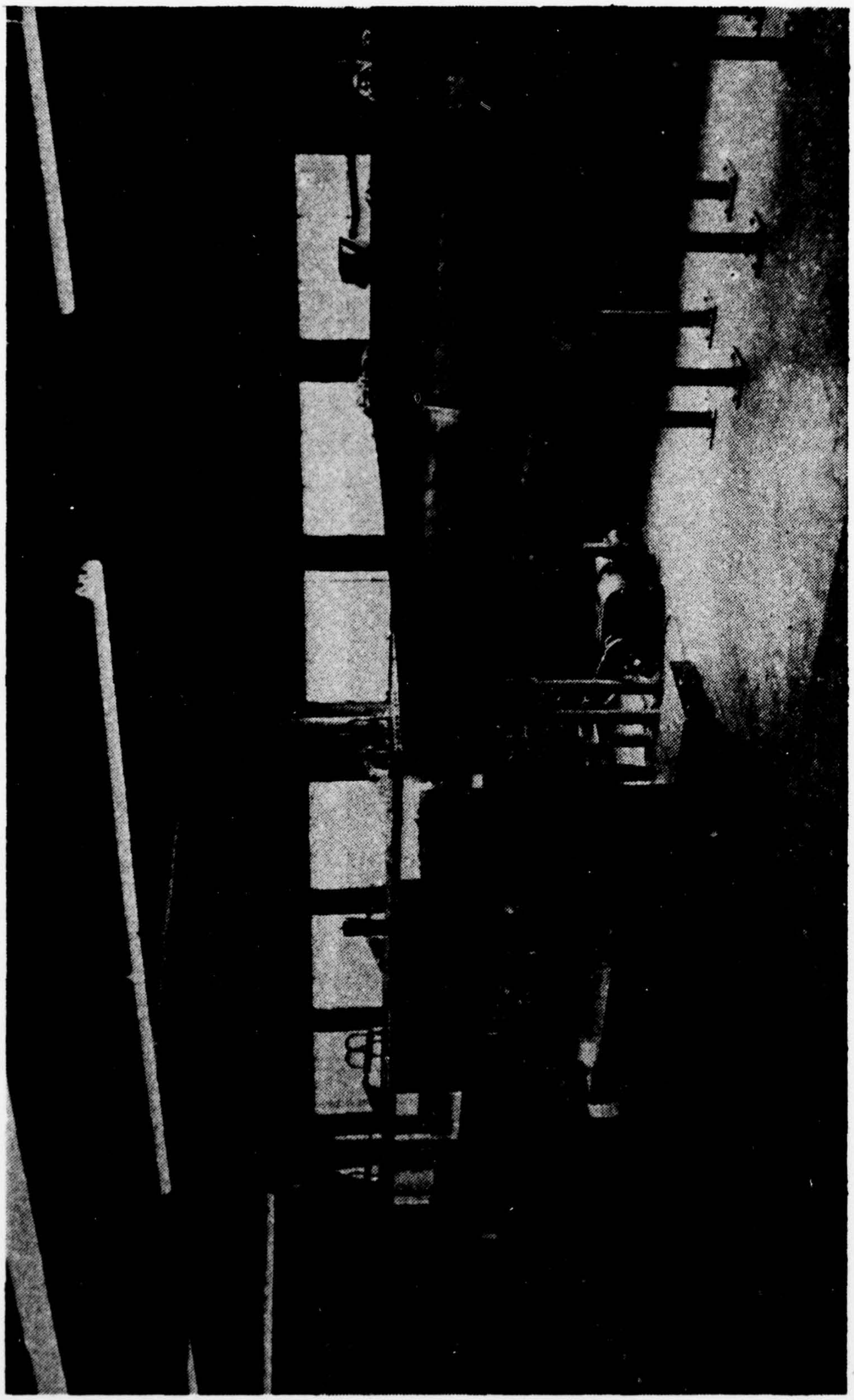

FIGURE I

OSCILLATING FLOW WIND TUNNEL AND INSTRUMENTATION

2. Rotating Shutter Valve

The most successful method of obtaining an oscillating flow with large ranges of frequency and amplitude is that first employed by Karlsson [26], later by Miller [27] in his investigation of transition, and subsequently by Despard [28]. A rotating shutter valve, immediately downstream of the test section, is used to superimpose a periodic variation of velocity on the mean flow. The present shutter valve consists of four horizontal steel shafts equally spaced across the test section. The shafts are slotted to accommodate flat blades of various widths, forming a set of four butterfly valves spanning the test section. Figure 2 is a schematic of the shutter valve. Each blade drives its immediate neighbor by means of a timing belt and pulley arrangement. The bottom shaft is driven by a five-horsepower variable-speed electric motor through a timing belt and pulley. An intermediate shaft between the motor and shutter valve permits a variety of pulley arrangements and a frequency range of from two to 240 Hz. The amplitude of oscillation is controlled by blade width. Test section closure may be varied from 25 to 100 percent. The resulting amplitude of oscillation of test section velocity is a function of frequency, mean velocity and pressure gradient. In this investigation, blades producing 50.0, 66.7 and 82.5 percent closure were used, resulting in an amplitude range of from 3 to 40 percent of the local mean freestream velocity.

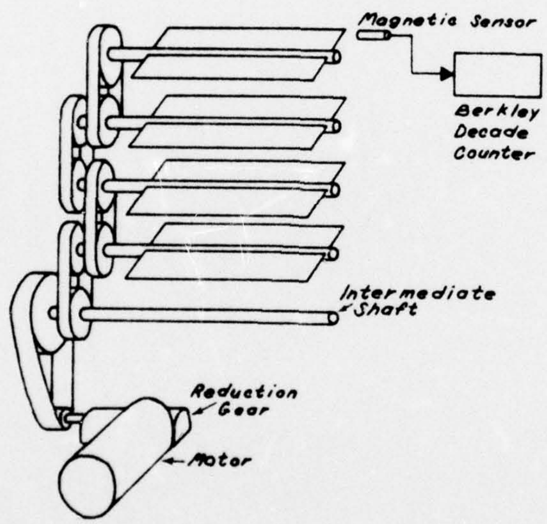

FIGURE 2. ROTATING SHUTTER VALVE

3. Test Section

Continuous pieces of two-inch thick aluminum, 24 inches wide and 223 inches long, form the upper and lower test section walls. Each of the side walls consists of three two-inch thick panels, two of stress-relieved Lucite and the center of plywood to facilitate the mounting of model and instrumentation. The Lucite panels on the console side of the test section are hinged and may be raised hydraulically, providing access to the test section. The heavy construction of the test section is dictated by the desire to reduce deflections induced by rapid changes in static pressure. As reported by Despard [28], freestream velocity profile variation is less than one percent from the mean to within three inches of any wall.

4. Tunnel Calibrations

In order to calibrate the flow in the tunnel, a series of tests were conducted without the model installed. A hotwire, a total pressure probe, and a static pressure probe were installed in the test section at approximately the mid-chord location. The shutters were operated from 0 to 50 Hz using both the 3 and 4 inch blades, and RMS, DC and phase angle data were recorded from each of the sensors. The full details of these measurements are presented by Lancaster [34]. Figure 3 illustrates typical results obtained with the 3-inch blades. Of note is the pressure perturbation peak at approximately 21 Hz. At this frequency the velocity and pressure waveforms are very

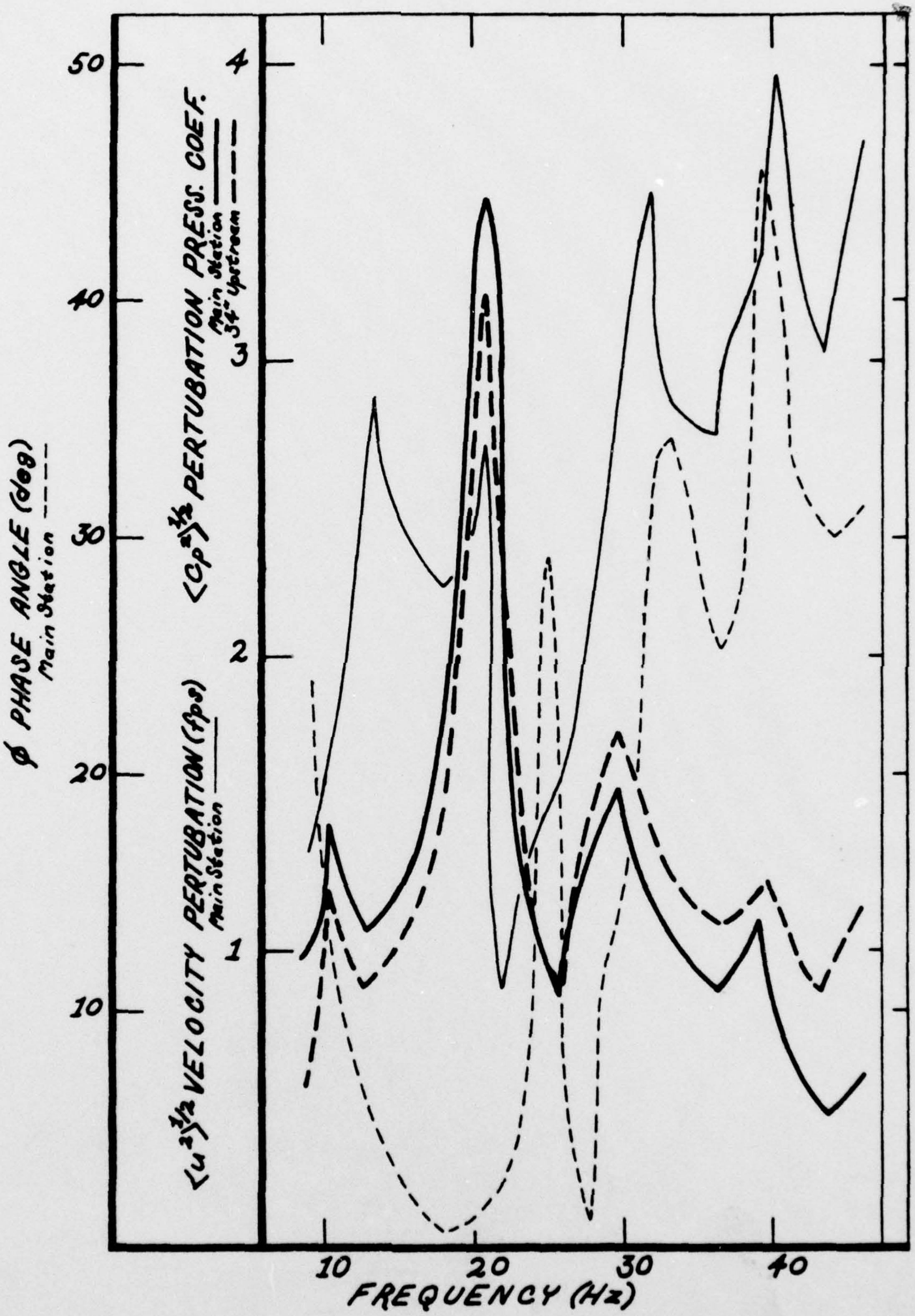

FIGURE 3. OSCILLATING FLOW WIND TUNNEL FREQUENCY RESPONSE CALIBRATION

nearly sinusoidal. The peak is attributed to acoustic resonance from the mouth of the tunnel. This resonant frequency also appeared in a steady flow frequency spectrum analysis of the wall static pressure conducted with a Spectral Dynamics Real Time Analyzer with the airfoil installed. Blower fan noise at 480 Hz was also detectable, as were intermediate frequencies of 90 and 120 Hz whose source could not be identified. Through appropriate filtering, the tunnel noise was removed from the data signals.

B. THE AIRFOIL

The airfoil model was a prototype section obtained from the Lockheed Phase I Study on Circulation Control Rotor (CCR) Design Feasibility [16] and modified in the Department of Aeronautics model shop to correct defects in the injection slot structure. Designed from an ellipse with a 10.215 inch chord, it had a shortened trailing edge of 0.48 inch radius with an adjustable slot located at X/C = .9951 on the upper surface. The reduced chord was 10.206 inches, the camber 3 percent, and the thickness ratio 0.214. Although slot width was adjustable by means of jack screws located every two inches along the span, tests were only conducted at a constant slot height of 0.016 inches. Figure 4 is a cross-sectional view depicting the location of the slot and the 54 midspan pressure taps. There were 5 additional taps on the upper surface, 3 at

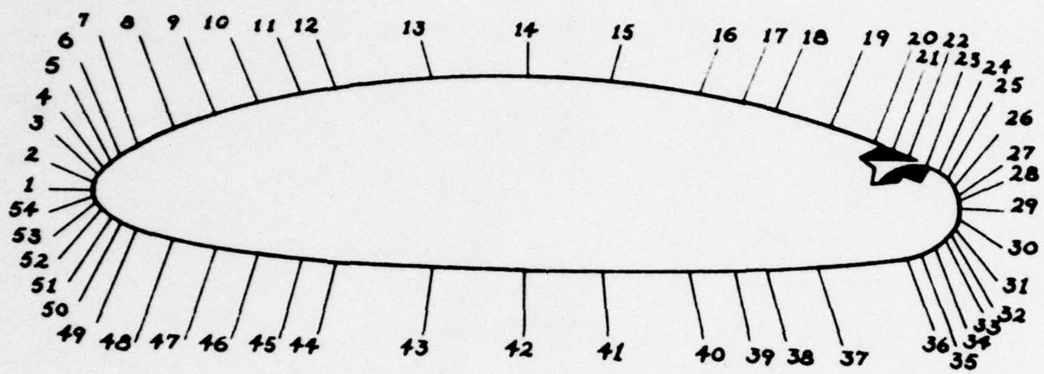

FIGURE 4. CC AIRFOIL CROSSSECTIONAL VIEW DEPICTING MIDCHORD SURFACE PRESSURE TAP LOCATIONS

midchord 6, 9 and 10.5 inches from midspan, and 2 at the three-quarter chord 6 and 9 inches from midspan. Surface pressure tap locations are listed in Appendix A. In addition to the surface taps a pressure tap was located in the plenum.

The airfoil spanned the 24-inch width of the tunnel test section and protruded through the walls approximately four inches on either side. The portions of the slot not in the tunnel were permanently sealed. The model was fitted through and held in position by aluminum disks with elliptical openings centered on their axes of rotation. Through slip rings the airfoil and disks could be rotated as a unit to set the angle of attack. The no-blowing zero-lift value was found to be approximately -5 degrees. The airfoil section ends were capped by flat plates through which passed a 1.5-inch diameter supply line for slot injection air.

C. SLOT INJECTION AIR SYSTEM

1. Air Compressor

A Carrier, 3-stage, 300-Hp centrifugal compressor was used to supply the slot injection air. It had a 6.057-inch flow metering nozzle installed in its 12-inch diameter inlet pipe. The 8-inch outlet pipe entered a distribution manifold from which extended a bypass line to control surge and a 3-inch supply line to the test area. At the test site the supply line was reduced to a 1.5-inch diameter for compatibility with the mass-flow control system and airfoil.

2. Mass Flow Control

As illustrated in Fig. 5 the mass flow control system consisted of a mean flow control globe valve immediately downstream of a Fischer and Porter Rotameter (a variable area flow meter), an oscillation control valve developed by Bauman [29] approximately two additional feet downstream with a hotwire immersed in the center of the 1.5-inch steel pipe three feet beyond it, and bypasses for the Rotameter and the oscillation control valve.

The oscillatory control valve consisted of an elliptical Lucite cam which rotated inside a two-inch steel pipe to provide a cross-section area which varied as a sine function of twice its angular position. The maximum cross-section area of the valve was approximately equal to the total exit area of the airfoil slot.

A globe valve installed in the rotating valve bypass line provided control of the ratio of steady flow component to oscillating component of C_μ. C_μ, therefore, could be made a function of the form $C_\mu = A(1 + B \sin \omega t)$ where A and B were adjusted by means of the oscillatory bypass and mean flow control globe valves. The frequency ω was set by driving the rotating valve with the variable speed motor employed to rotate the shutter valve. Provision for mechanically introducing phase angles was designed into this drive.

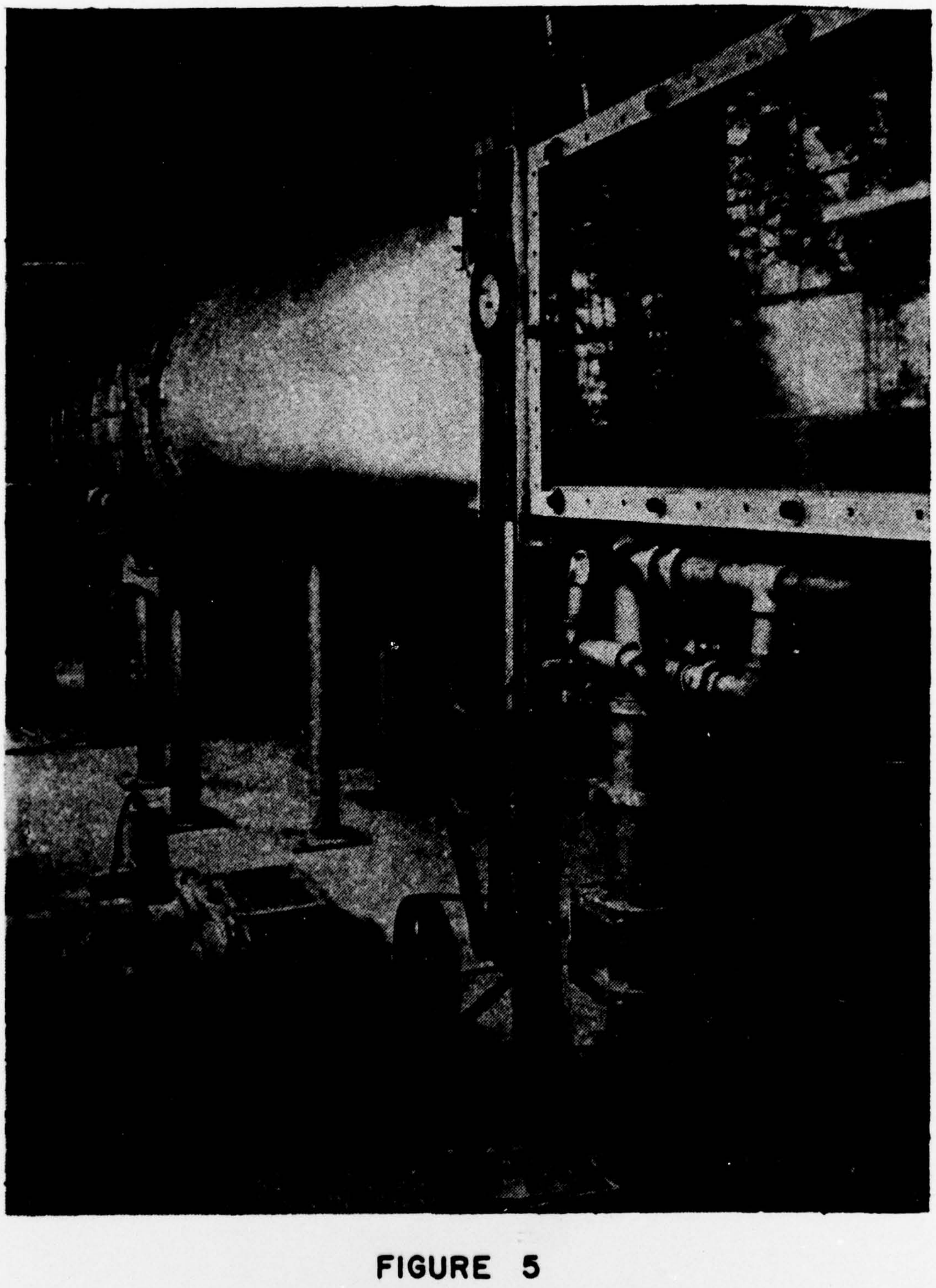

FIGURE 5

MASS FLOW CONTROL

3. Mass Flow Measurements

The steady blowing mass flow rate was measured using the calibrated rotameter. Nonsteady injection mass flow rates were measured by a supply line hotwire anemometer calibrated against the rotameter in steady flow. The anemometer was used to set the mean injection rate and the injection oscillation amplitude. When setting the mean injection rate, the mean plenum pressure was used as a cross-reference. The hotwire signal was observed on an oscilloscope in order to monitor mass flow waveform.

D. WAKE TRAVERSING MECHANISM

A wake traversing mechanism shown in Fig. 6 was designed to provide a two-dimensional hotwire mapping of the wake at the quarter span. To enable examining the flow at a constant distance from the trailing edge, the track on which the mechanism rides was designed to pivot about the origin of the airfoil's trailing edge radius.

The angular drive mechanism was mounted in a common housing with the radial drive to reduce flow interference. The housing was 1.5 inches high, 6 inches across, and spanned 48 degrees. The angular drive permitted coverage of 72 degrees. Through a screw and track aligned on a radial line, the probe could be positioned radially from 0 to 2.0 inches from the wall. Probe location was reported electronically with resolution of 0.001 inches and 0.1 degrees.

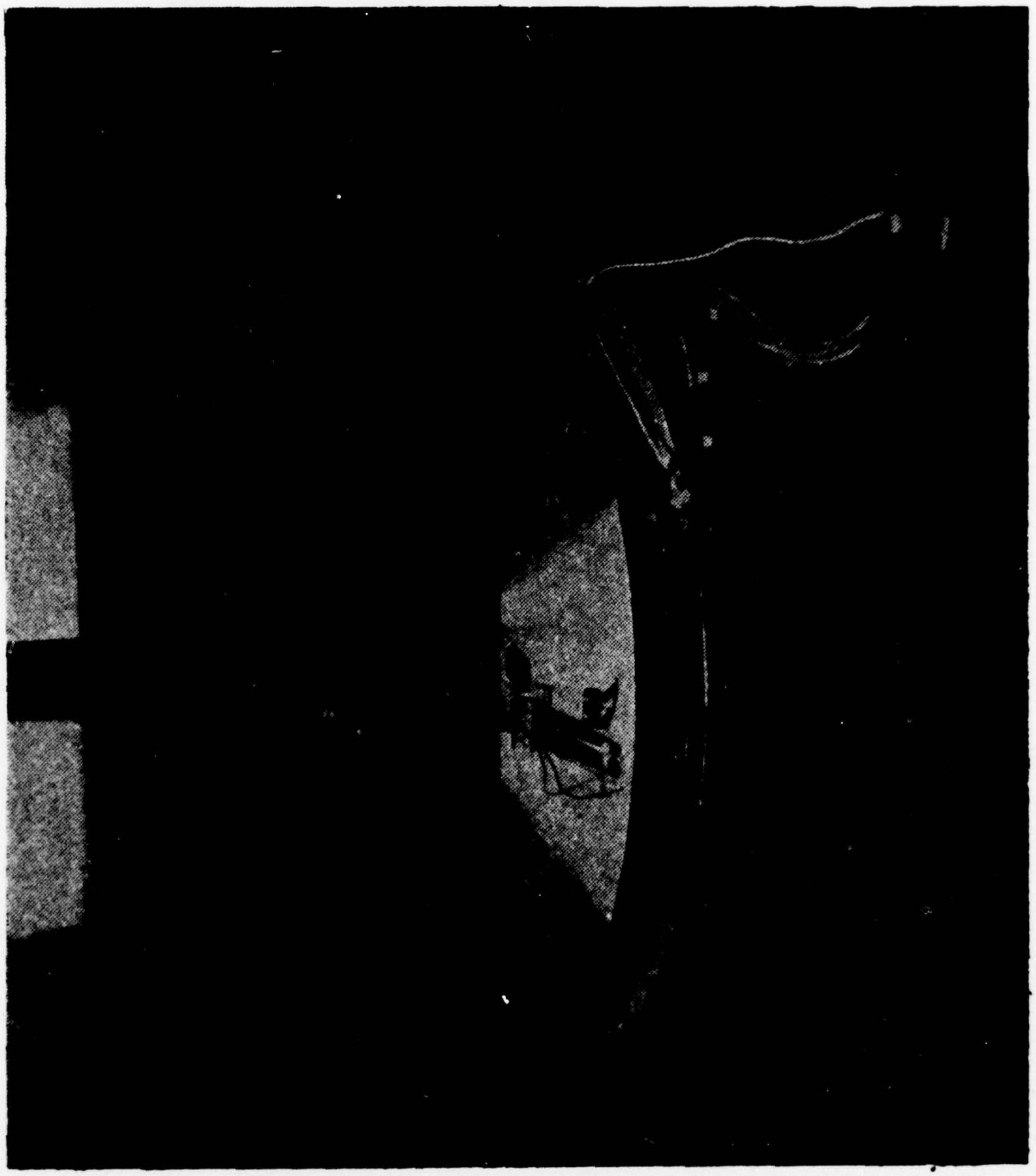

FIGURE 6

HOT WIRE WAKE TRAVERSING MECHANISM

The entire mechanism was mounted on an aluminum base plate which in turn was bolted to the angle of attack disk on the far wall from the console. This permitted moving the mechanism with the airfoil when the angle of attack was changed. The tunnel far wall was selected to permit convenient visual observation of the mechanism by the operator and to enable determination of its flow interference effects (via the half and three-quarter chord pressure taps spanning that half of the airfoil). The uncertainty in the aerodynamic characteristics introduced by the traversing mechanism is C_μ dependent but in no case exceeded six percent. The traversing mechanism was positioned on the airfoil mounting disk to place the separation region for $C_\mu = 0.04$ in the center of its field of view. This permitted evaluation of the entire range of C_μ without having to relocate the mechanism.

The hotwire probes were 5.5 inches long with a 0.125 inch diameter that was flared to 0.25 inches for the last 1.5 inches to facilitate mounting in the probe holder. The steel tips were 0.3 inches long, spaced 0.15 inches apart and spanned by 0.00015 inch diameter tungsten filaments. The filaments were copper plated at both ends to facilitate mounting and had effective sensing lengths of 0.085 inches. The hotwire signals were processed by a Security Associates Model 100 single channel, linearized constant temperature anemometer and then displayed on a digital voltmeter, an RMS meter, and an oscilloscope for data acquisition, Fig. 7.

FIGURE 7

WAKE TRAVERSING MECHANISM TEST CONSOLE

The anemometer output was calibrated to indicate 1 volt DC with the probe at -55 degrees, 2 inches out, a point assumed to be in the freestream. The mechanism was then rotated through the 72 degrees in increments which were adjusted to ensure coverage of the profile variations encountered. During the preliminary tests 15 data points for each radial distance were recorded. Subsequently, this was increased to 26 to improve profile definition. At each point, the angle from the chordline, the digital voltmeter DC value, and the true RMS voltage were recorded. The hot-wire signal was also displayed on an oscilloscope for visual analysis. The same procedure was used for the steady and unsteady tests although the preliminary steady tests did not include RMS data acquisition.

E. PRESSURE DATA ACQUISITION SYSTEM

The airfoil surface pressure acquisition system illustrated in Fig. 8 employed two remote transducers connected via scanivalves to a number of surface points by means of an extended length of tubing. This technique reduces the possibility that the dynamics of the test setup may influence transducer response and is more cost effective, but there exists an additional complexity posed by the transfer function associated with the tubing.

A phase lag and amplitude decrease results as a signal of the form:

$$P_i(t) = \overline{P}_i + P_i \sin \omega t$$

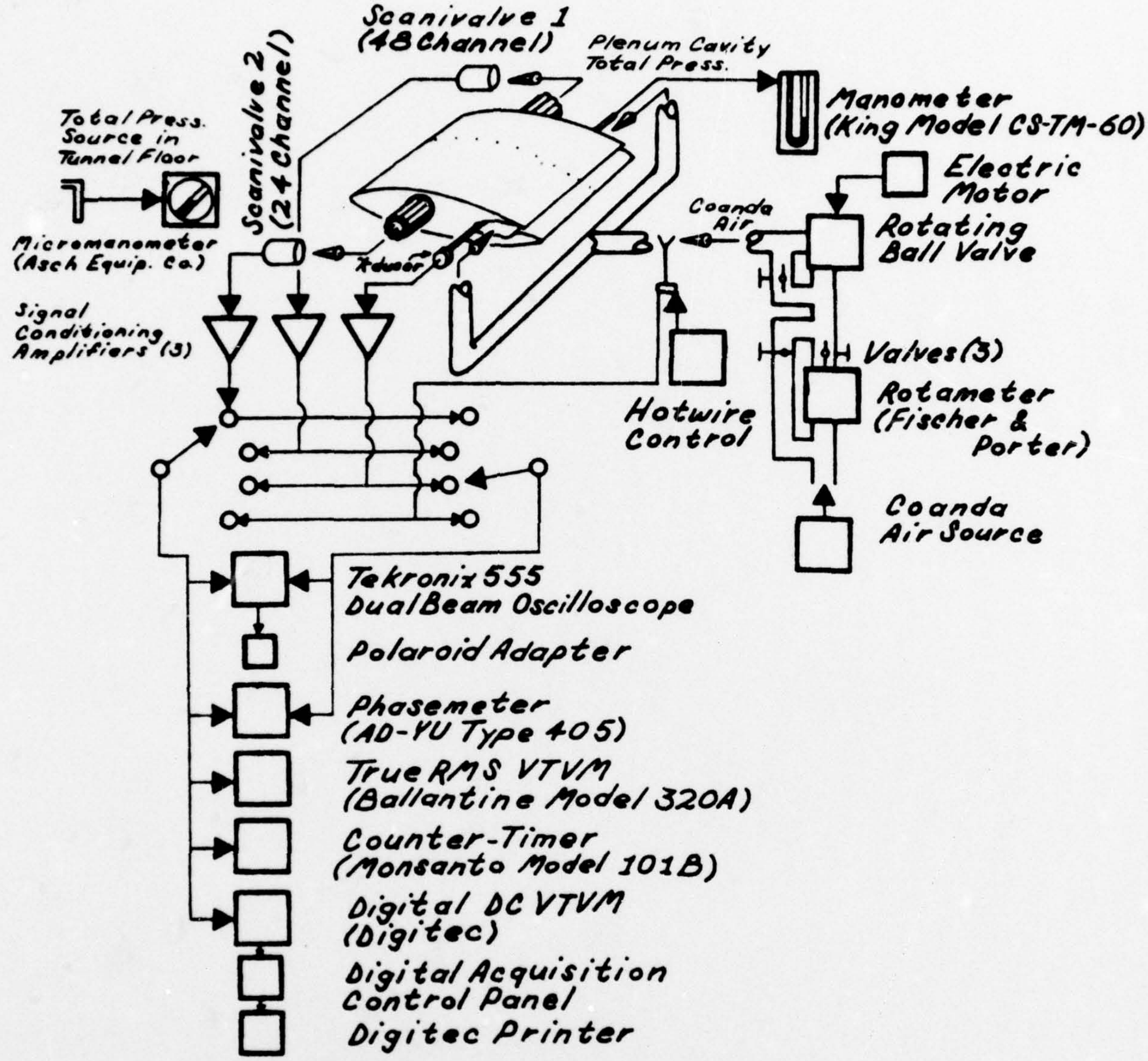

FIGURE 8

SCHEMATIC OF THE SURFACE PRESSURE ACQUISITION SYSTEM

is transmitted from the airfoil surface through the 25.5 inches of 0.033-inch I.D. steel tubing and then via either 2- or 3-inch plastic tubing (coupling length depends on scanivalve) to the scanivalve, Fig. 9. The signal sensed by the pressure transducer in the scanivalve was of the form:

$$P_o(t) = \overline{P}_i + p_o \sin(\omega t + \phi)$$

where

$\overline{P}$ = mean pressure,

p = amplitude of unsteady pressure

ϕ = phase shift (function of frequency)

and the frequency dependent dynamic gains is:

$$|G(\omega)| = p_o/p_i.$$

To determine the dynamic gain and phase shift as functions of frequency, each scanivalve lead was connected via the same length tubing to a resonator and the output compared to that of a reference transducer as illustrated in Fig. 10. The acoustic drive of the resonator was located in the center of the cavity and from the two pressure taps provided comparative signals with an estimated accuracy of one degree in phase angle. The dynamic response curves for scanivalves

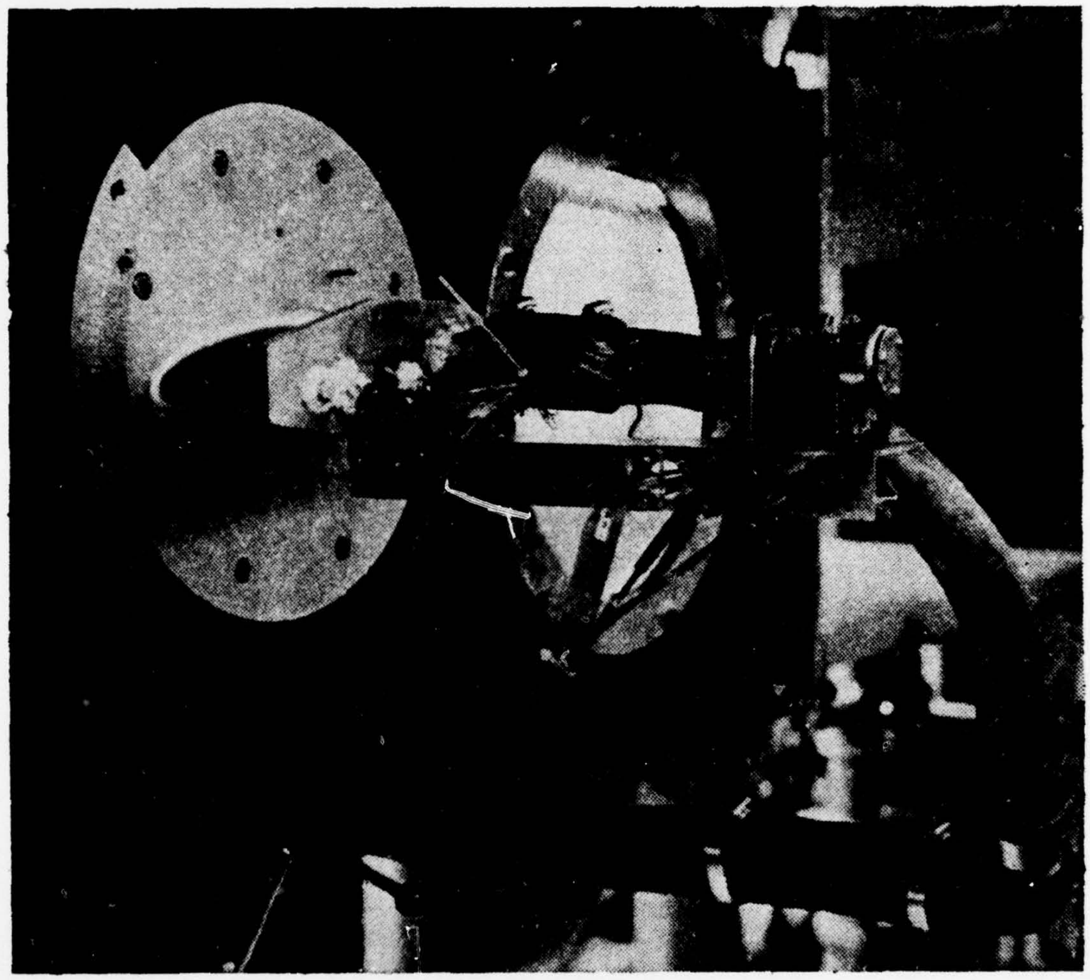

FIGURE 9

SCANIVALVE ATTACHMENT

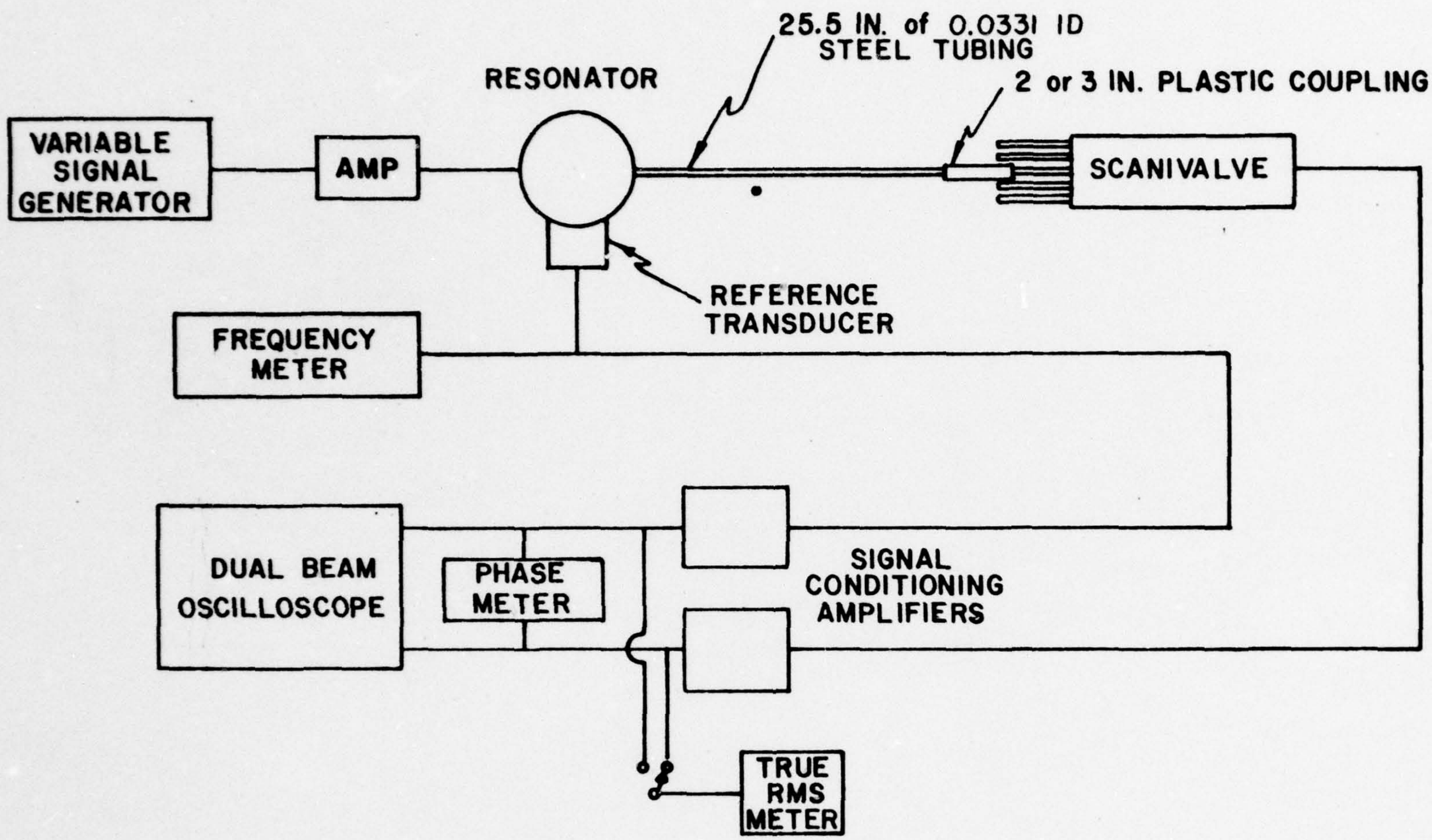

FIGURE 10

SCHEMATIC DIAGRAM OF SCANIVALVE DYNAMIC CALIBRATION INSTRUMENTATION

1 and 2 are depicted in Fig. 11 and the associated static response curves are illustrated in Fig. 12.

This pressure sensing technique was first demonstrated and theoretically analyzed by Bergh [30,31]. Details of its application have been presented by Johnson [32] and Banning [33]. Briefly, with the transfer function of the pressure line determined, phases and amplitudes measured at the distal end were corrected by a numerical application of the inverse of the measured transfer function to yield the pressure history at the surface tap. The DC data were automatically logged by a Digitec printer during the steady flow tests. During the unsteady tests, the counter-timer was manually sequenced to permit recording the true RMS value of the pressure signal at approximately the same time the mean value was printed. The comparative steady-flow data were obtained in the same manner. For both the steady and unsteady tests, the DC signal was processed through a low-pass filter with a two second time constant.

A plenum pressure probe with its own transducer was incorporated as a cross reference to the injection pipe hotwire signal and to provide the clock for surface presure data correlation. The pressure waveform of the scanivalve channel being scanned could be displayed on a dual-beam oscilloscope with a channel of the alternate Scanivalve or the plenum. These signals could also be compared on the phasemeter although only order of magnitude data was obtainable. The pressure data acquisition system was

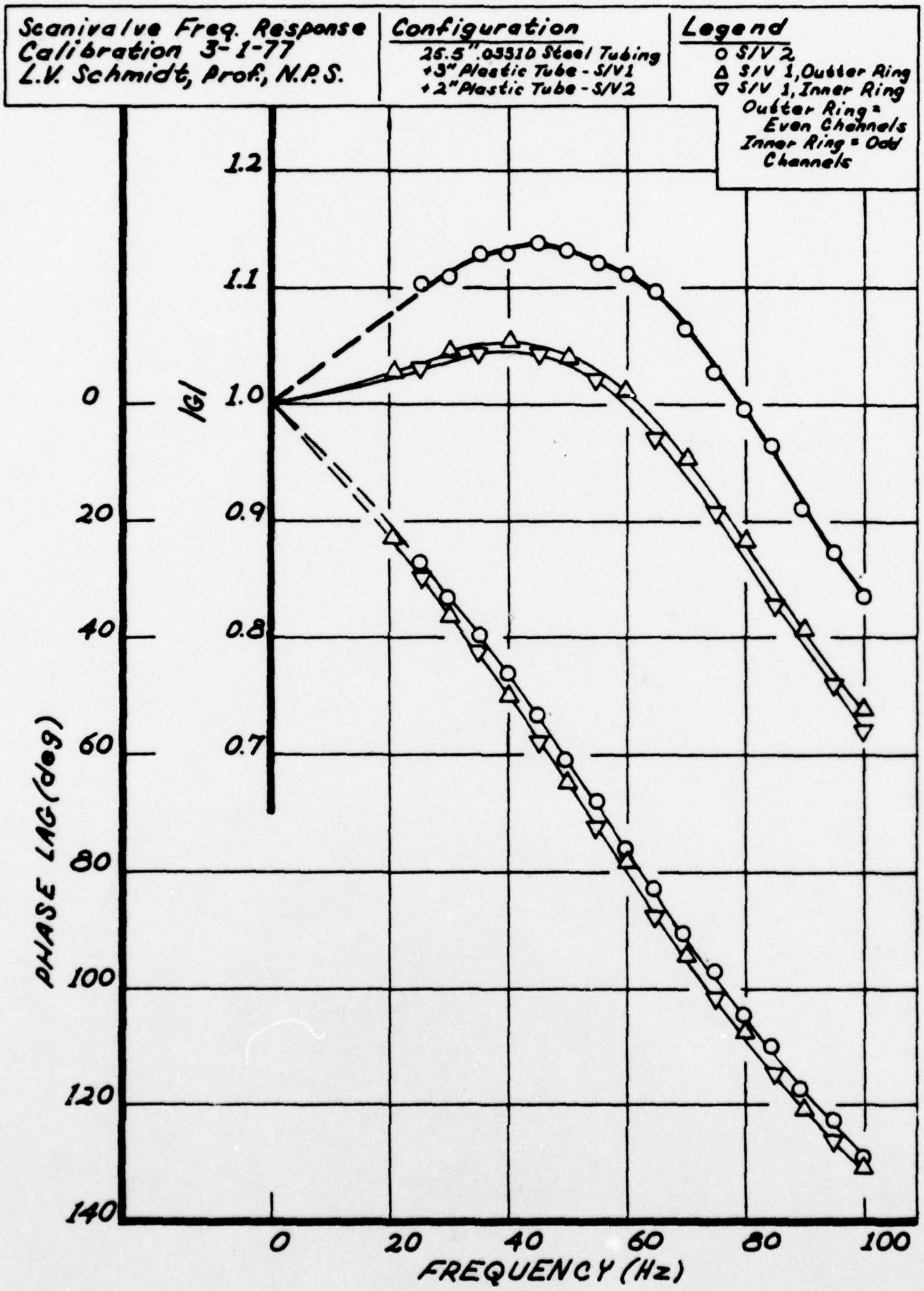

FIGURE 11

SCANIVALVE DYNAMIC FREQUENCY RESPONSE CURVES

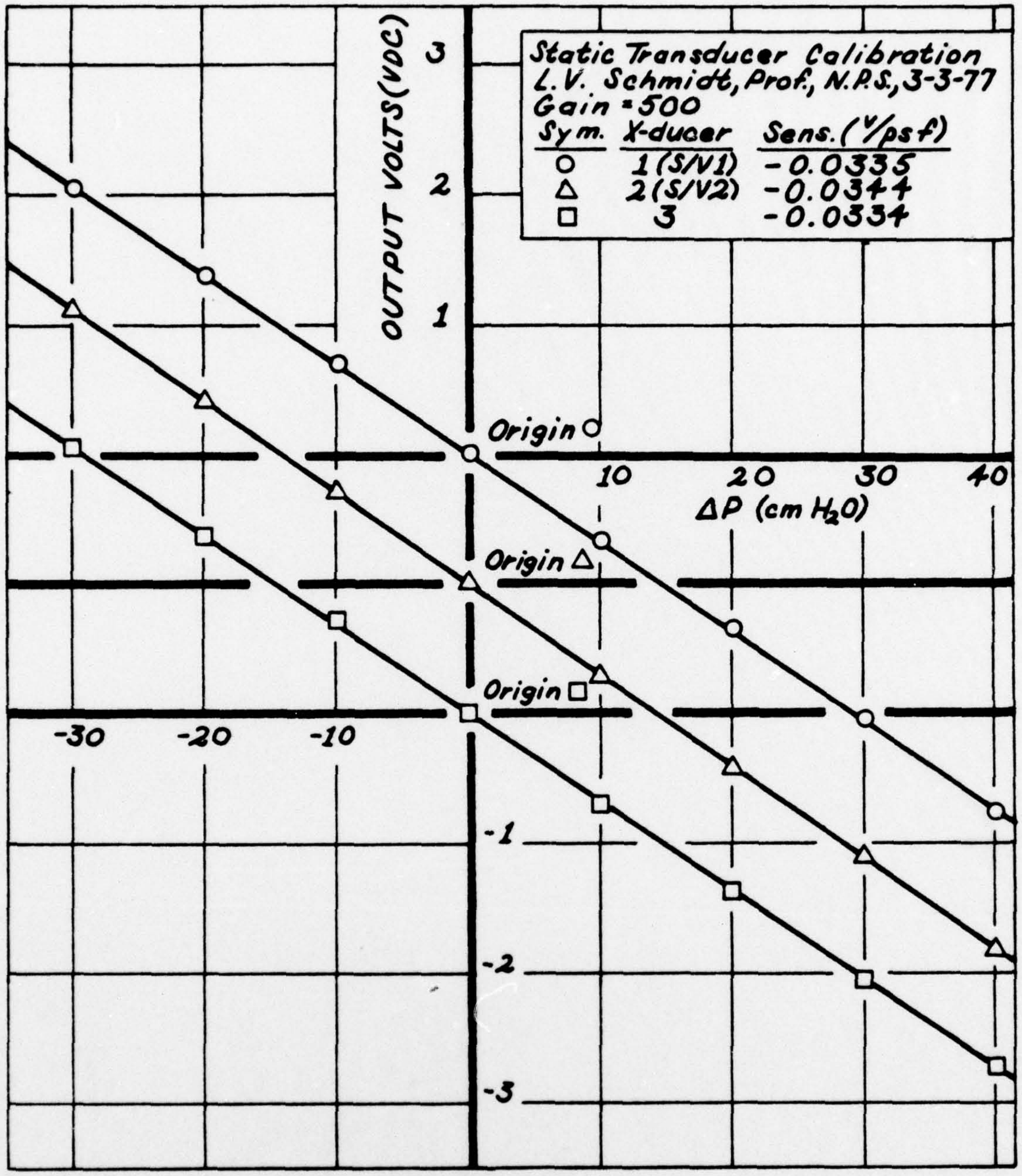

FIGURE 12

STATIC TRANSDUCER CALIBRATION CURVES

estimated to be accurate to within 1 percent of mean pressure. In addition to surface pressures each scanivalve received P_o, P_T and P_{atm} for calibration purposes. A plenum pressure line was also connected to a water manometer to provide the mean value of the steady and oscillating plenum pressure. Tunnel q was monitored by a micromanometer and pitot-static tube installed in the test section. Figure 13 is a photograph of the pressure data acquisition system console.

FIGURE 13

PRESSURE ACQUISITION SYSTEM CONSOLE

IV. CALCULATION OF BLOWING AND AERODYNAMIC COEFFICIENTS

A. STEADY FLOW

The steady blowing coefficient C_μ may be defined as:

$$C_\mu = \frac{\dot{m}\, V_j}{qS}$$

where $\dot{m}$ is the mass flow rate, V_j is the velocity of the Coanda jet at the slow, q is the test section dynamic pressure, and S the model planform area. Mass flow rate was obtained directly from rotameter readings. The jet velocity was obtained from the isentropic relationship

$$V_j = \{\frac{2R}{M} T_i \left(\frac{k}{k-1}\right)[1 - \left(\frac{p_\infty}{p_i}\right)^{\frac{k-1}{k}}]\}^{1/2}$$

where i denotes a plenum value, and tunnel q was calculated from the freestream pitot-static measurements. Conventional aerodynamic coefficients defined by surface integrals were approximated by numerical integrations since data were available only at a finite number of pressure tap locations. The steady normal force, chord force, and pitching moment coefficients are:

$$C_N = \int_0^{1.0} (C_{p_\ell} - C_{p_u})\, d(X/C)$$

$$C_c = \int_{Y/C(min)}^{Y/C(max)} (C_{p_f} - C_{p_r})\, d(Y/C)$$

$$C_{M(TE)} = \int_{Y/C(min)}^{Y/C(max)} (C_{p_f} - C_{p_r})(Y/C)\, d(Y/C)$$

$$+ \int_{0}^{1.0} (C_{p_\ell} - C_{p_u})(X/C)\, d(X/C)$$

Including the effects of angle of attack and a moment transfer to the half and quarter-chord positions, these force coefficients may be written as the usual aerodynamic coefficients:

$$C_L = C_N \cos \alpha - C_c \sin \alpha$$

$$C_D = C_N \sin \alpha + C_c \cos \alpha$$

$$C_{M(C/4)} = C_{M(TE)} - 0.75\ C_N$$

$$C_{M(C/2)} = C_{M(TE)} - 0.5\ C_N$$

The conversion from pressure data to coefficient of pressure data, and the subsequent calculation of the aerodynamic coefficients were performed on a Hewlett-Packard Model 9830 calculator. The computer program may be found in Ref. [36].

B. OSCILLATING FLOW

For the unsteady blowing test, an oscillation was imposed on the mass flow in the air injection supply line such that the pipe hotwire indicated a velocity fluctuation of the form:

$$V_{pipe} = \overline{V}(1 + \varepsilon \sin \omega t)$$

where ε was varied from 0 to 0.4. For incompressible self-similar flow, this implies that

$$\dot{m} = \overline{\dot{m}}(1 + \varepsilon \sin \omega t)$$

Therefore, assuming that the velocity amplitude ratio in the pipe was the same as that occurring at the slot,

$$C_\mu(t) = \frac{\overline{\dot{m}}\, V_j}{qS} (1 + \varepsilon \sin \omega t)^2$$

or

$$C_\mu(t) = \overline{C_\mu} \left[1 + 2\varepsilon \sin \omega t + \frac{\varepsilon^2}{2} (1 + \cos 2\omega t)\right]$$

with the maximum velocity amplitude ratio $\varepsilon = 0.4$, $\varepsilon^2 = 0.16$ and as a first approximation, ε^2 was neglected. Then to first order $C_\mu(t) = \overline{C_\mu}\,(1 + 2\varepsilon \sin \omega t)$. The implications of neglecting the second order term and assuming no transfer function from the pipe to the slot are discussed in Section V.

With $\dot{m}$ proportional to the pipe velocity, and thus the hotwire signal, the mass flow amplitude ratio was defined as

$$\varepsilon = \sqrt{\left[\frac{e_{RMS}}{\bar{e}}\right]^2_{oscillating} - \left[\frac{e_{RMS}}{\bar{e}}\right]^2_{steady}}$$

where $\left[\frac{e_{RMS}}{\bar{e}}\right]_{steady}$ accounts for the turbulence intensity of the supply line in steady flow.

With the dynamic gain approximately equal to one for frequencies on the order of 10 Hz, numerical integration of the unsteady static pressure distribution can be performed in a manner similar to the steady pressure integration, provided relative phase information is available. Unfortunately the real time acquisition system designed and constructed by Englehardt [35] was not completed in time for the present investigation. With the exception of the no blowing harmonic resonance case examined by Pickelsimer [36], only mean and RMS pressure data could be obtained.

The pressure and lift coefficient amplification ratios, ε_p and ε_L, were defined in a similar manner to :

$$\varepsilon_p = \sqrt{\left[\frac{p_{RMS}}{\bar{p}}\right]^2_{oscillating} - \left[\frac{p_{RMS}}{\bar{p}}\right]^2_{steady}}$$

and

$$\varepsilon_L = \sqrt{\left[\frac{C_{LRMS}}{\overline{C}_L}\right]^2_{oscillating} - \left[\frac{C_{LRMS}}{\overline{C}_L}\right]^2_{steady}}$$

where C_{LRMS} was obtained by running the aerodynamic coefficient program with the RMS pressure data.

V. RESULTS AND DISCUSSION

A. PRELIMINARY STEADY AND OSCILLATORY BLOWING TESTS

Initial testing produced a dC_L/dC_μ of only one half that reported by others for similar profiles. Examination of the composite model revealed the structure to be delaminating in the area of the injection slot.

Before repairing the airfoil, a temporary fix was performed to permit completion of the mass flow control evaluation reported by Bauman [29]. With oscillating mass flow rate amplitudes of up to 43% of the mean, no noticeable effect could be observed on the forward stagnation point. In fact, it was not possible to observe surface pressure fluctuations beyond the point of separation for $C_\mu = 0.03$ or 0.05. These results raised questions as to the nature of the fluid dynamics occurring in the Coanda jet and the near-wake.

While the airfoil internal structure was being repaired and a steel slot lip constructed, the hotwire wake traversing mechanism was designed and constructed to allow investigation of the near-wake flow field. At the same time tunnel and surface pressure acquisition system calibrations were performed. These procedures and results were discussed in Section III.

B. STEADY FLOW, STEADY BLOWING TESTS

1. Airfoil Performance

With the steel slot lip installed, the slot height was set at 0.016 inches based on advice from Wilkerson.* Under maximum pressurization for the range of blowing coefficients investigated, the slot height increased less than 15 percent, and did not show evidence of change during extensive testing.

The steady flow lift augmentation results are illustrated in Fig. 14 and associated aerodynamic characteristics are listed in Table I. For $\alpha_g = -5$, the approximate zero-lift geometric angle of attack, $dC_L/dC_\mu = 30.5$. This data was compiled without incorporation of wall and effective angle of attack corrections because of the need for comparable data to that obtained in the unsteady tests where such corrections are not possible. Although the augmentation appears well below the value of 70 obtained by Englar [21], it is felt that results to follow are indicative of what could be obtained on a production airfoil.

Of note is the linear relationship existing between the ratio of plenum-to-jet pressure, $PR = p_j/p_i$ and the blowing coefficient, C_μ as shown in Fig. 15. Treating the jet pressure at the slot as the value obtained at tap 22

---

*Personal communication

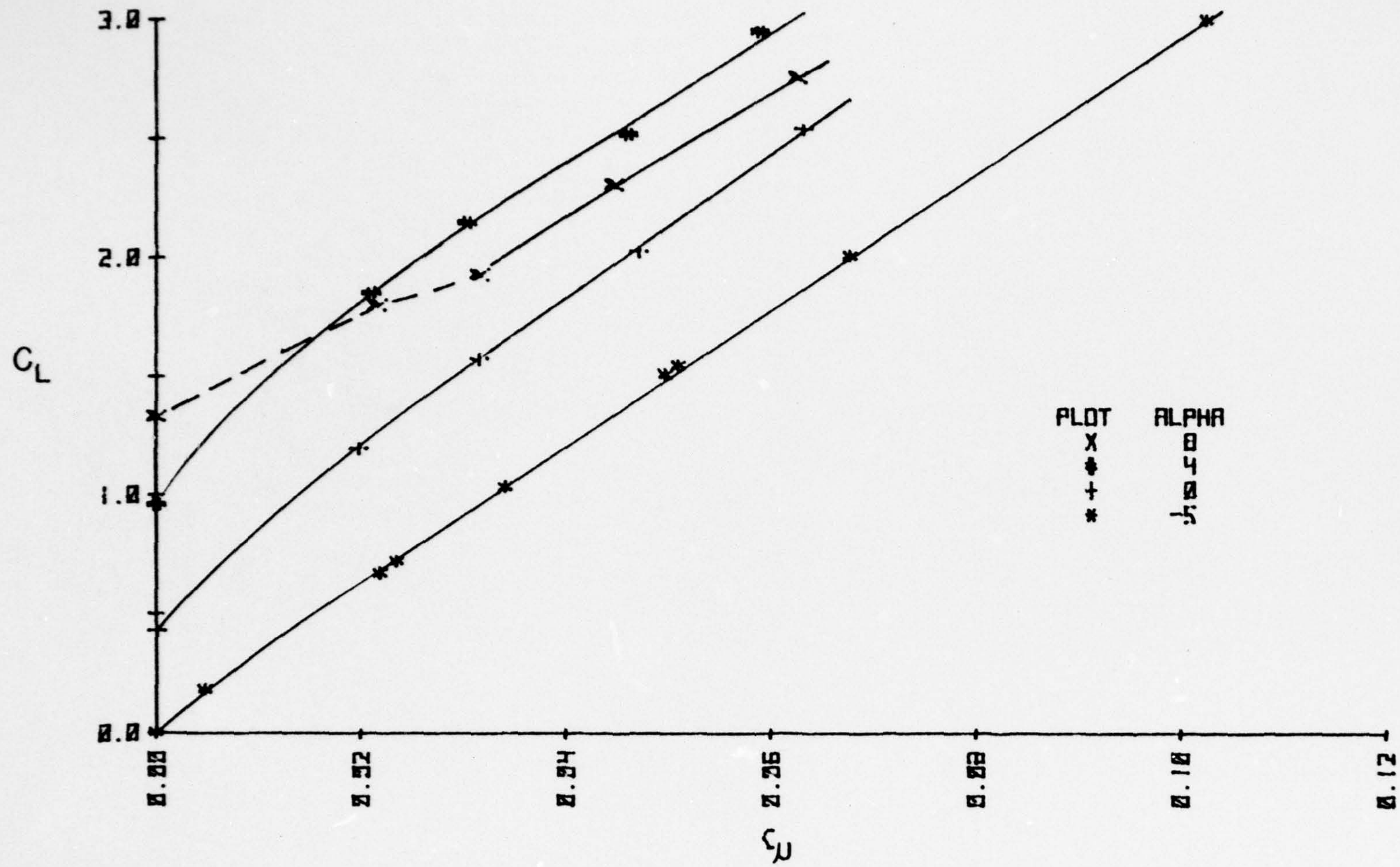

FIGURE 14
C_L VS C_μ FOR STEADY BLOWING

TABLE I

STEADY FLOW, STEADY BLOWING AERODYNAMIC CHARACTERISTICS

RUN	C_L	C_D	$C_{M(C/4)}$	$C_{M(C/2)}$
		$\alpha = -5°$		
32501	0.0080	0.0483	-0.1173	-0.1163
32502	0.7252	0.0423	-0.3354	-0.1558
32503	1.0360	0.0461	-0.4211	-0.1641
32504	1.5109	0.0790	-0.5588	-0.1842
32505	2.0111	0.1126	-0.7129	-0.2145
		$\alpha = 0°$		
32506	0.4311	0.0557	-0.1101	-0.0023
32507	1.1979	0.0482	-0.3210	-0.0216
32508	1.5746	0.0596	-0.4211	-0.0334
32509	2.0272	0.0833	-0.5558	-0.0490
32510	2.5412	0.1197	-0.6962	-0.0609
		$\alpha = 4°$		
33101	0.9619	0.0525	-0.1299	0.1109
33102	1.8540	0.0704	-0.3763	0.0873
33103	2.1499	0.0742	-0.4611	0.0764
33104	2.5190	0.1113	-0.5587	0.0715
33105	2.9507	0.1195	-0.6950	0.0789
		$\alpha = 8°$		
33106	1.3341	0.0515	-0.1259	0.2061
33107	1.8004	0.0930	-0.2594	0.1896
33108	1.9301	0.1095	-0.2803	0.2013
33109	2.3029	0.1726	-0.4061	0.1700
33110	2.7566	0.1395	-0.4744	0.2129

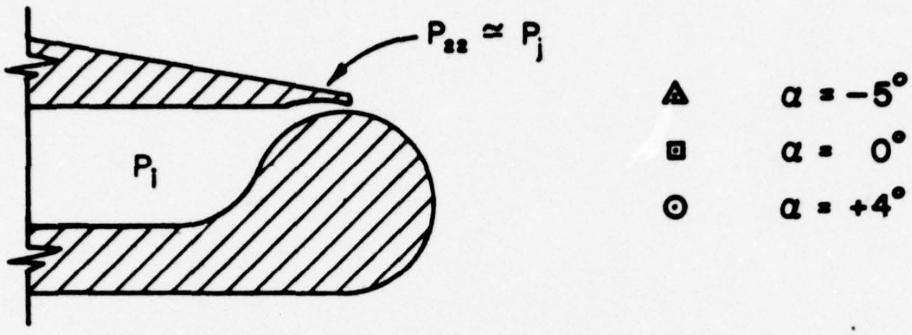

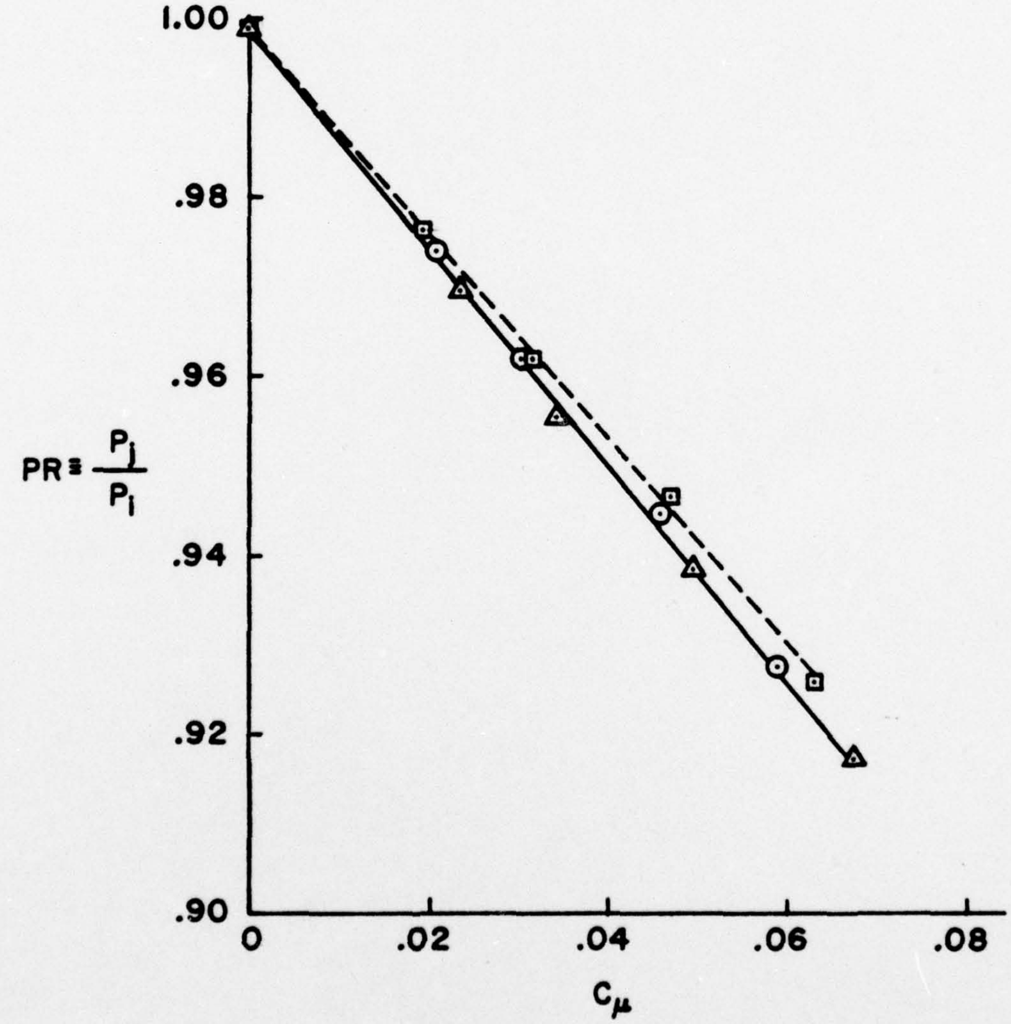

FIGURE 15

COMPARISON OF JET-TO-PLENUM PRESSURE RATIOS AS A FUNCTION OF C_μ FOR VARIOUS α

(0.15 inches upstream of the slot), $d(PR)/dC_\mu$ varied from -1.15 to -1.25 depending on angle of attack.

Figures 16 and 17 illustrate the upper surface pressure variation with spanwise distance from the wall at mid-chord and three-quarter chord respectively. From these plots and through tests with tufts and a wand, it was concluded that the wall interference propagated not more than three inches from the wall at the trailing edge.

2. Trailing Edge Flow Environment

Trailing edge pressure distributions for the C_μ tested at $\alpha_g = -5°$ are illustrated in Fig. 18. As noted in Section I, the Coanda sheet separates when the pressure coefficient reaches a positive near-constant value just beyond the suction peak. Thus for the blowing cases, separation in terms of the angular coordinate measured from the slot lip ranges from 70 to 100 degrees for C_μ between 0.02 and 0.07.

Kind [18] and Gibbs [20] assert that the near constant value defines a separation bubble which extends over 100 degrees beyond the Coanda jet separation point for low blowing rates. The lower limit of the bubble defines the lower surface boundary layer separation point, (for typical rotor Reynolds numbers, the boundary layer is turbulent). In plotting the pressure distribution versus Y/C, this region becomes more evident, Fig. 19. A review of C_p data for C_μ from 0.0089 to 0.0854 indicated that the lower boundary layer

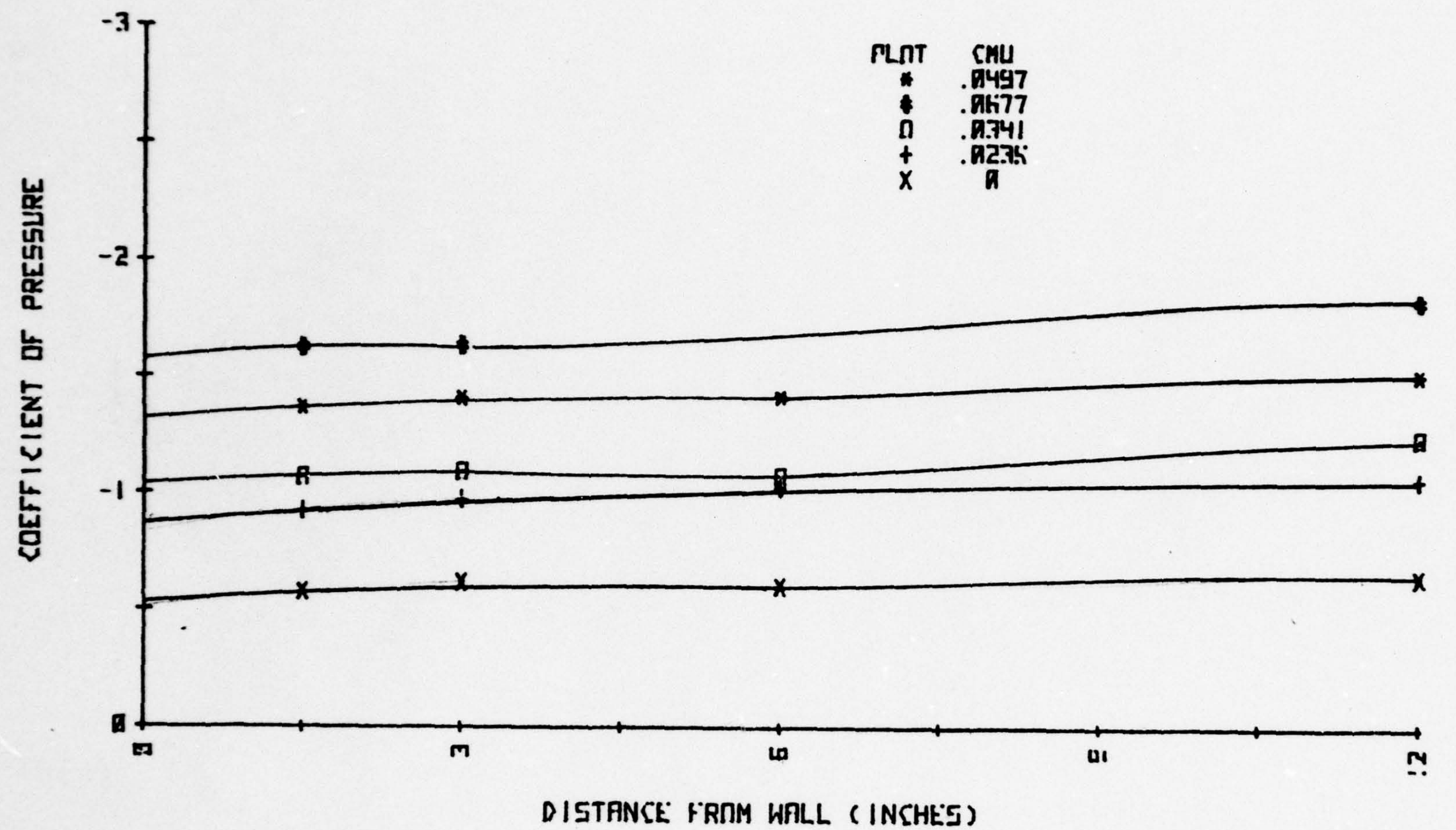

FIGURE 16

COEFFICIENT OF PRESSURE VS DISTANCE FROM WALL

ALONG 0.50*(X/C) FOR ALPHA = -5

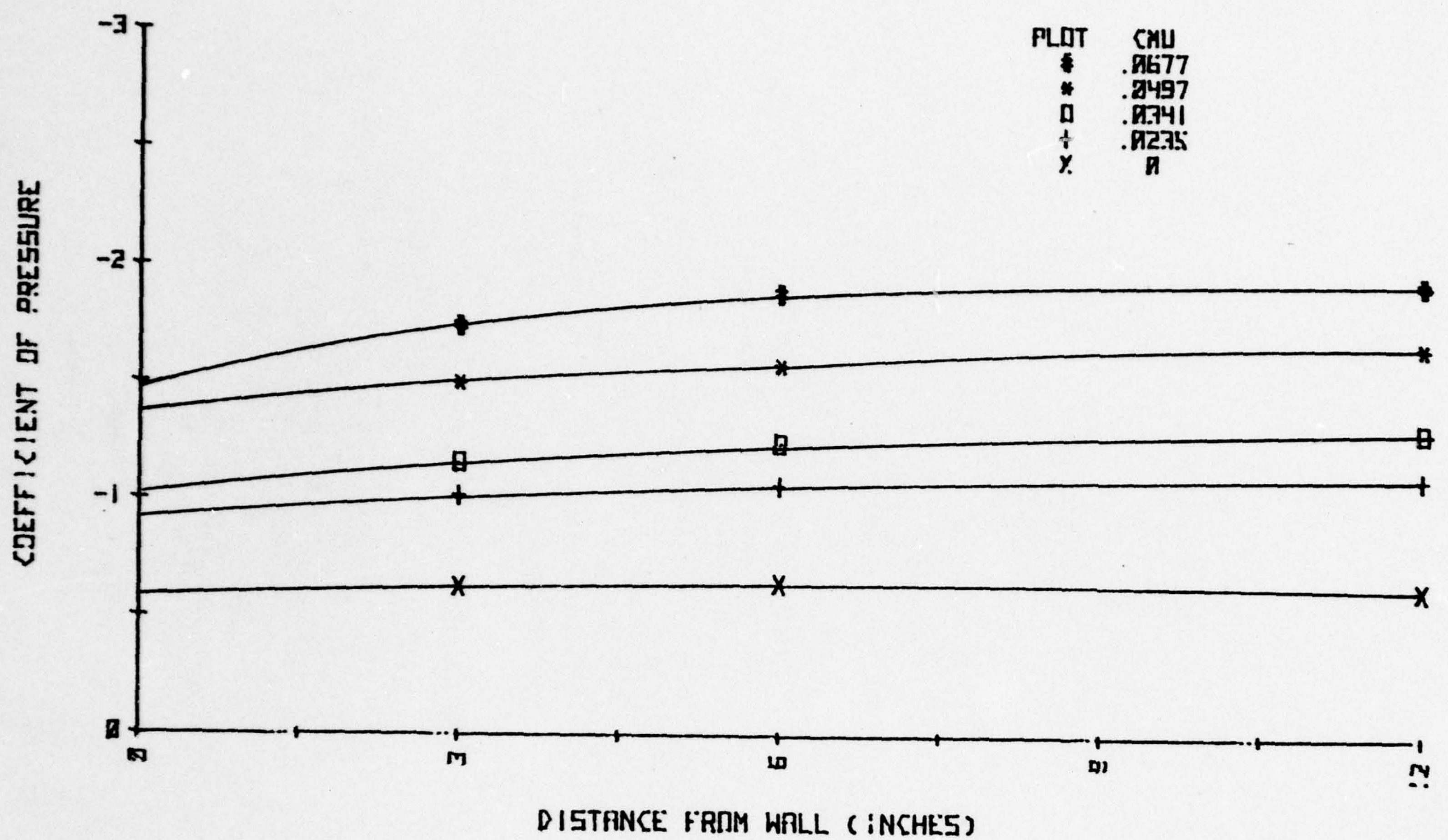

FIGURE 17

COEFFICIENT OF PRESSURE VS DISTANCE FROM WALL

ALONG 0.75*(X/C) FOR ALPHA = -5

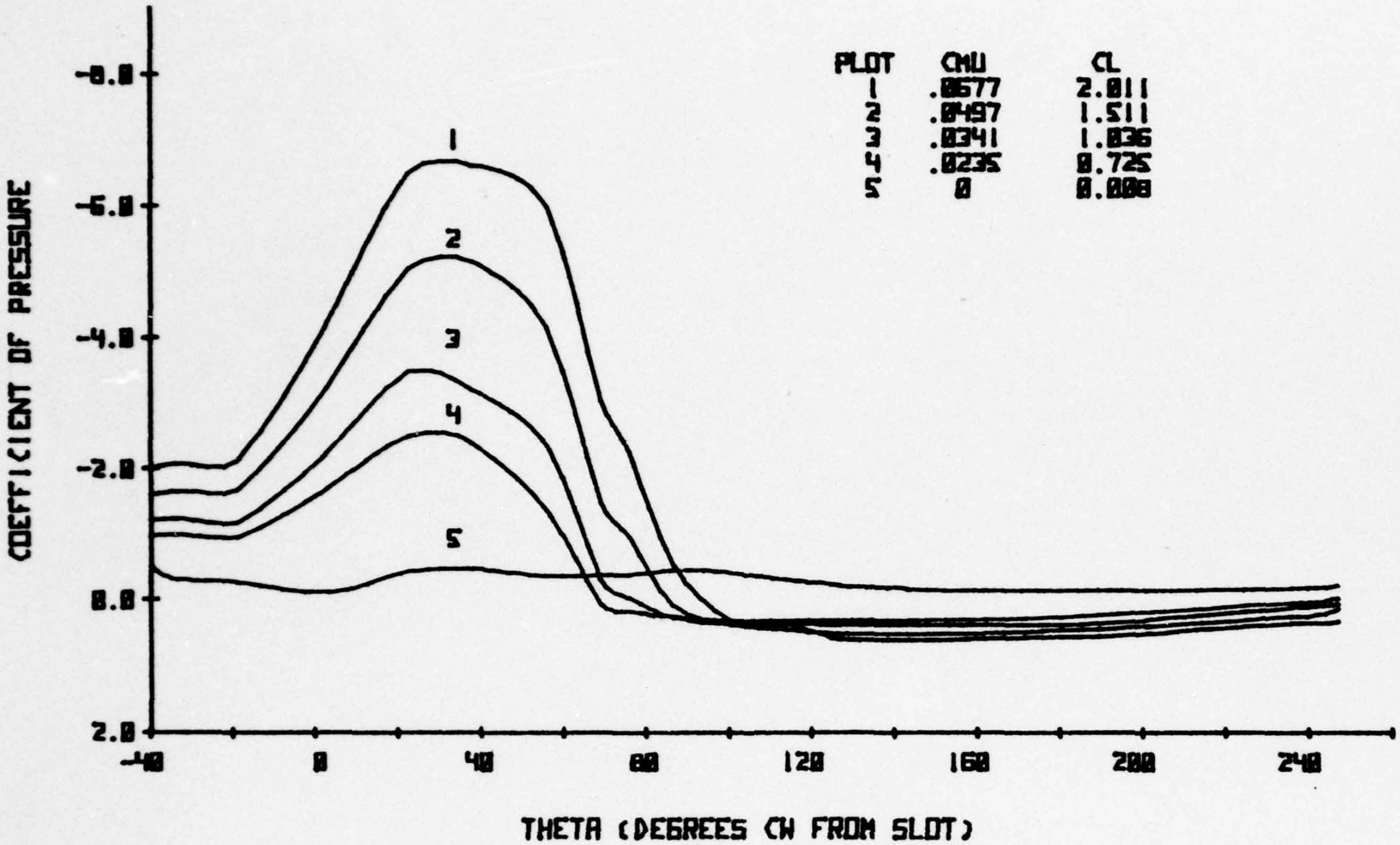

FIGURE 18

COEFFICIENT OF PRESSURE VS THETA FOR ALPHA = -5

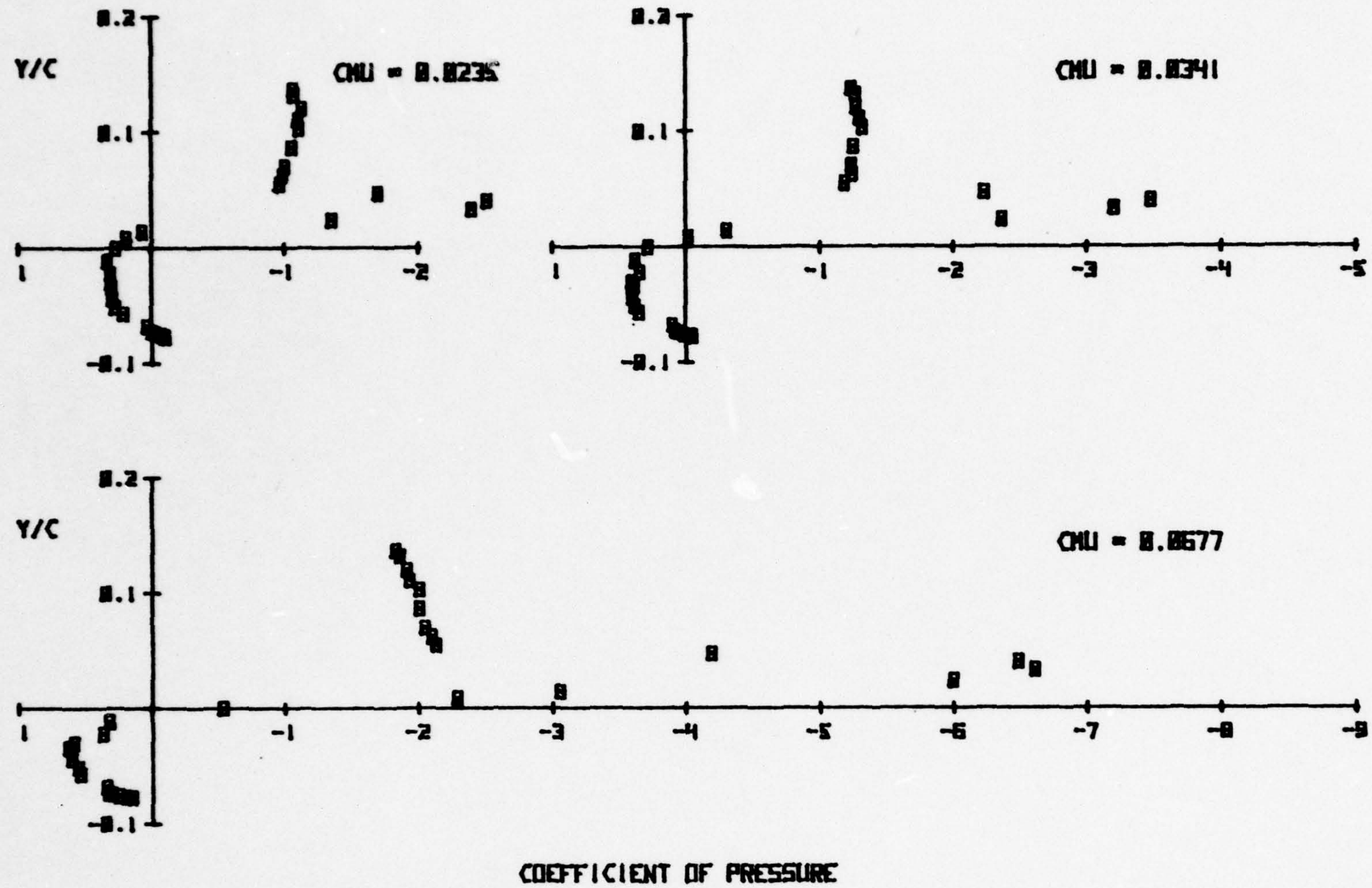

FIGURE 19

REAR PRESSURE DISTRIBUTIONS VS Y/C FOR VARIOUS CMU, ALPHA=-5

separation point occurred between 170 and 190 degrees from the slot. No information existed concerning correlation of bubble depth to C_μ.

3. Wake Traversing Mechanism Effects on Airfoil Performance

With the wake traversing mechanism installed, flow blockage was observable at 1.5 inches and to a lesser extent at 3 inches from the wall. At the quarter-span, the pressure coefficients varied as a function of C_μ and seemed to have the greatest deviation from the unobstructed flow results in the range of C_μ less than 0.03. Figure 20 is a comparison of typical pressure data obtained with and without the mechanism installed. Additional spanwise pressure data are contained in Appendix B. Note that at values of C_μ greater than 0.035, the ratio $C_{p(b/4)}$ to $C_{p(b/2)}$ decreases less than 4 percent from the half to three-quarter chord with the mechanism installed. Therefore, at least for C_μ greater than 0.035, it is assumed that the flow reaching the hotwire was two-dimensional and indicative of that measured at midspan.

This conclusion is consistent with the lift augmentation results compared in Fig. 21. For C_μ between 0.01 and 0.025 the C_L loss reached 30 percent, but for C_μ greater than 0.035 the loss was less than 5 percent. For C_μ greater than 0.055 the influence of the mechanism was not detectable.

The aerodynamic characteristics obtained with the mechanism installed are listed in Table II. As shown in Fig. 22, the influence of the mechanism on pressure drag was small.

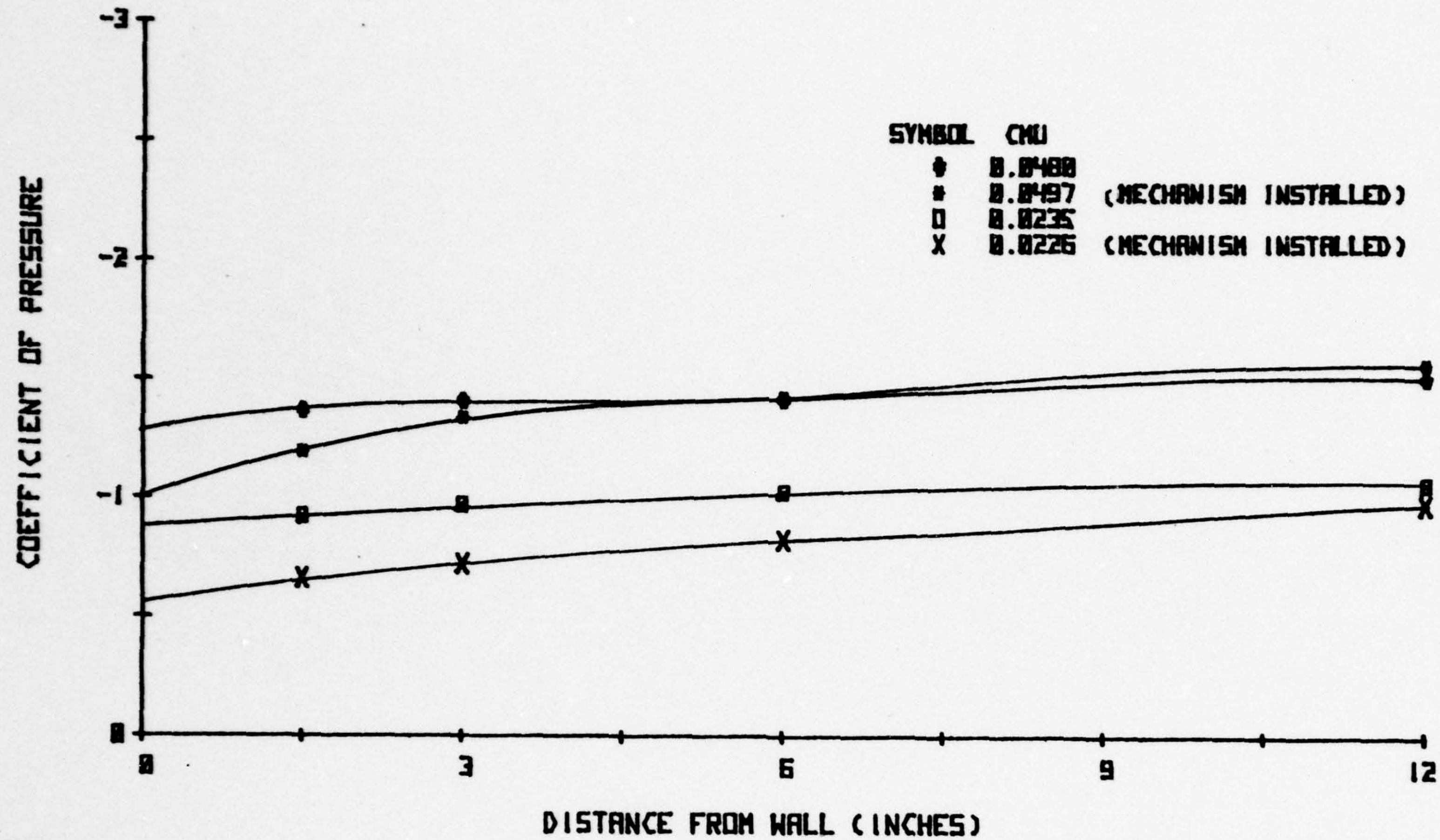

FIGURE 20

COEFFICIENT OF PRESSURE VS DISTANCE FROM WALL

ALONG 0.50*(X/C) FOR ALPHA = -5

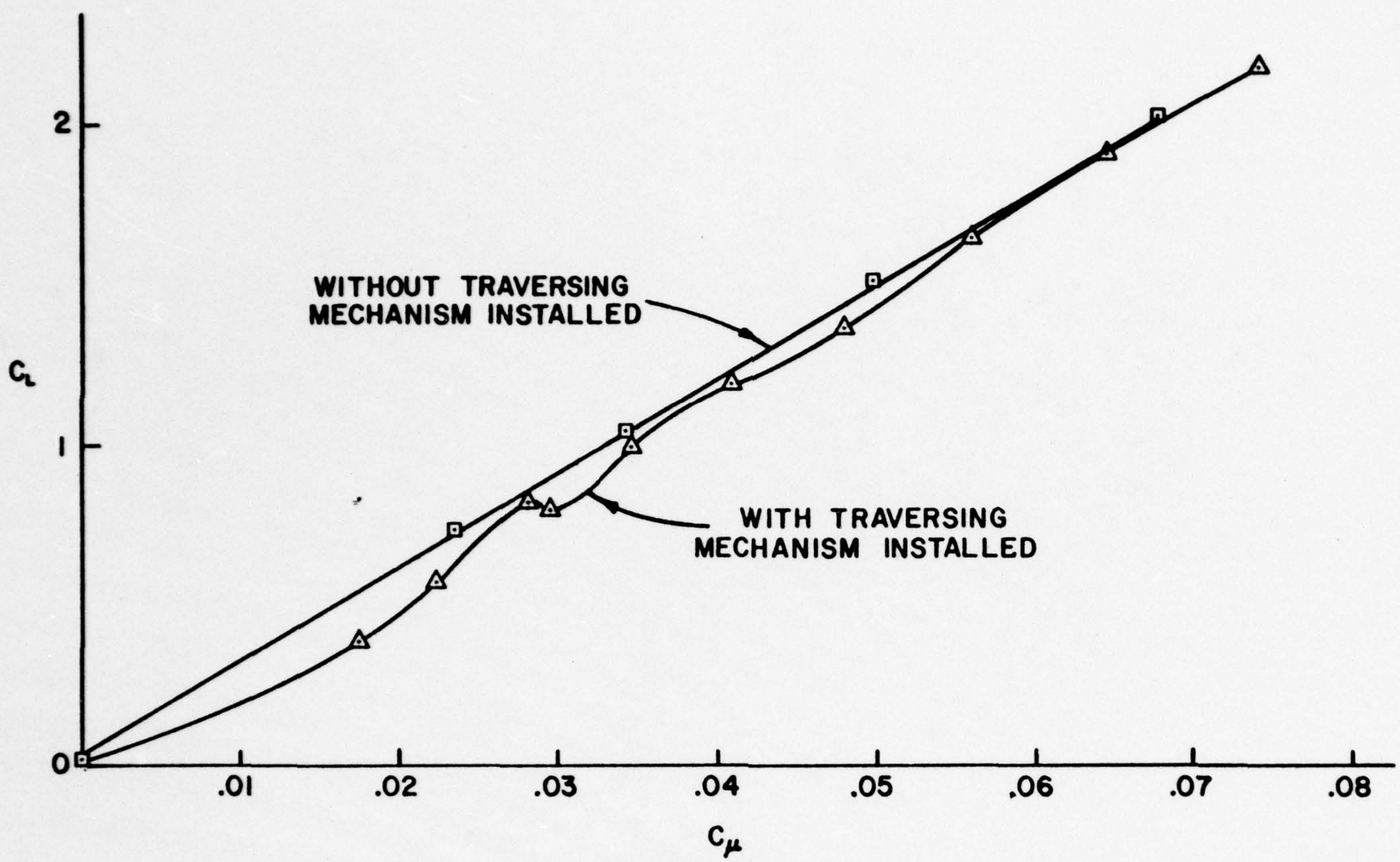

FIGURE 21

COMPARISON OF LIFT AUGMENTATION OBTAINED WITH AND WITHOUT THE WAKE TRAVERSING MECHANISM INSTALLED

TABLE II

STEADY FLOW, STEADY BLOWING AERODYNAMIC CHARACTERISTICS WITH THE WAKE TRAVERSING MECHANISM INSTALLED

RUN	C_L	C_D	$C_{M(C/4)}$	$C_{M(C/2)}$
50201	1.0881	0.5900	0.0621	
51003.1	1.1836	0.0733	0.4795	-0.1863
51003.2	-0.0521	-0.0160	0.0238	0.0112
51002	1.2088	0.0130	-0.4884	-0.1889
51011	0.1555	0.0214	-0.1713	
51012	0.2517	0.0404	-0.1991	
51013	0.4402	0.0392	-0.2314	
5130.1	0.0067	0.0148	0.0020	0.0033
51301	1.2560	0.0725	-0.4815	-0.1702
51701	1.4971	0.0511	-0.5418	
52001	2.7322	0.1077	-0.8917	-0.2136
52002	2.6563	0.1208	-0.8854	-0.2265
52002.1	0.0765	0.0315	-0.0308	-0.0124
52601	1.3785	0.0598	-0.5282	-0.1862
52604	1.8370	0.0991	-0.6594	-0.2040
52603	1.3103	0.0849	-0.4942	-0.1697
52602	1.3531	0.0604	-0.5317	-0.1960
52605.1	0.0536	0.0328	-0.0295	-0.0169
52604.1	0.0090	0.0094	-0.0037	-0.0017
52603.1	0.0650	0.0392	-0.0403	-0.0250
52602.1	0.0575	0.0164	-0.0175	-0.0036
52605	1.9903	0.0651	-0.6801	-0.1858
52601.1	0.0107	0.045	-0.0039	-0.0013

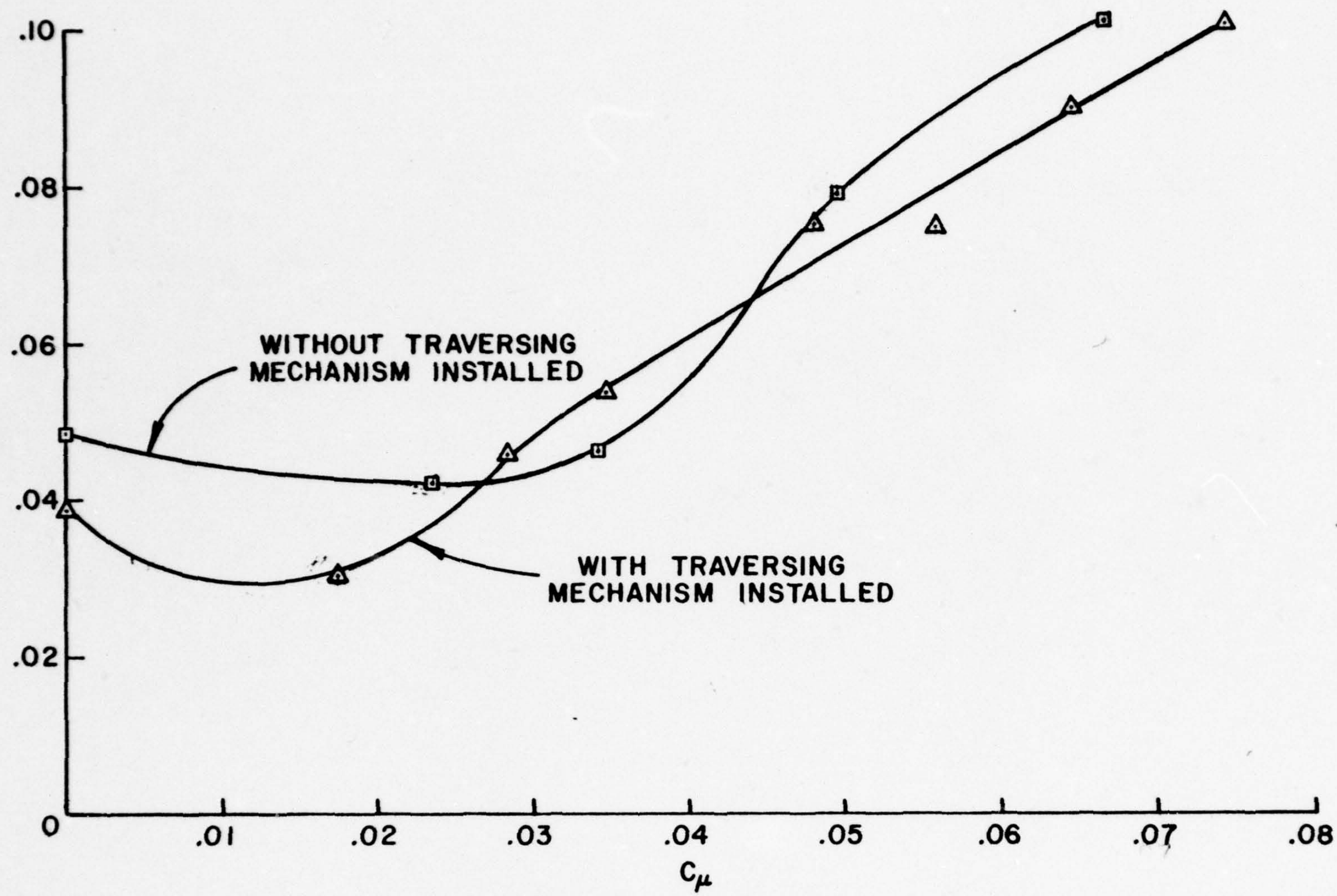

FIGURE 22

COMPARISON OF PRESSURE DRAG VS BLOWING COEFFICIENT WITH AND WITHOUT WAKE TRAVERSING MECHANISM INSTALLED

4. Wake Survey

The initial purpose of the wake traversing mechanism was to provide a means to map near-wake velocity distributions and to permit observation of the flow phenomena occurring just beyond the separation bubble. The mechanism was also to provide diagnostic information that could be correlated during oscillatory blowing with surface static pressure results to assist in identifying the contributing mechanics to the unsteady aerodynamic transfer functions.

After conducting preliminary tests, it became evident that the hotwire traversing mechanism could provide information sufficient to define the location of separation of the Coanda jet. The objective of these tests was accordingly expanded to include ocrrelation of the location of separation with flow parameter variation.

Determination of the initial location of the wake traversing mechanism required reference to the trailing edge pressure data. With separation occurring roughly between 70 and 100 degrees from the slot for C_μ between 0.02 and 0.07, the mechanism was located to span 48 to 120 degrees.

Figures 23 and 24 are examples of the mean velocity data obtained for a range of hotwire distances from the surface of 0.025 to 0.75 inches. Except for evidence of the velocity maximum for 0.025 inches in Fig. 24 (the higher C_μ case), the first 25 degrees offered little useful information.

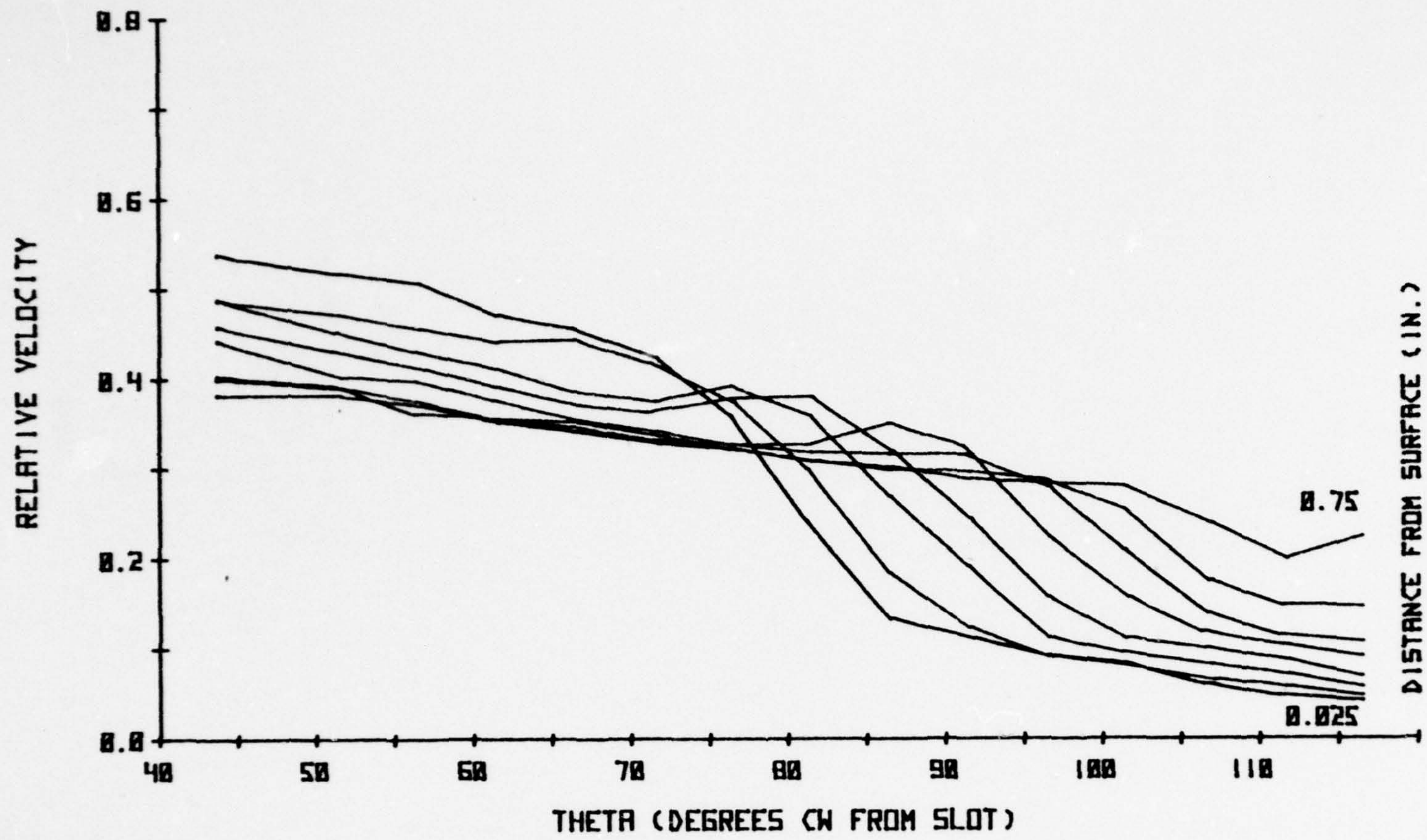

FIGURE 23

RELATIVE VELOCITY VS THETA FOR ALPHA = -5 CMU = 0.0332
0.025, 0.05, 0.1, 0.15, 0.25, 0.375, 0.5, 0.75 IN. FROM SURFACE

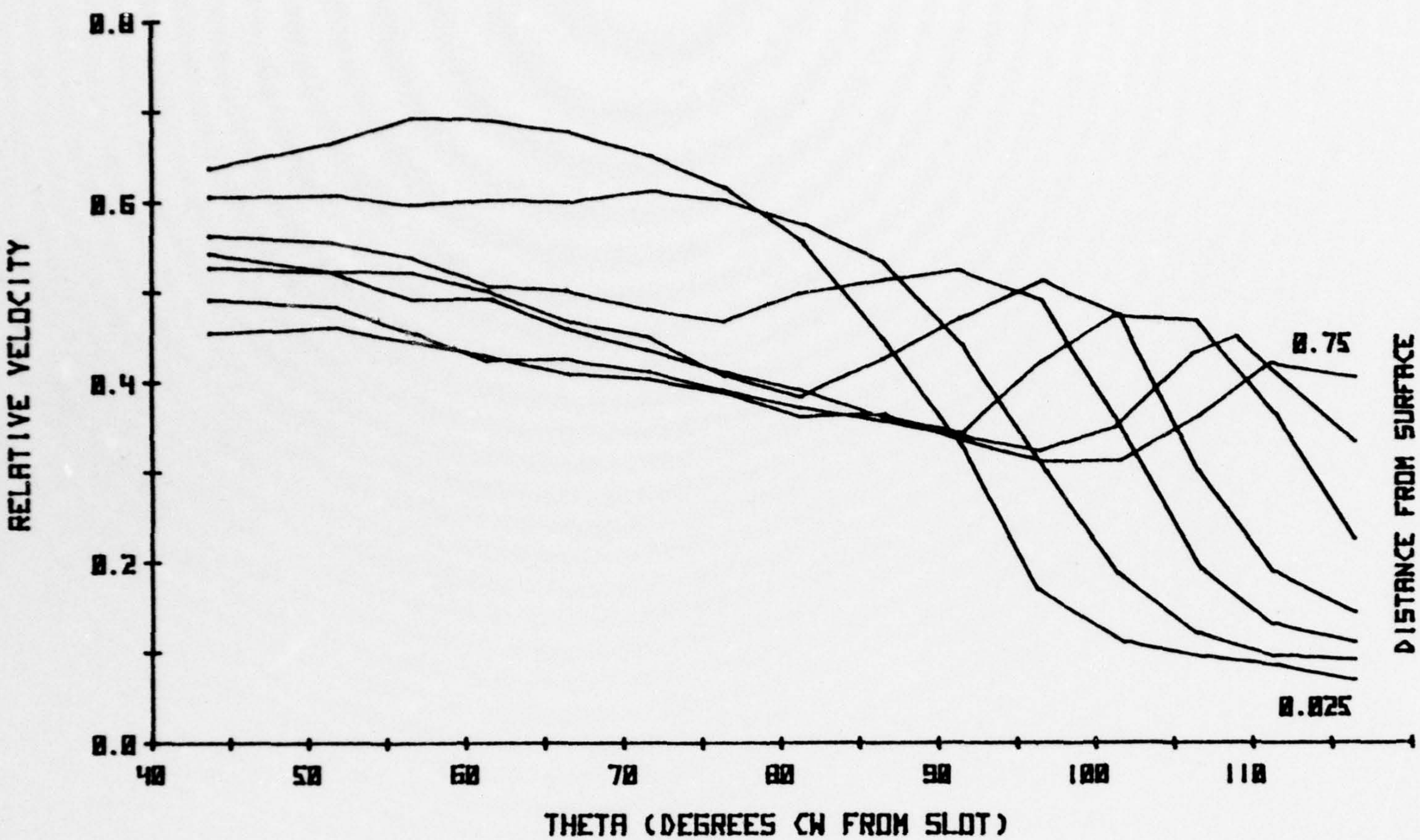

FIGURE 24

RELATIVE VELOCITY VS THETA FOR ALPHA = -5 CMU = 0.0575
0.025, 0.05, 0.1, 0.25, 0.375, 0.5, 0.75 IN. FROM SURFACE

Moreover, only a partial picture of the velocity minimum side of the wake was obtained. In order to permit mapping of the entire wake including the shear layer, the mechanism was relocated to span 79.4 to 151.4 degrees (15 degrees above the chord line to 55 degrees below it).

Figures 25 and 26 illustrate the behavior of the mean velocity in the vicinity of the near-wake. In comparing the 0.75 and 1.5-inch (surface distance) velocity profiles for $C_\mu = 0.0215$, it appeared that the velocity might be approaching a constant value for theta greater than 125 degrees. When the probe was traversed at 151.4 degrees out to 2 inches, the velocity increased less than 4 percent passing 1.75 inches and was steady from there out to 2 inches. A similar behavior was observed at higher C_μ's.

For the remainder of the surveys, the velocity data was normalized adopting the value at 151.4 degrees, 2 inches out as the freestream reference value.

From the mean velocity data there did not appear to be sufficient information to determine the location of the rear stagnation streamline. The expected maximum-minimum velocity profiles across the wake were obtained, but it was not clear whether the streamline intersected the points of minimum velocity or the midslopes between the maximums and minimums. The maximum velocity points were excluded for they yielded at 0.025 inches from the wall, streamline positions further above the chord line than theta (separation) determined from corresponding C_p data.

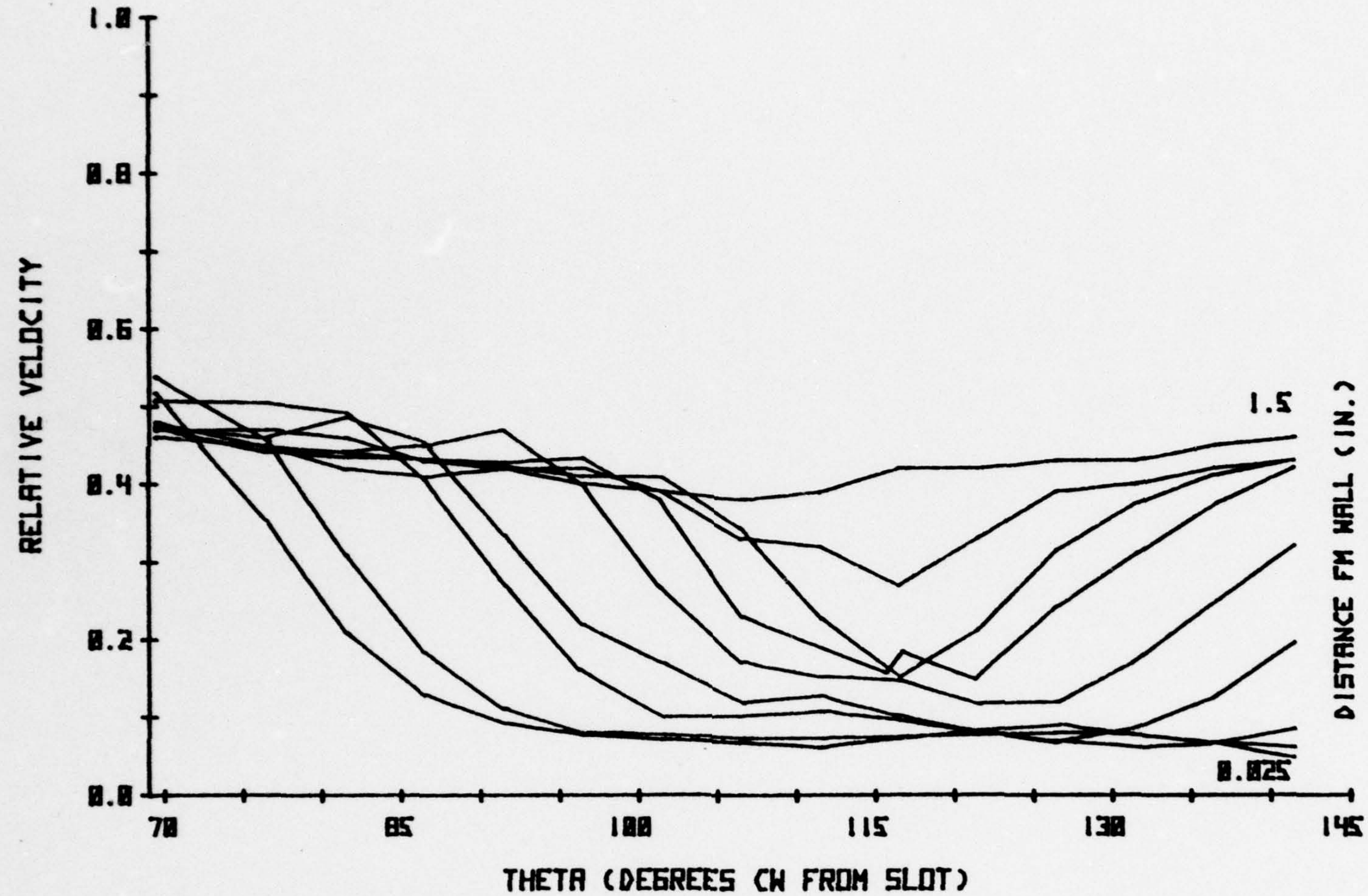

FIGURE 25

RELATIVE VELOCITY PROFILES FOR ALPHA=-5 CMU = 0.0215

AT 0.025, 0.05, 0.1, 0.15, 0.25, 0.375, 0.5, 0.75, 1.5 IN. FM WALL

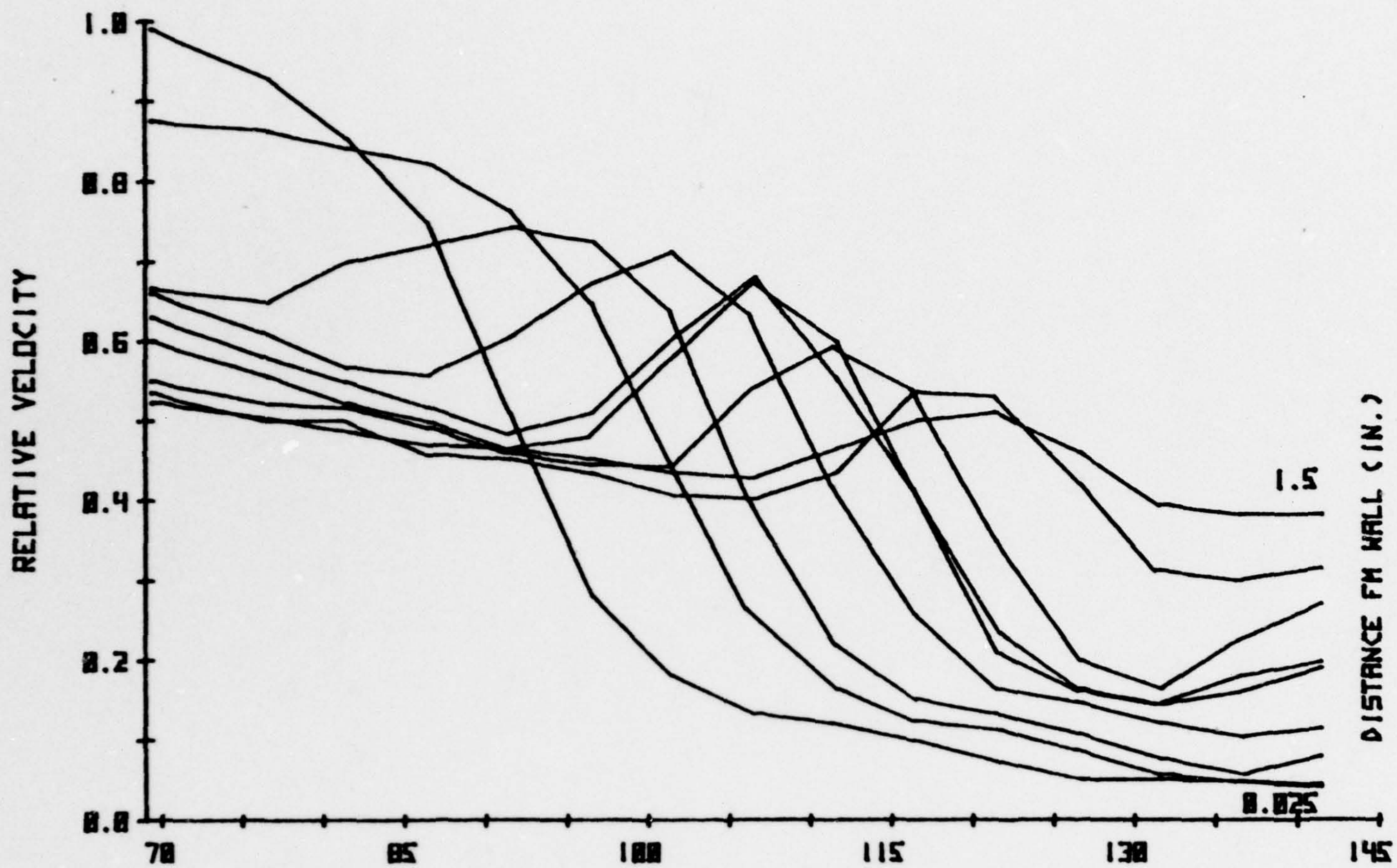

FIGURE 26

RELATIVE VELOCITY PROFILES FOR ALPHA=-5 CMU= 0.0617
AT 0.025, 0.05, 0.1, 0.15, 0.25, 0.375, 0.5, 0.75, 1.5 IN. FM WALL

As illustrated in Fig. 27, there was a wide region close to the surface where the flow velocities were low and nearly constant. The point of minimum velocity was defined as the point of maximum change in the shear stress in this region.

When turbulence intensity data were compared to corresponding C_p data as in Fig. 28, the point of peak turbulence at 0.025 inches from the wall was within 2 degrees of the point of separation, and corresponded to the midslope point, Fig. 27. The minimum velocity points were 5 to 10 degrees beyond the midslope points and thus are not indicative of the point of separation.

Figure 29 depicts the stagnation streamlines based on the "midslope" criteria for representative values of C_μ. As C_μ increased the streamlines appeared to become unsteady, and the detachment angle increased.

Figure 30 is a composite picture of the near-wake constructed from data illustrated in Fig. 27. Figure 31 shows velocity profiles in the boundary layers of the trailing edge for various angular position from the chord line. As discussed by Collins and Simpson [37], it is not possible to tell the local flow direction from the mean felocity data. The inflection point apparent at 2.5 degrees may well indicate a flow reversal. The turbulence intensity data for the case presented in Fig. 32 suggest separation occurred between 5 and 7.5 degrees above the chord plane but the precise point of separation is not indicated.

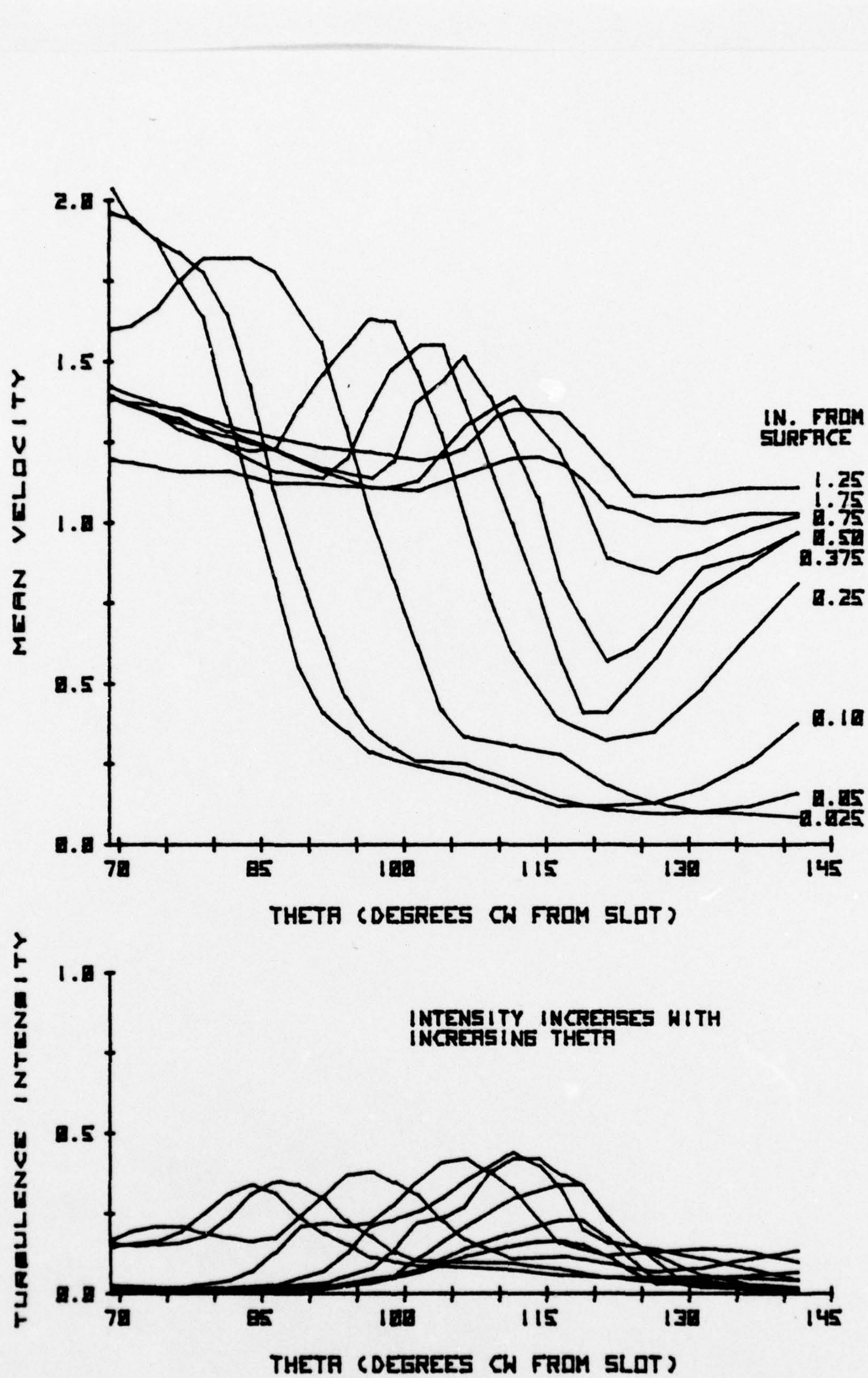

FIGURE 27

NONDIMENSIONAL MEAN VELOCITY AND TURBULENCE INTENSITY PROFILES VS THETA FOR ALPHA=-5 CMU= 0.0451, 0.025 TO 1.75 IN. FROM SURFACE

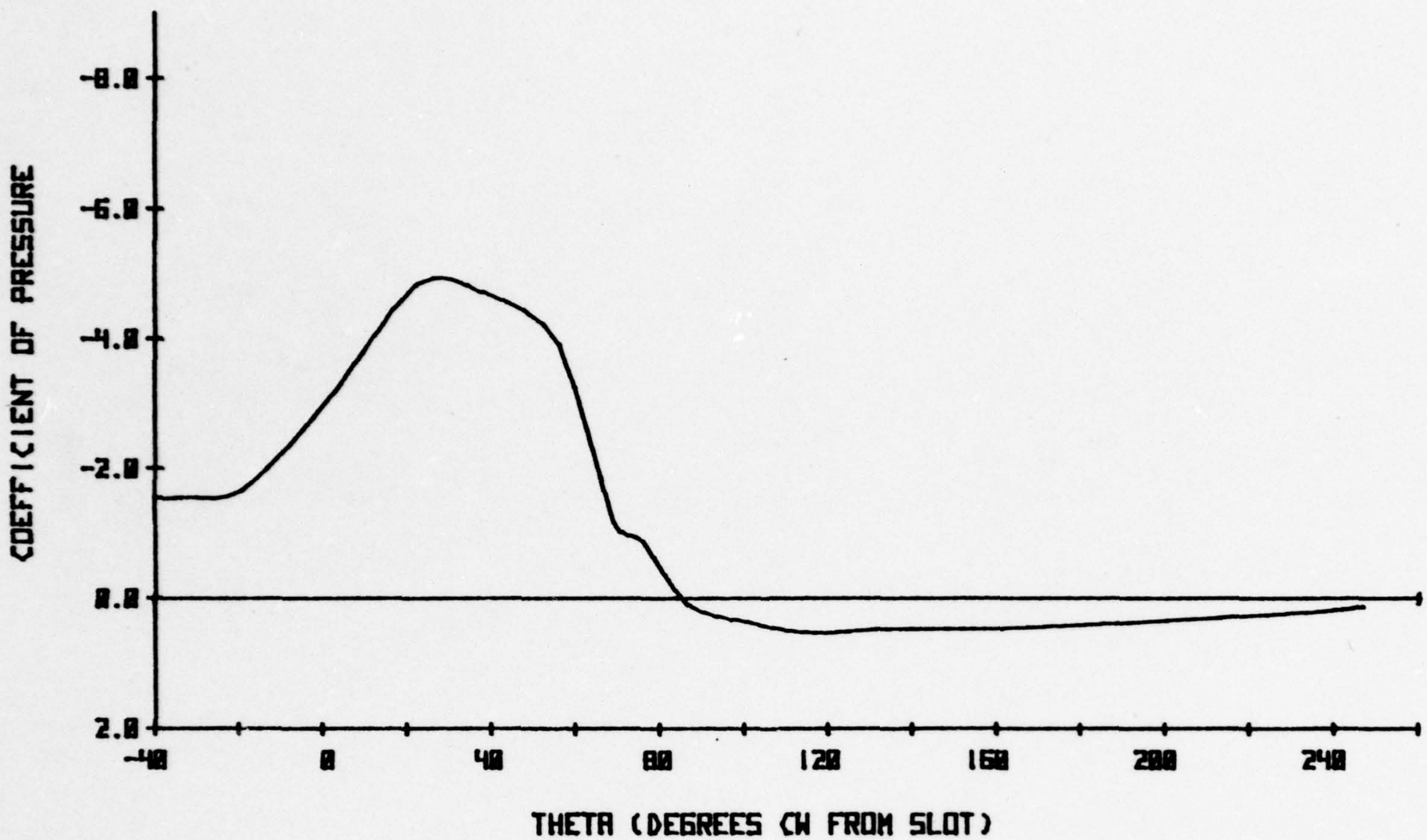

FIGURE 28

COEFFICIENT OF PRESSURE VS THETA FOR ALPHA = -5 CMU = 0.0451

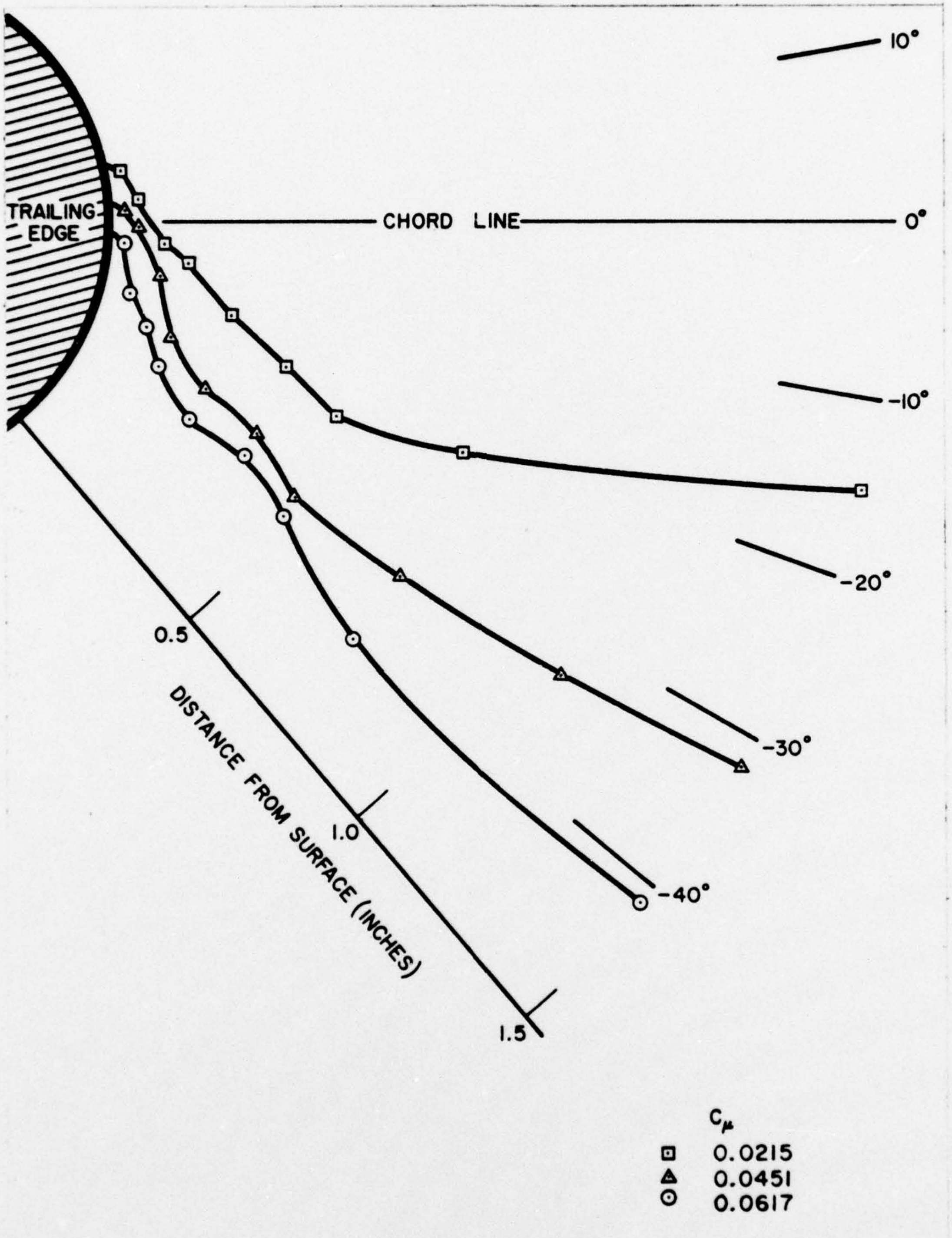

FIGURE 29

NEAR-WAKE STAGNATION STREAMLINES DETERMINED FROM MID-SLOPE METHOD FOR VARIOUS BLOWING COEFFICIENTS WITH $\alpha = -5°$

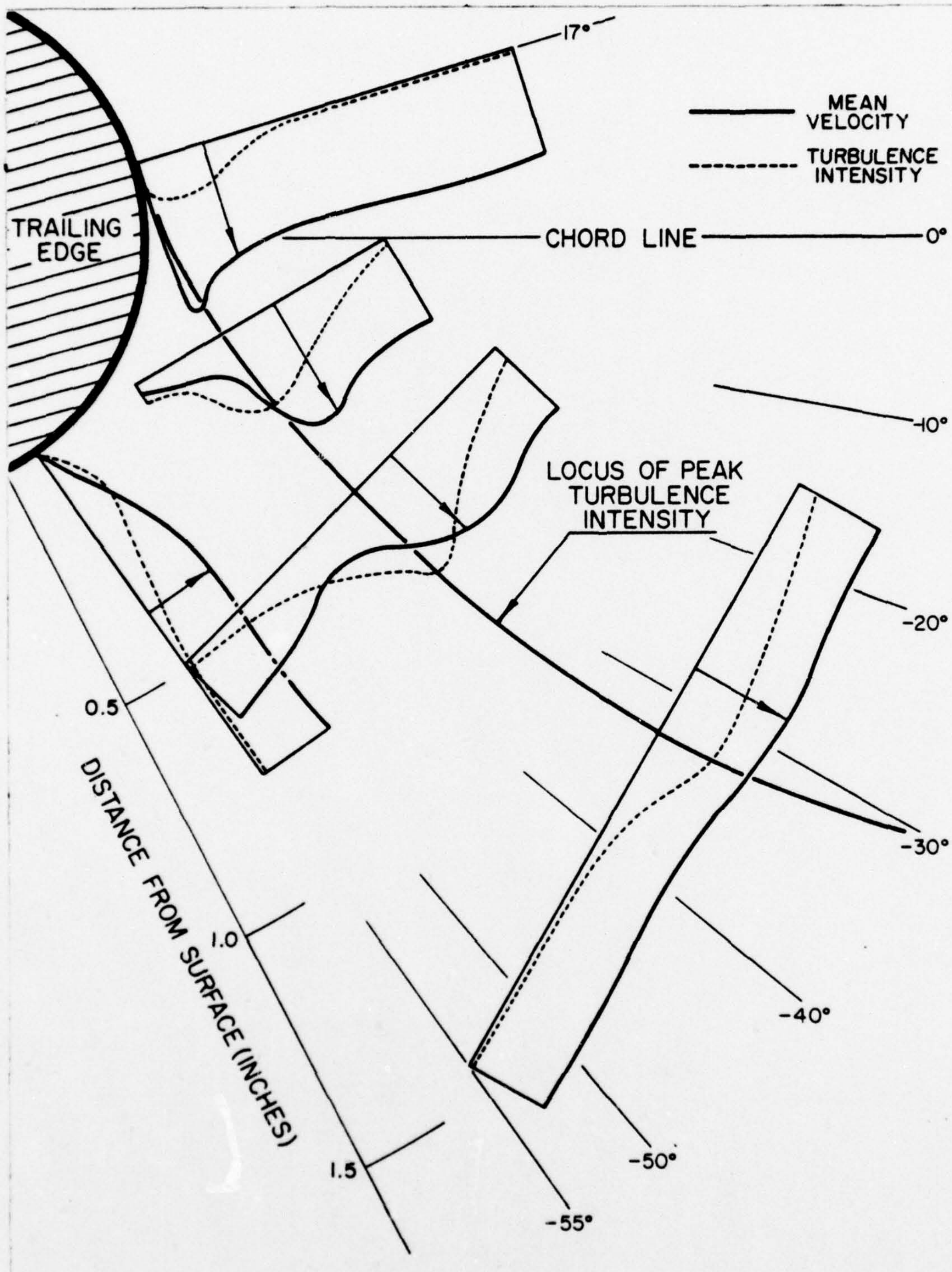

FIGURE 30

REPRESENTATIVE VELOCITY PROFILES AND TURBULENCE INTENSITY IN NEAR-WAKE FOR $\alpha = -5$, $C_\mu = 0.0451$

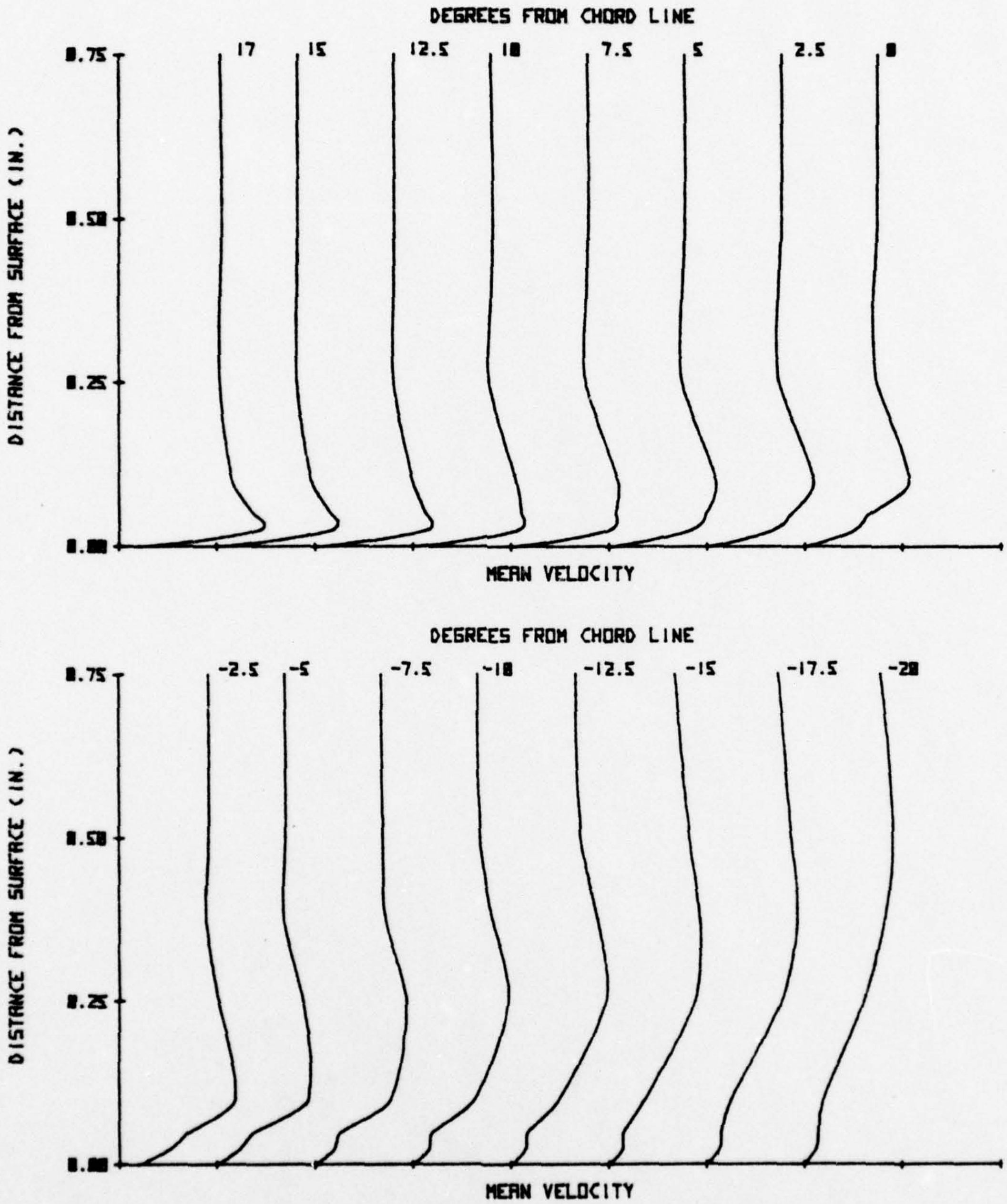

FIGURE 31

BOUNDARY LAYER PROFILES OVER THE TRAILING EDGE AS A FUNCTION OF ANGULAR POSITION FOR ALPHA = −5 C_{μ} = 0.0451

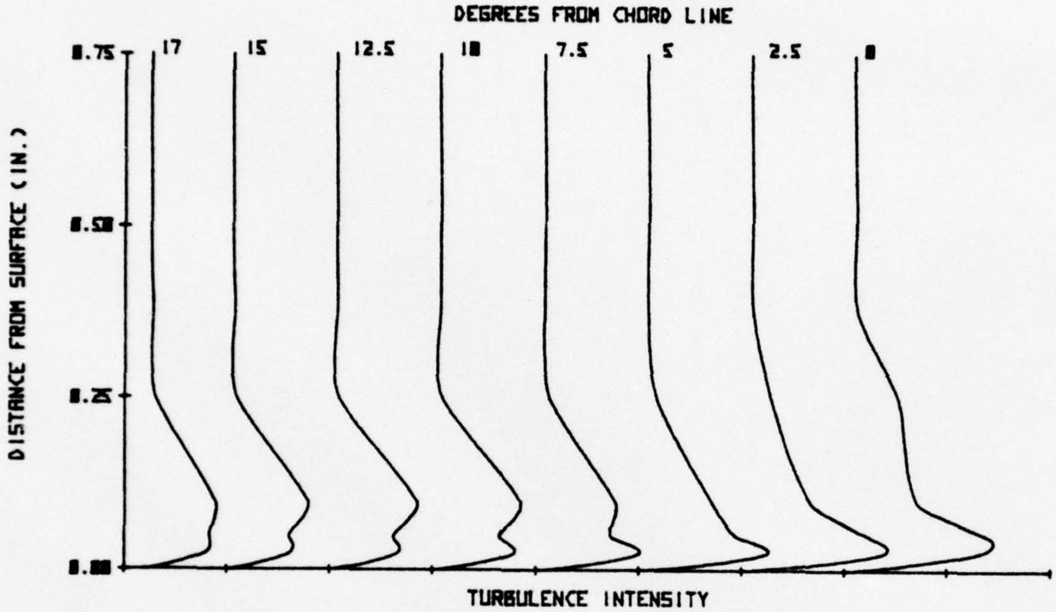

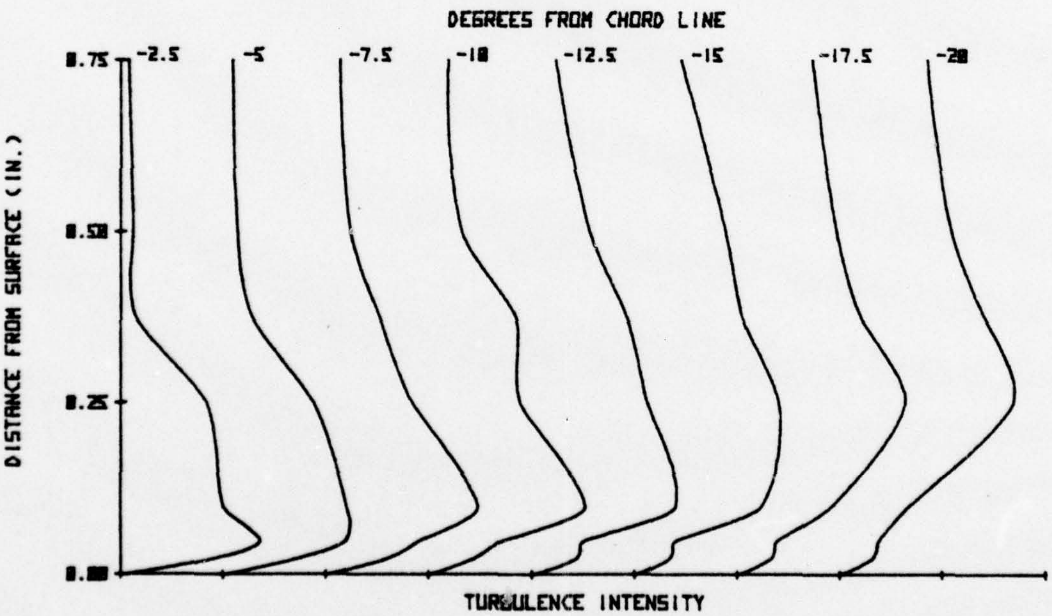

FIGURE 32

COMPARISON OF TURBULENCE INTENSITY VS DISTANCE FROM SURFACE AS A FUNCTION OF ANGULAR POSITION FOR ALPHA = -5 CMU = 0.0451

Figure 33 depicts the location of separation based on the point of peak turbulence intensity at 0.025 inches from the surface, as a function of C_μ. The corresponding relationship of separation point location compared with lift coefficient is plotted in Fig. 34. The flow anomaly apparent on both graphs was accompanied by a sinusoidal waveform superimposed on the turbulent signal as indicated in Fig. 35. No fluctuation was observable in the plenum.

Englar [9] indicated that shed vorticity occurs at the wall-airfoil boundary layer interface over the aft portion of the airfoil in two-dimensional CC testing. This three-dimensional effect appreciably influences the flow close to the wall. As noted in Section V.B.3, the wake traversing mechanism caused reduced lift augmentation and influenced the spanwise pressure distribution up to 6 inches from the wall at lower blowing rates (below 0.035). Thus the wake traversing mechanism appeared to increase vortex shedding. However, examination of the spanwise pressure coefficient data vs. C_μ provided no insight as to the specific cause of the sinusoidal waveform or the flow anomaly.

With the occurrence of the flow anomaly, there was not sufficient information to formulate a mathematical correlation between the separation point and the lift and blowing coefficients.

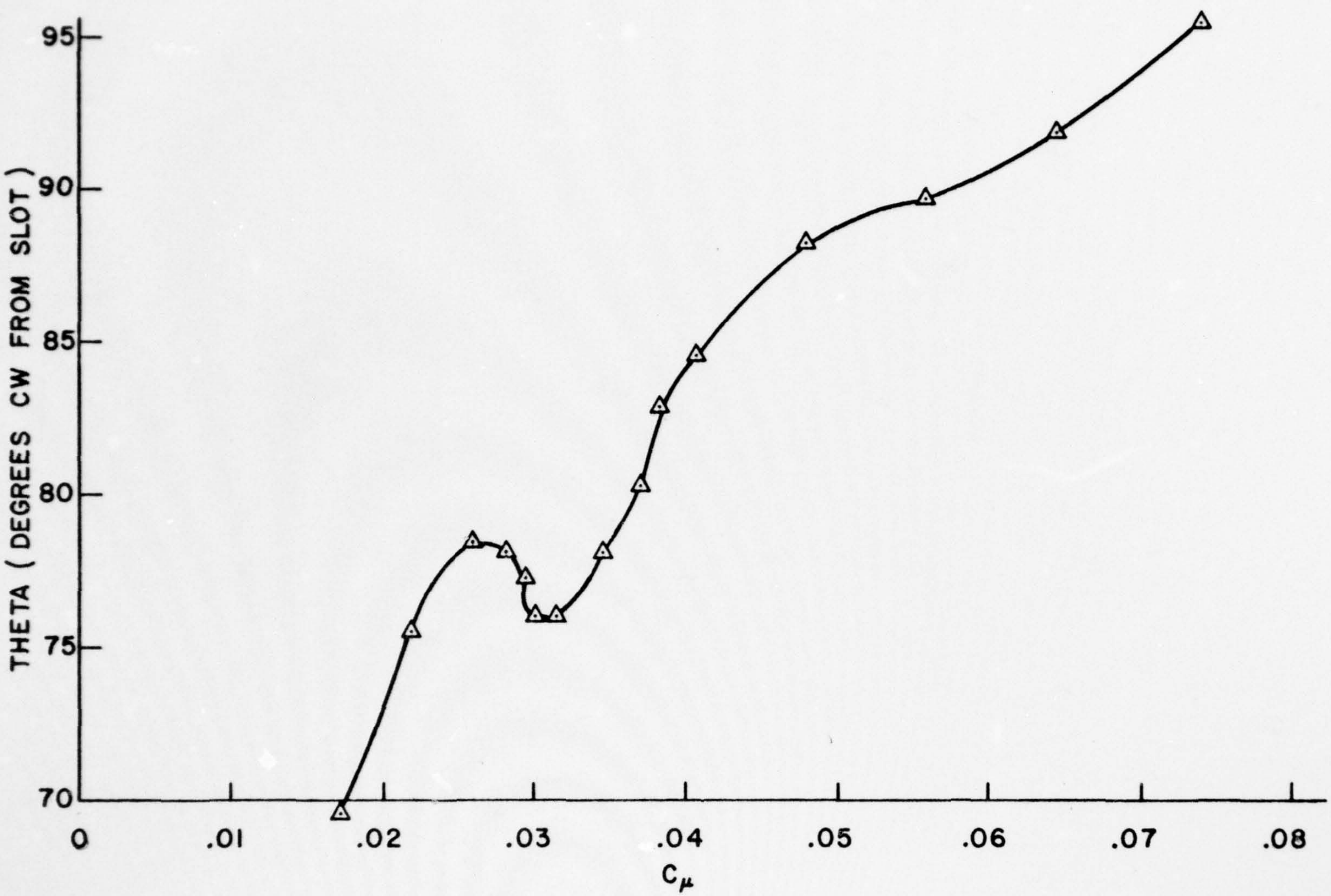

FIGURE 33

SEPARATION POINT IN DEGREES FROM SLOT VS BLOWING COEFFICIENT

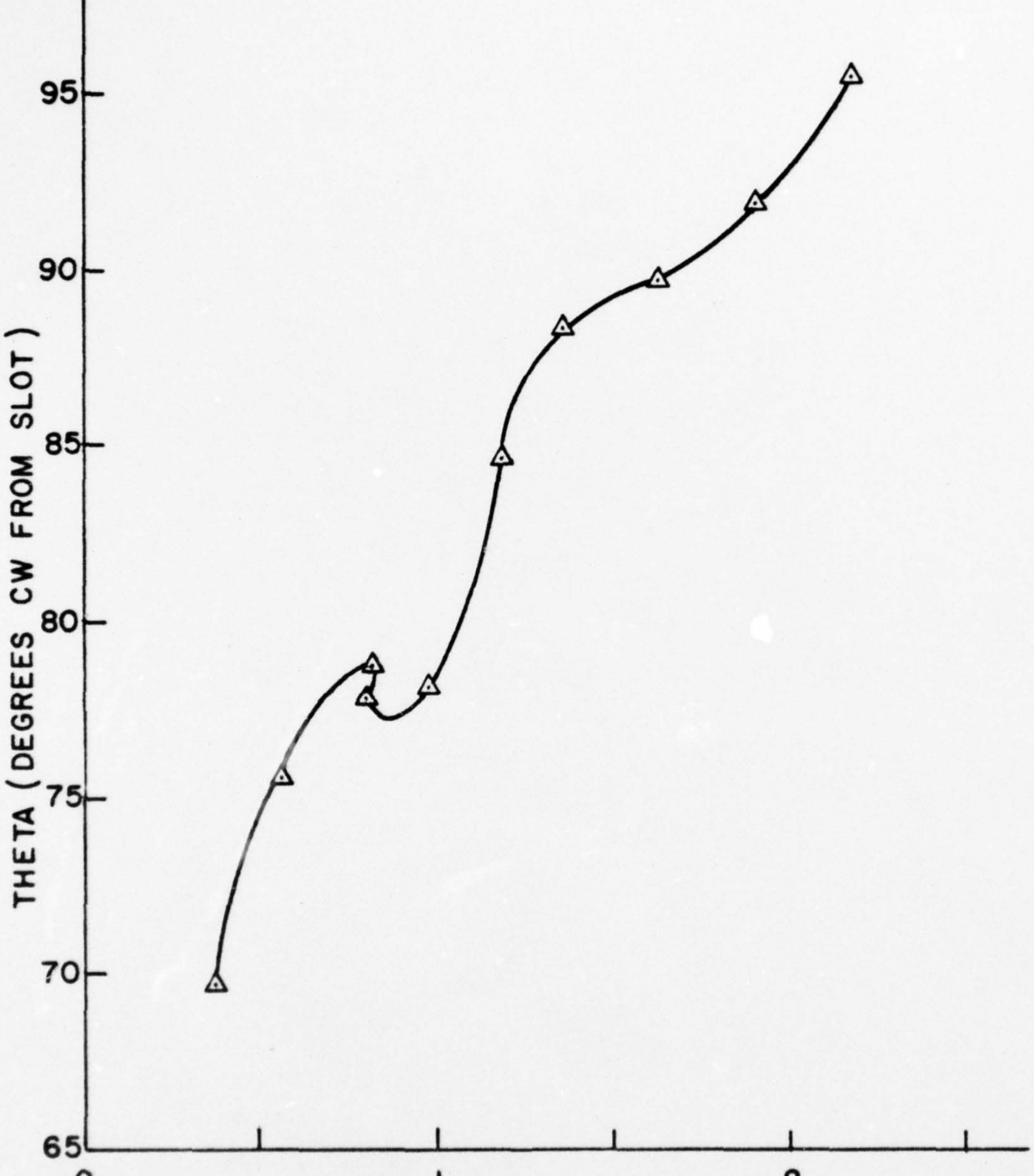

FIGURE 34

SEPARATION POINT IN DEGREES
FROM SLOT VS LIFT COEFFICIENT

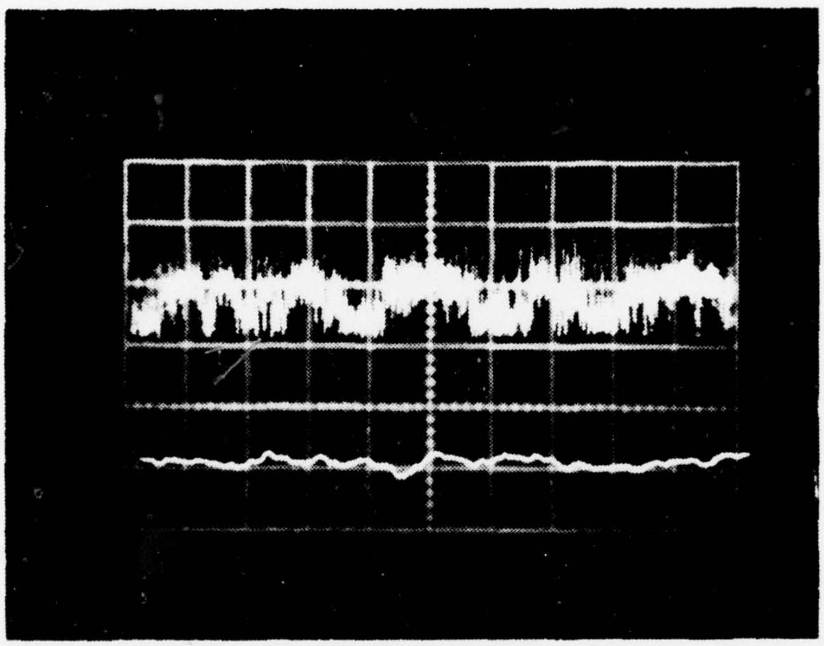

FIGURE 35

Wake Hotwire vs Plenum Pressure for $C_\mu = 0.0258$ (10 msec/cm; Top: Hotwire 76° from slot, 0.025" from wall, 1 v/cm; Bottom: Plenum Pressure, 0.1 v/cm)

C. TESTS WITH OSCILLATING INJECTION

The objective of this portion of the investigation was to assess the feasibility of employing a CC airfoil with a modulated blowing coefficient of the form:

$$C_\mu(t) = \overline{C}_\mu(1 + \varepsilon \sin \omega t)$$

for ε of the order of unity.

The range of frequencies applicable to helicopter aerodynamics when scaled to the model is roughly from 3 to 10 Hz. Below about 5 Hz data acquisition by analog readout becomes a problem because of instrument limitations. Moreover, the quality of the mass flow rate waveform decays with decreasing frequency. Thus 9 Hz was the minimum frequency available with an acceptable waveform.

1. Pressure Wave Propagation

The first portion of these tests addressed the question of whether or not the modulated blowing created a pressure wave which propagated around the airfoil. To determine this the plenum pressure signal and that from taps in the region of the forward stagnation point, and the upper and lower midchord points were examined on a dual beam oscilloscope. Figures 36 and 37 illustrate typical waveforms observed. Note the plenum pressure appears to lead the forward stagnation signal by 180 degrees.

As shown in Fig. 38 the pressure perturbation over the lower surface of the airfoil was obscured by tunnel noise.

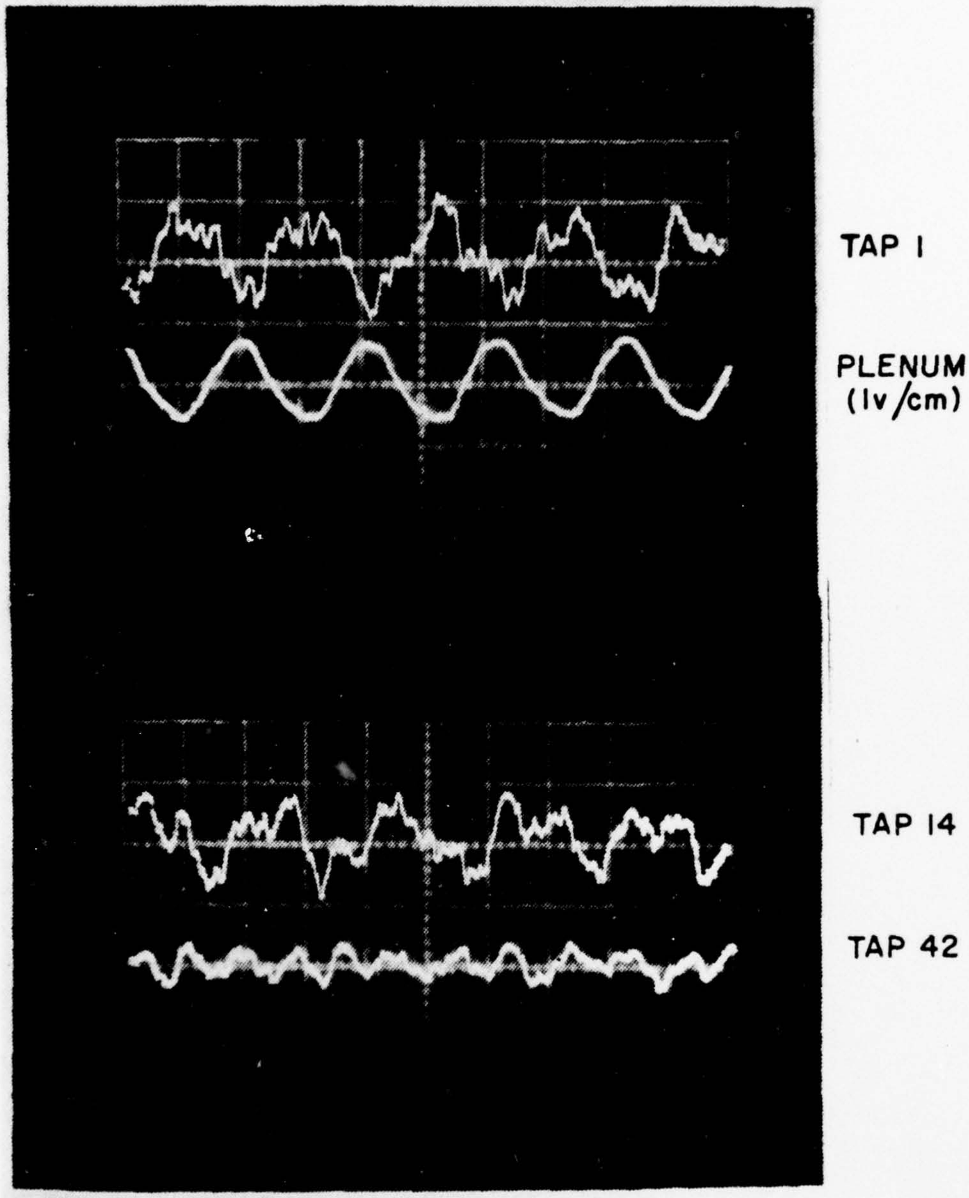

FIGURE 36

COMPARISON OF PRESSURE WAVEFORMS FOR
$C_\mu = 0.0854$, $\epsilon = 27.4\%$, $f = 9$ Hz
(50 msec/cm ; 0.1 v/cm)

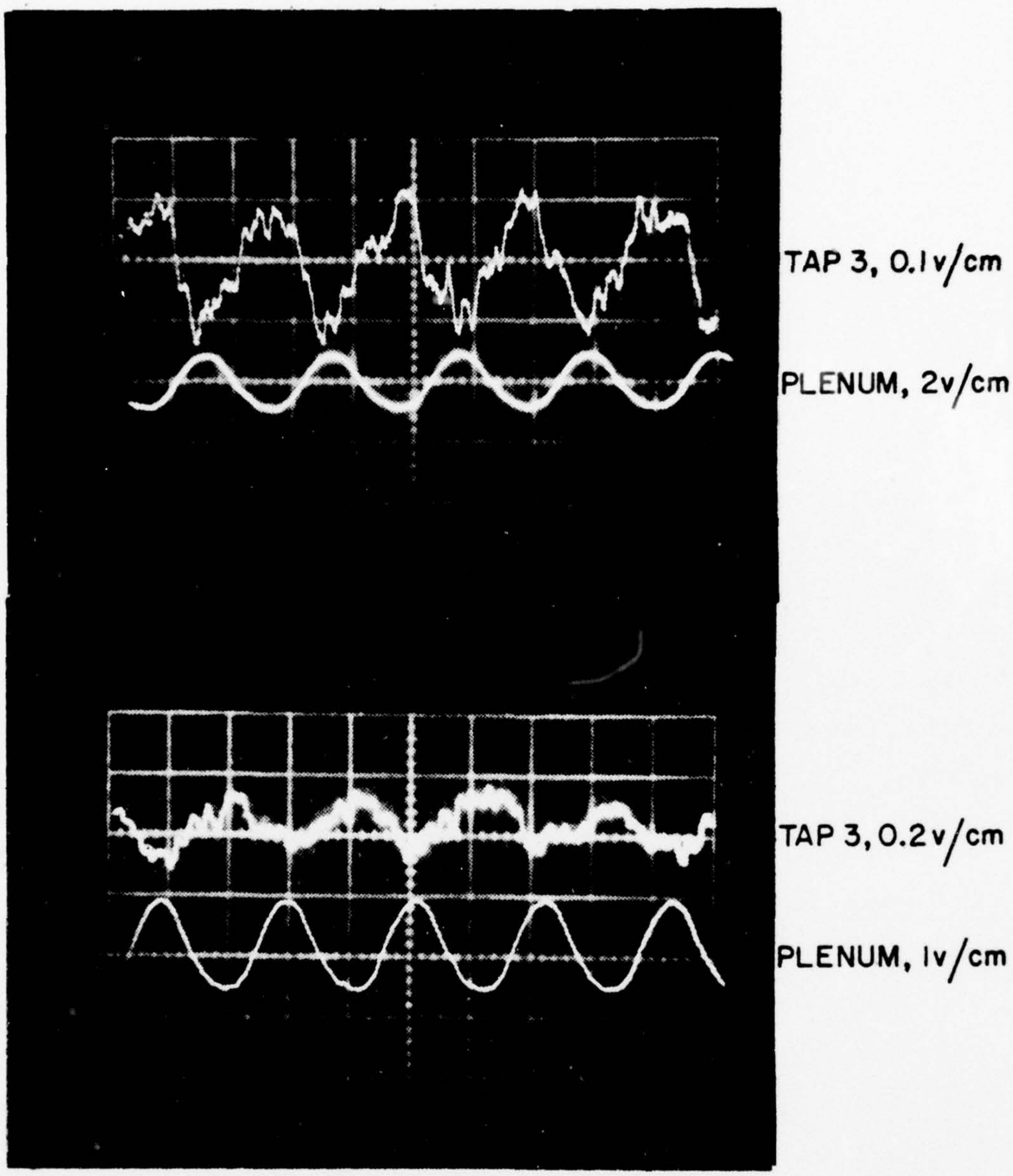

FIGURE 37

COMPARISON OF PRESSURE WAVEFORMS FOR $C_\mu = 0.0457$, $\epsilon = 47.4\%$ AND $C_\mu = 0.0645$, $\epsilon = 30.2\%$ FOR $f = 9$ Hz (50 msec/cm)

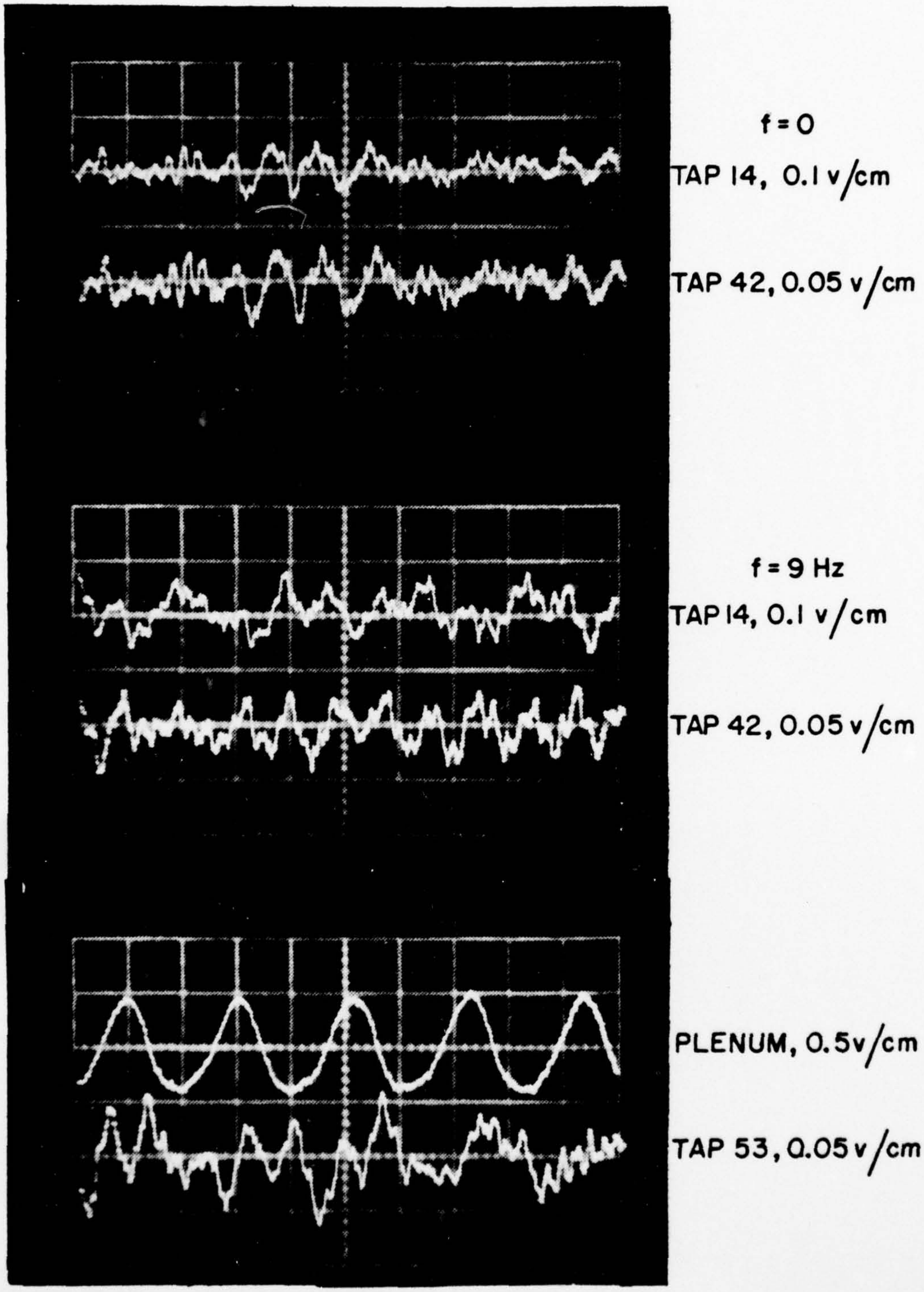

FIGURE 38

COMPARISON OF PRESSURE WAVEFORMS FOR $C_\mu = 0.045$ WITH $\epsilon = 30\%$, f = 9 Hz vs f = 0 (50 msec/cm)

Although the DC signals were filtered and steady RMS signals were subtracted from the observed unsteady data, it has not been determined what effect this noise has in wave propagation over the airfoil. However, what is suggested is that the momentum flux occurring at the slot induces a fluctuating rate of entrainment, and that the primary signal propagation is over the upper surface of the airfoil.

From the previous three figures, it is apparent that for relatively large values of ε the pressure fluctuation does propagate over the airfoil, but with substantial attenuation. What this means in terms of lift augmentation is illustrated in Table III. No conclusive trends concerning lift augmentation were observed. In only 3 of the 5 cases where RMS data were taken did $\langle C_L^2 \rangle^{1/2} + \overline{C}_L \simeq C_{L\ STEADY}$. The associated drag and moment coefficients listed in Table IV also provided no correlation with $C_\mu(t)$. The limit of ε available at $C_\mu = 0.045$ was approximately 65%, while for $C_\mu = 0.085$ only 30% could be obtained because of air supply limitations.

2. The Near-Wake in Oscillatory Blowing

The near-wake behavior of the mean velocity and turbulence intensity is illustrated in Figs. 39, 40, and 41. The slope of the mean velocity changes slightly, but the significant information appears to lie in the change in the turbulence intensity. As noted in Figs. 39 and 42 there appears to be a region of near-constant maximum intensity which becomes wider with increasing oscillation

TABLE III

BLOWING AND LIFT COEFFICIENTS FOR
STEADY FREESTREAM, OSCILLATORY BLOWING

C_μ	ε_{C_μ} (% of C_μ)	C_{LS}	C_L	$\frac{\Delta C_L}{C_{LS}}$	$\langle C_{LS}^2 \rangle^{1/2}$	$\langle C_L^2 \rangle^{1/2}$	ε_{C_L} (% of C_L)
.0441	15.4	1.2018	1.2560	4.5		.0067	0
.0438	23	1.2088	1.1836	- 2.1		.0521	5.1
.0457	47.4	1.3785	1.3103	- 4.9	.0107	.0650	4.9
.0451	65	1.3561	1.4971	10.3*			
.0645	30.2	1.837	1.990	8.3	.0090	.0536	2.65
.0856	27.4	2.7322	2.6563	- 2.8		.0765	7.6

* signal not passed through low-pass filter

TABLE IV

STEADY FLOW, 9 Hz OSCILLATORY BLOWING AERODYNAMIC CHARACTERISTICS

RUN NUMBER	TYPE	C_μ	C_L	C_D	$C_{M(C/4)}$	$C_{M(C/2)}$
51303	SB	0.0441	1.2018	.0737	-.4826	-.1849
51301	MOB		1.2560	.0725	-.4815	-.1702
51301.1	ROB		.0067	.0148	.0020	.0033
51002	SB	0.0438	1.2088	.0732	-.4884	-.1889
51003.1	MOB		1.1836	.0733	-.4795	-.1863
51003.2	ROB		.0521	.0160	-.0238	-.0112
52601	SB	0.0457	1.3785	.0598	-.5282	-.1862
52601.1	RSB		.0107	.0045	-.0039	-.0013
52603	MOB		1.3103	.0849	-.4942	-.1697
52603.1	ROB		.0650	.0392	-.0403	-.0250
51701	SB	0.0451	1.3561	.0732	-.5353	-.1990
51702	MOB		1.4971	.0511	-.5418	-.1700
52604	SB	0.0645	1.8370	.0991	-.6594	-.2040
52604.1	RSB		.0090	.0094	-.0037	-.0017
52605	MOB		1.9903	.0651	-.6801	-.1858
52605.1	ROB		.0536	.0328	-.0295	-.0169
52001	SB	0.0856	2.7322	.1077	-.8917	-.2136
52002	MOB		2.6563	.1208	-.8854	-.2265
52002.1	ROB		.0765	.0315	-.0308	-.0124

SB Steady Blowing M Mean
OB Oscillatory Blowing R RMS

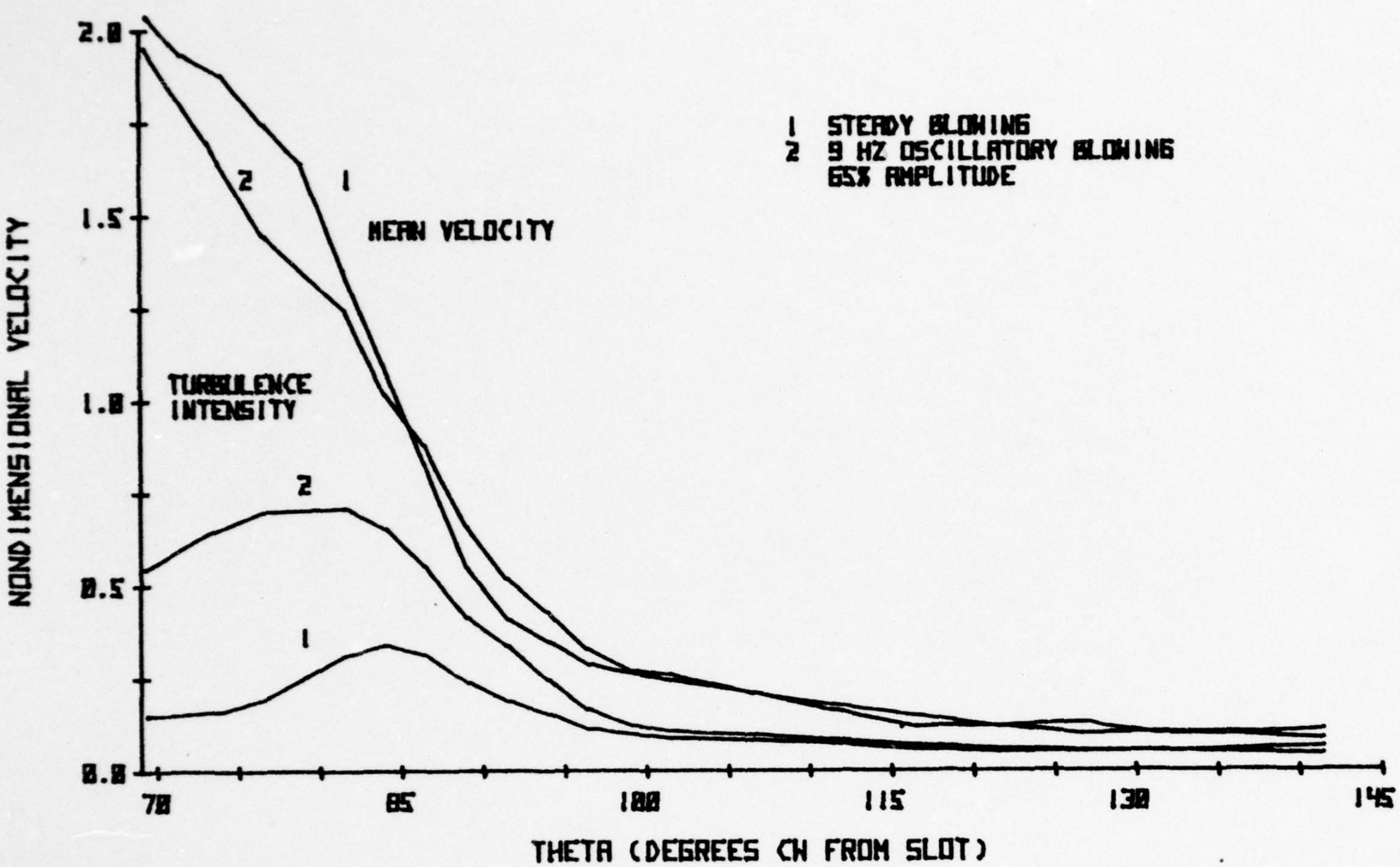

FIGURE 39

NONDIMENSIONAL MEAN VELOCITY AND TURBULENCE INTENSITY PROFILES VS THETA FOR ALPHA=-5 CMU= 0.0451 AT 0.025 IN. FROM SURFACE

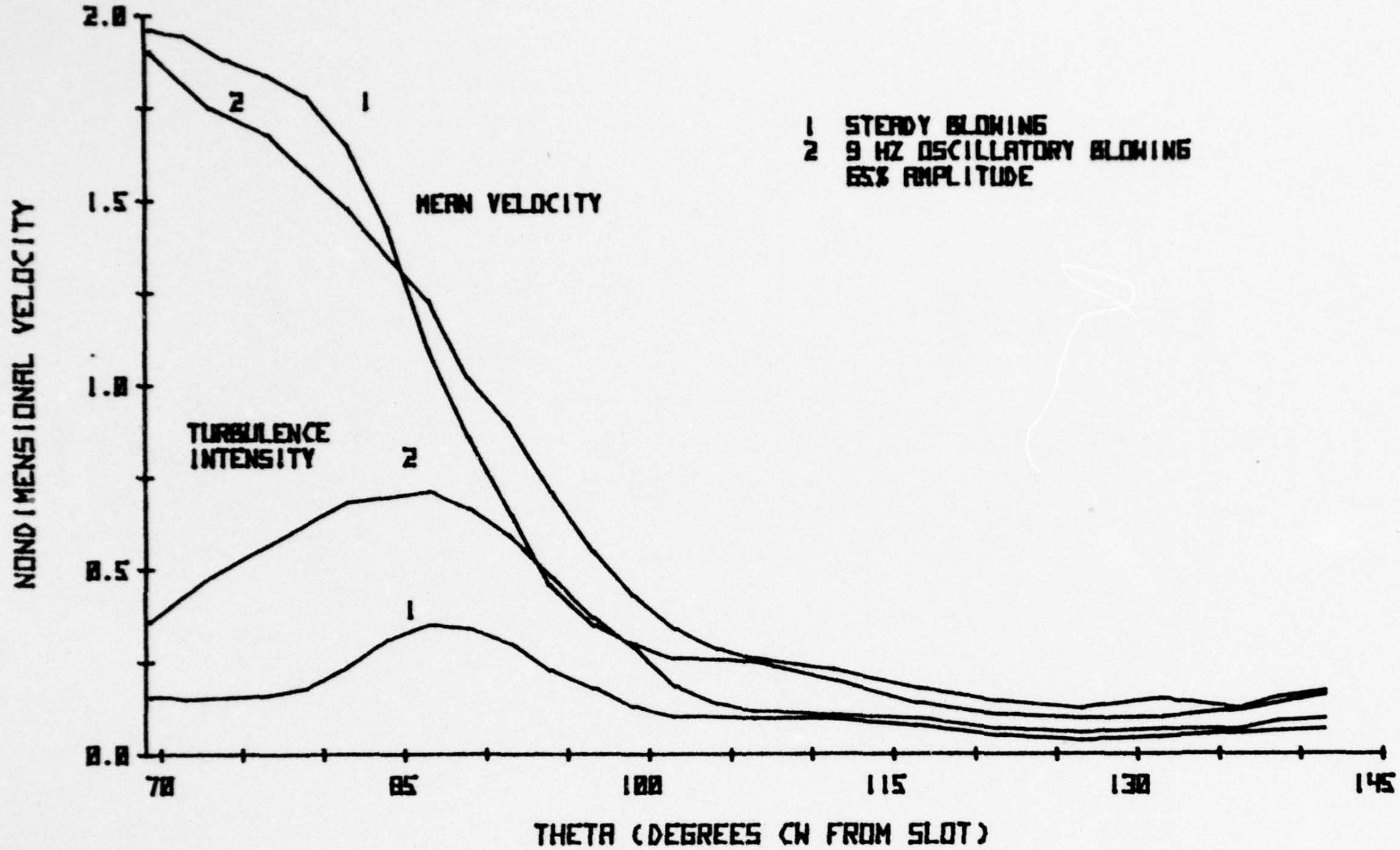

FIGURE 40

NONDIMENSIONAL MEAN VELOCITY AND TURBULENCE INTENSITY PROFILES
VS THETA FOR ALPHA=-5 CMU= 0.0451 AT 0.05 IN. FROM SURFACE

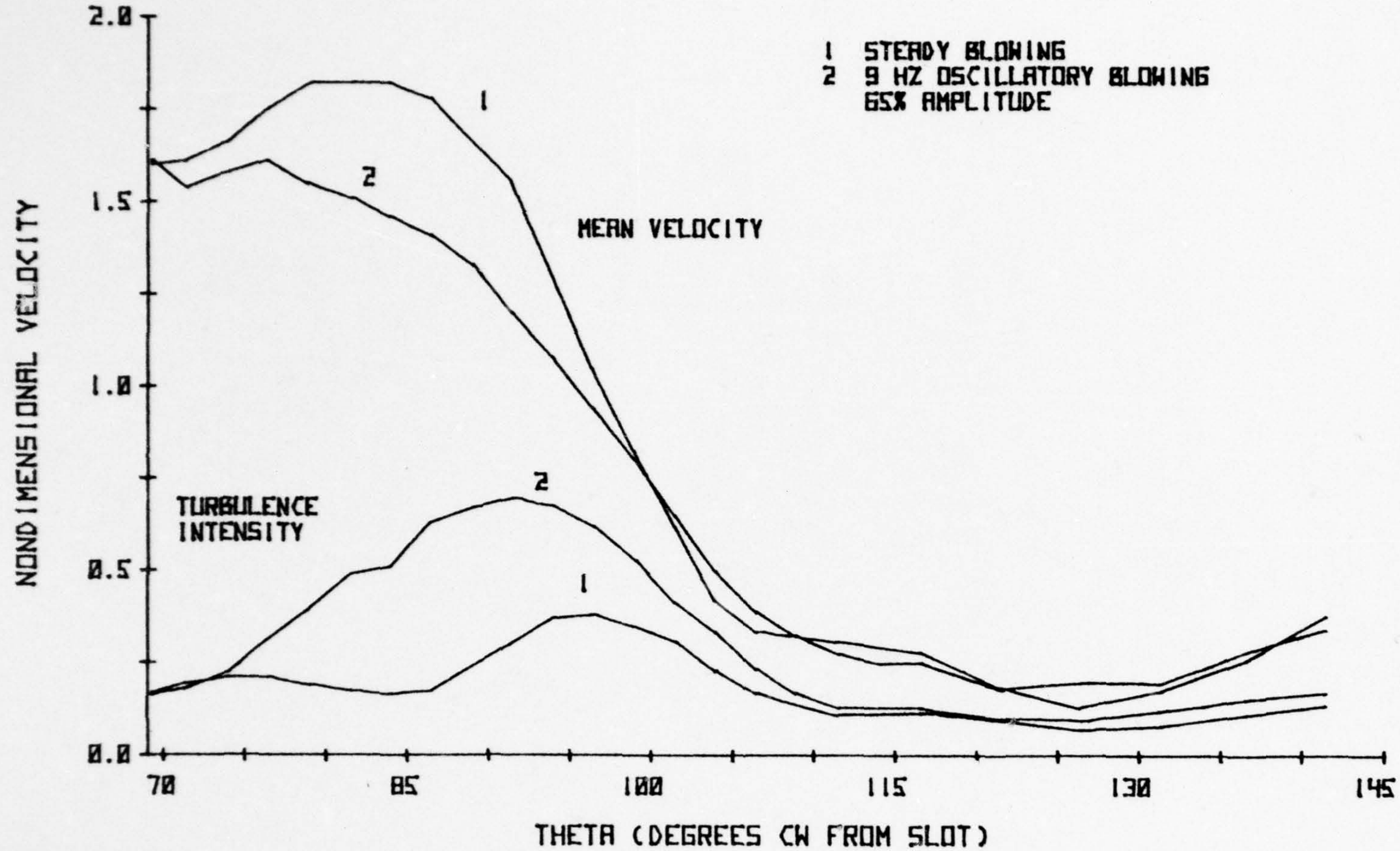

FIGURE 41

NONDIMENSIONAL MEAN VELOCITY AND TURBULENCE INTENSITY PROFILES VS THETA FOR ALPHA=-5 CMU= 0.0451 AT 0.10 IN. FROM SURFACE

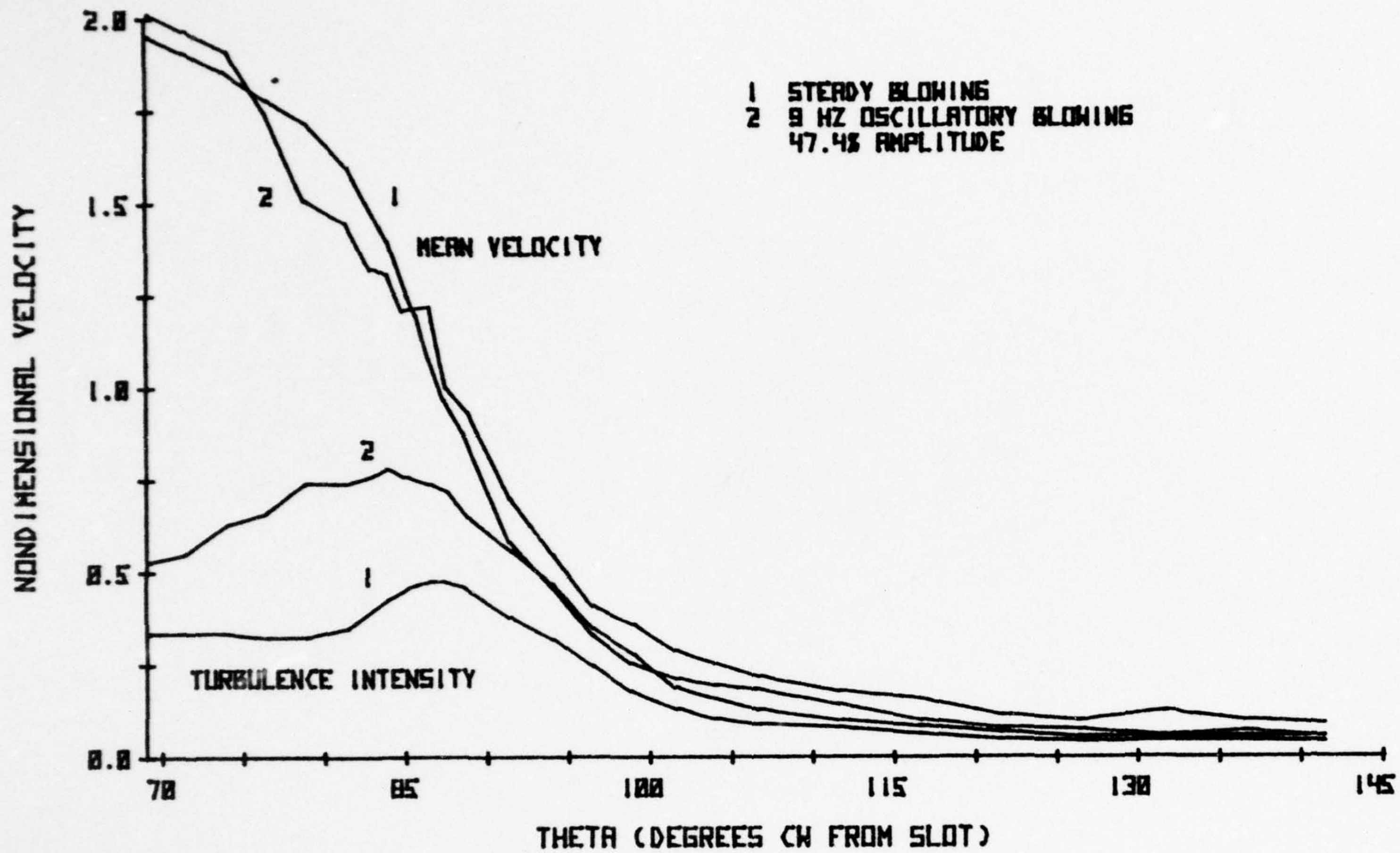

FIGURE 42

NONDIMENSIONAL MEAN VELOCITY AND TURBULENCE INTENSITY PROFILES VS THETA FOR ALPHA=-5 CMU= 0.0457 AT 0.025 IN. FROM SURFACE

amplitude. This suggests for example that the separation angle fluctuates about a mean of 83 degrees with roughly an 8-degree variation for ε = 65%, C_μ = 0.045. The unsteady variation is about 5 degrees less than one would expect for a quasi-steady flow based on steady flow measurements. For ε = 47.4% nearly the same results were obtained. Figures 43 and 44 for C_μ = 0.0645, ε = 30.2% and C_μ = 0.0853, ε = 27.4% indicate virtually no change in the mean location of the separation point. With the capability to acquire unsteady data now available at the Naval Postgraduate School, it should be possible for future investigators to correlate the instantaneous separation point to the fluctuating blowing.

Figure 45 illustrates that the pressure perturbation propagates around the trailing edge separation bubble, but with noticesable attenuation.

D. OSCILLATING FREESTREAM, STEADY BLOWING TEST

With the 3-inch blades rotating at 9 Hz, an amplitude ratio of 10.9 percent of the freestream was obtained. As illustrated in Fig. 46, the pressure signal at tap 1 was considerably cleaner than the signals observed during oscillatory blowing. Also illustrated is the fact that an oscillation in the freestream imposed an oscillation in the plenum of substantial amplitude.

Figure 47 indicates there is little change induced in the wake turbulence intensity by the oscillating freestream and no perceptible separation point oscillation. The influence

AD-A050 025 NAVAL POSTGRADUATE SCHOOL MONTEREY CALIF F/G 20/4
UNSTEADY SURFACE PRESSURE AND NEAR-WAKE HOTWIRE MEASUREMENTS OF--ETC(U)
SEP 77 K A KAIL

UNCLASSIFIED NL

2 OF 2
AD
A050025

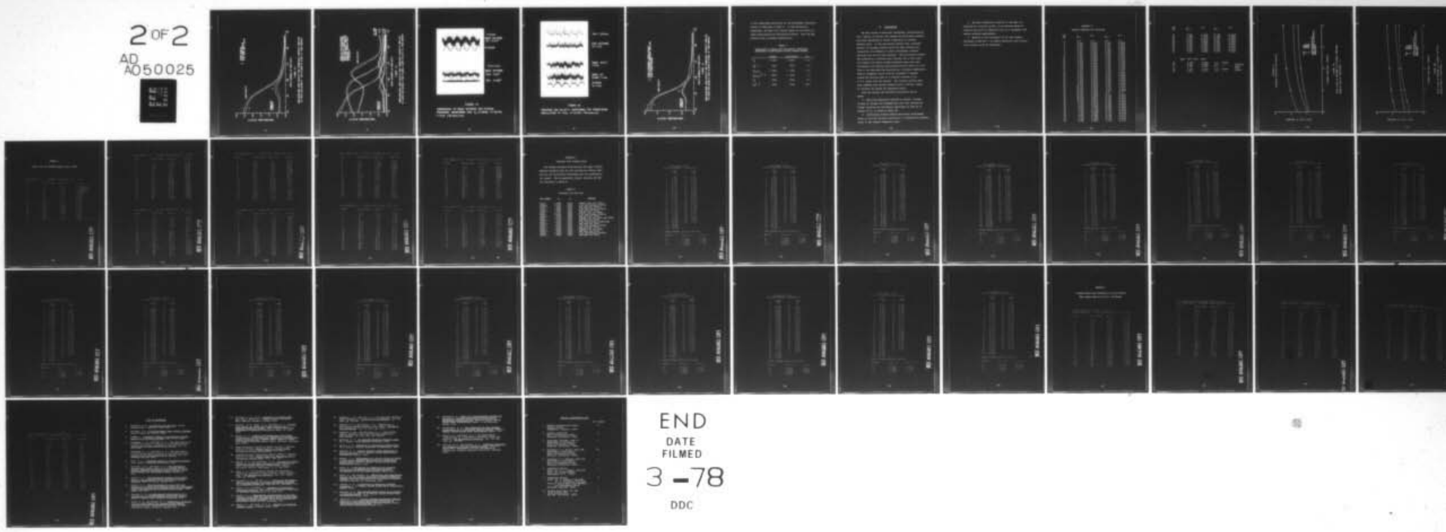

END
DATE
FILMED
3-78
DDC

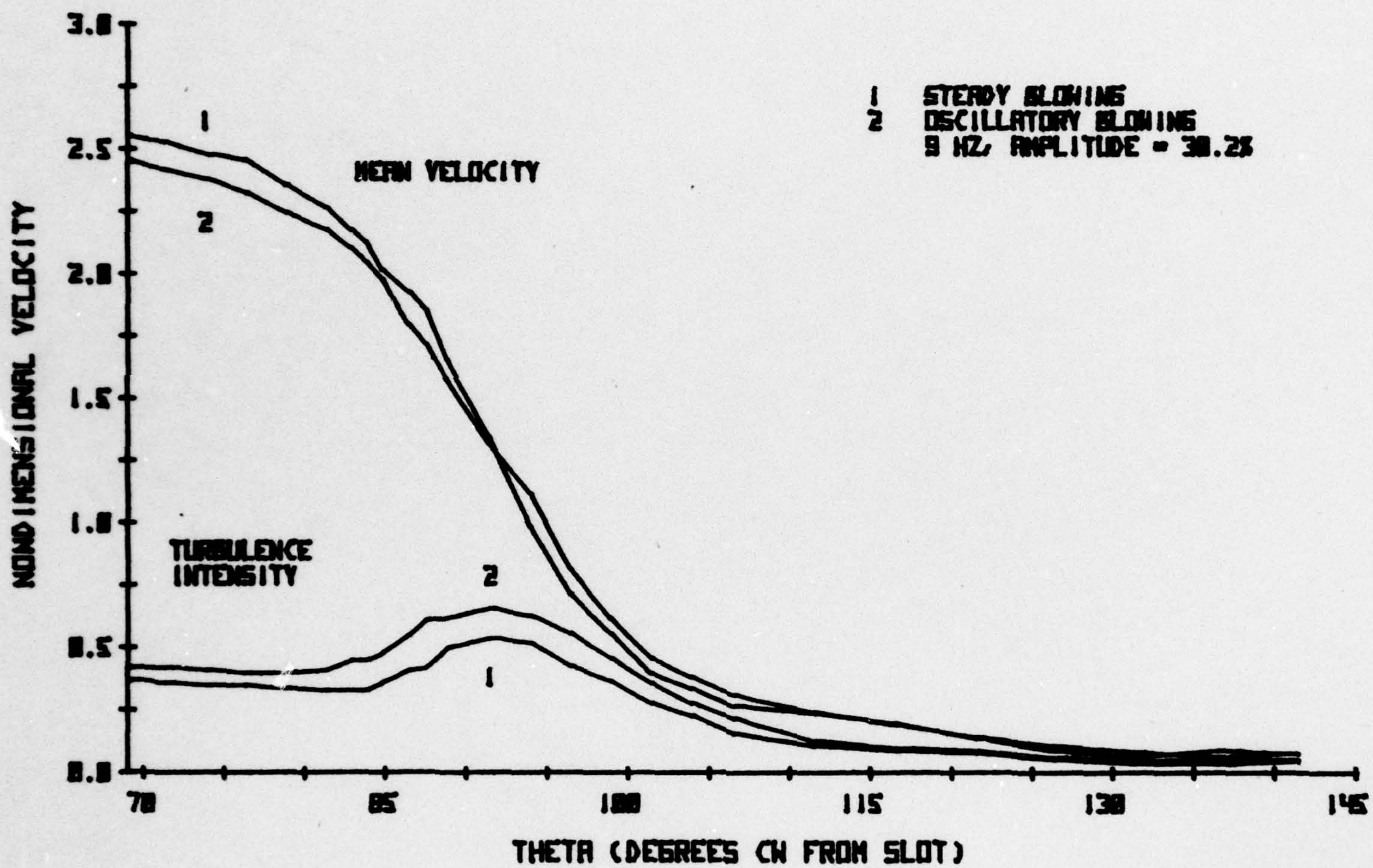

FIGURE 43

NONDIMENSIONAL MEAN VELOCITY AND TURBULENCE INTENSITY PROFILES VS THETA FOR ALPHA=-5 CMU= 0.0645 AT 0.025 IN. FROM SURFACE

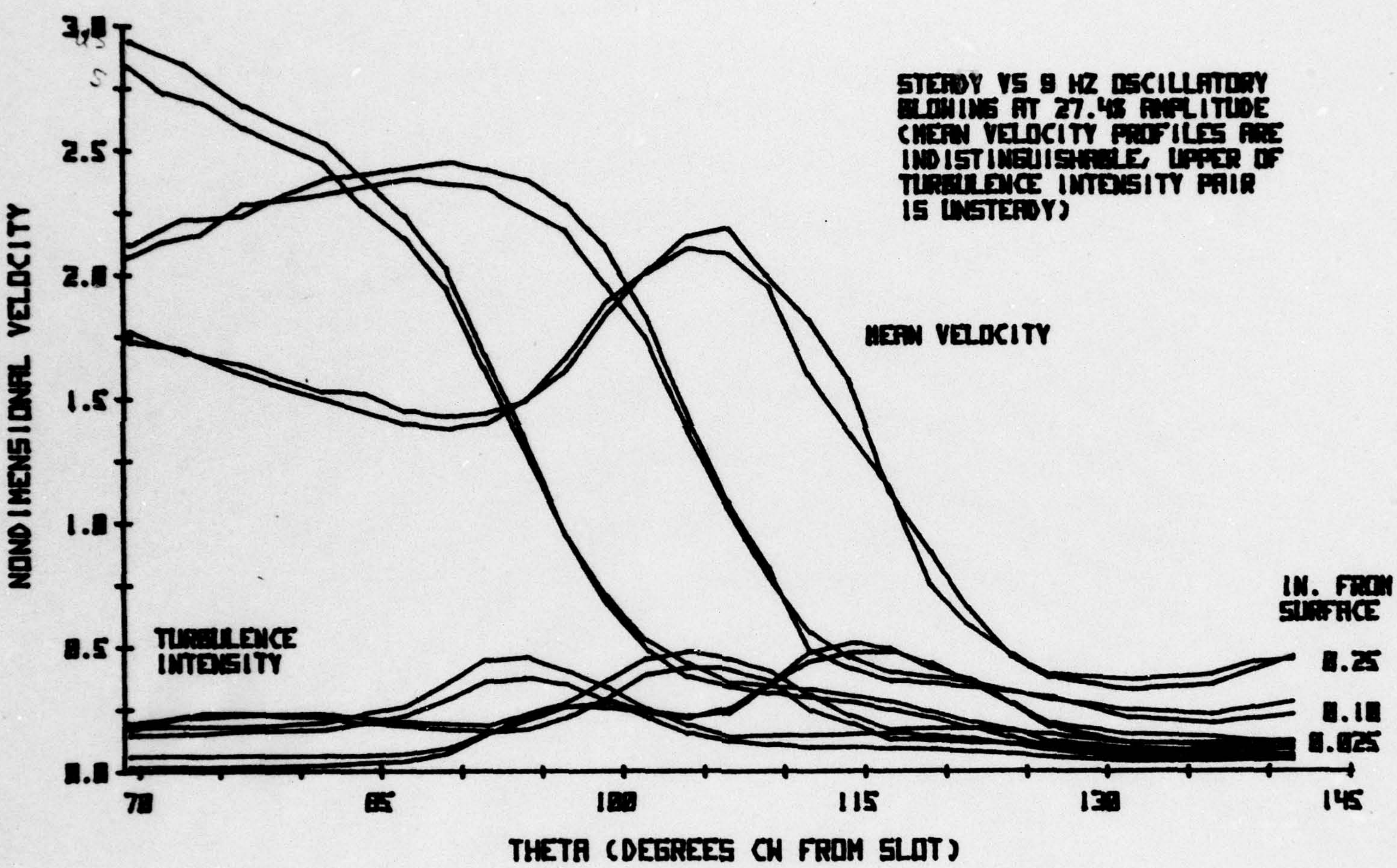

FIGURE 44

NONDIMENSIONAL MEAN VELOCITY AND TURBULENCE INTENSITY PROFILES VS THETA FOR ALPHA=-5 CMU= 0.0853, 0.025 TO 0.25 IN. FROM SURFACE

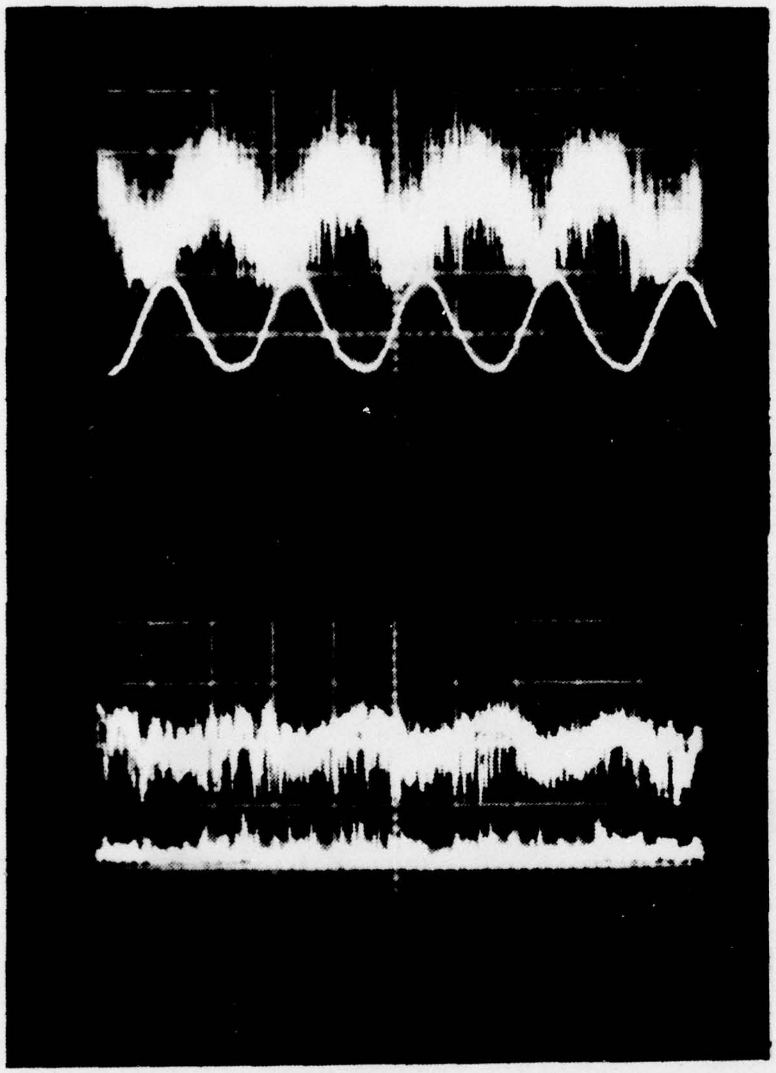

(1 v/cm)
WAKE HOTWIRE
-5°, 0.25"
PLENUM

(0.5 v/cm)
WAKE HOTWIRE
-55°, 0.25"
-55°, 0.025"

FIGURE 45

COMPARISON OF WAKE HOTWIRE AND PLENUM PRESSURE WAVEFORMS FOR $C_{\mu} = 0.0645$, $\epsilon = 30.2\%$, $f = 9$ Hz (50 msec/cm)

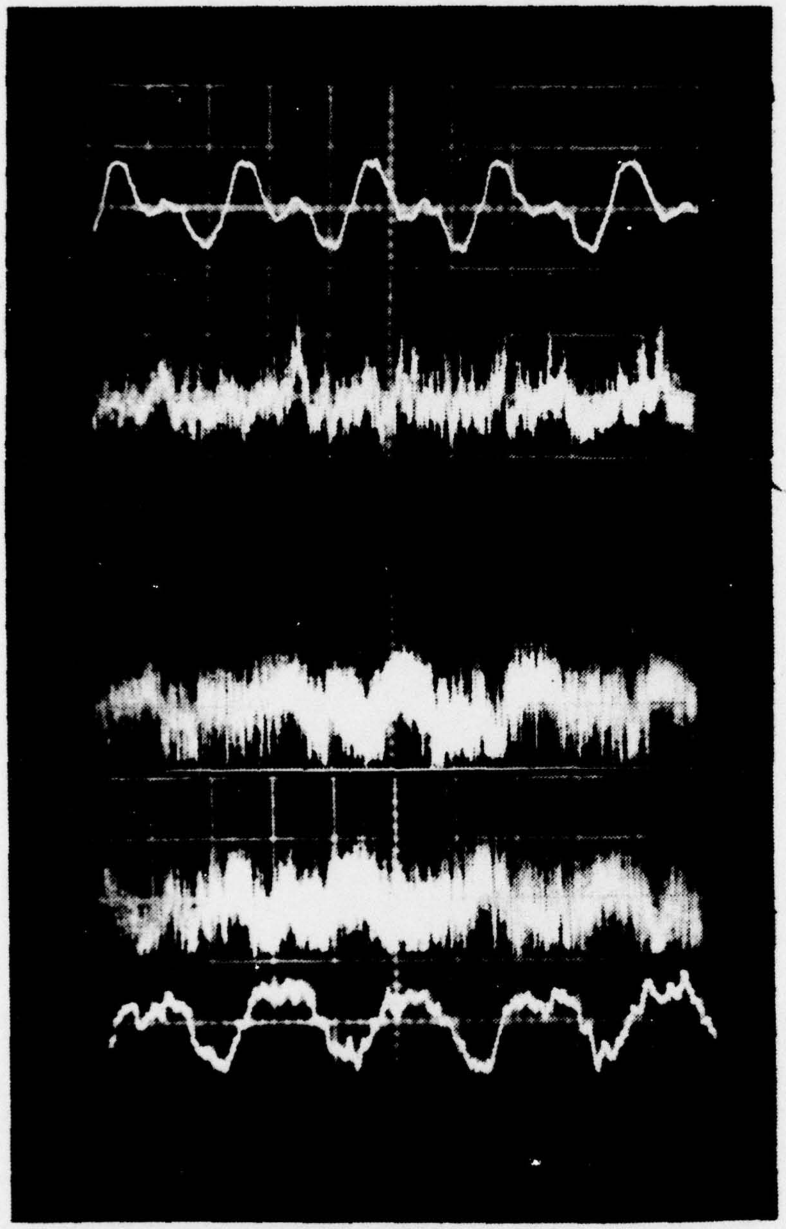

FIGURE 46

PRESSURE AND VELOCITY WAVEFORMS FOR FREESTREAM OSCILLATING AT 9 Hz, $\epsilon = 10.9\%$ (50 msec/cm)

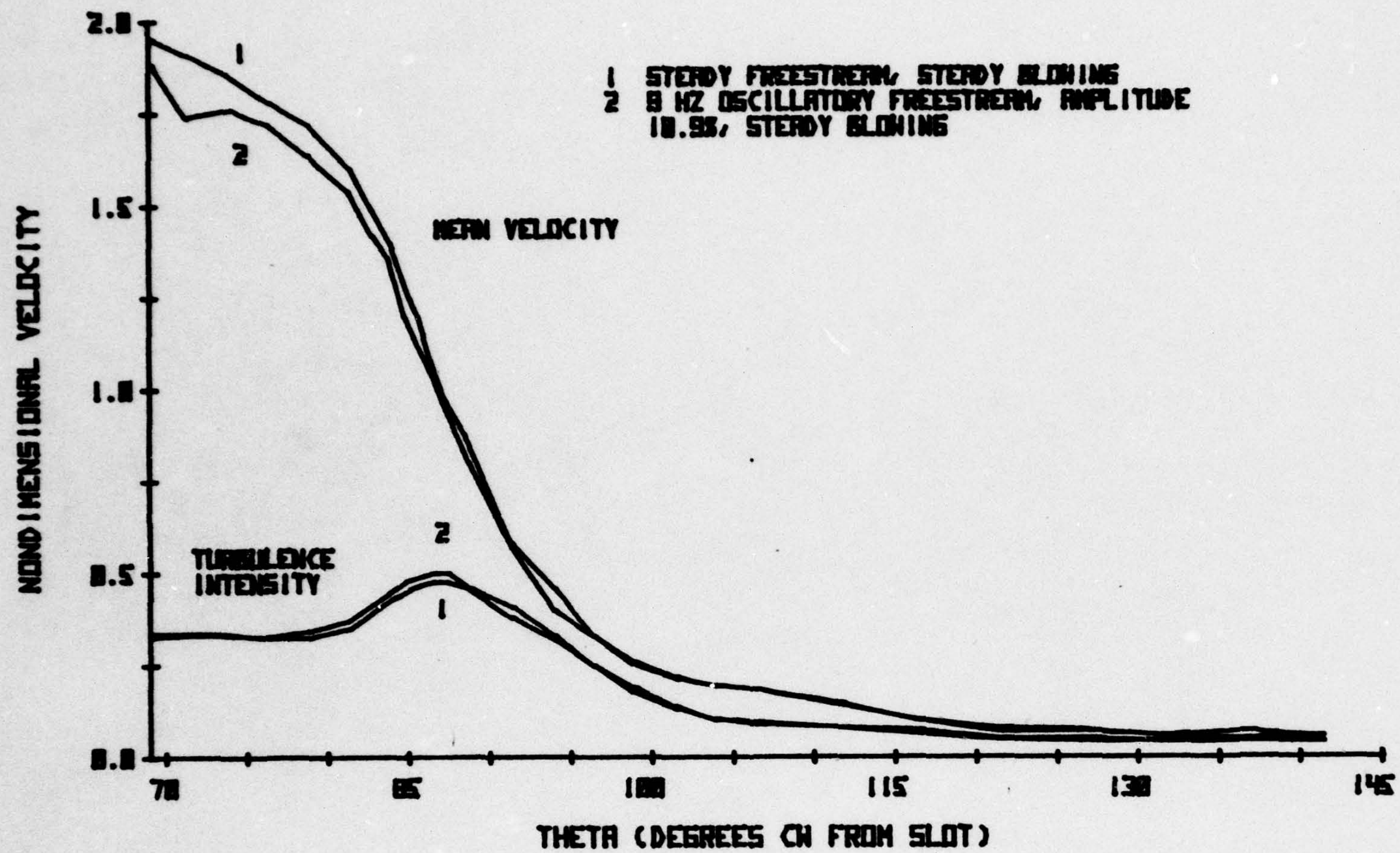

FIGURE 47

NONDIMENSIONAL MEAN VELOCITY AND TURBULENCE INTENSITY PROFILES VS THETA FOR ALPHA=-5 CMU= 0.0445 AT 0.025 IN. FROM SURFACE

of the freestream oscillation on the aerodynamic characteristics is indicated in Table V. In the oscillating freestream, the mean lift effects appear to be similar to those encountered with oscillatory blowing. Only the RMS pressure drag increased substantially.

TABLE V

COMPARISON OF STEADY AND OSCILLATING FREESTREAM AERODYNAMIC CHARACTERISTICS WITH STEADY BLOWING

	STEADY	OSCILLATING	ε (%)
$\bar{C}_L$	1.3785	1.3531	- 1.8
$\langle C_L^2 \rangle^{1/2}$	.0107	.0575	4.2
$\bar{C}_{M(C/2)}$	- .1862	- .1960	- 5.3
$\langle C_{M(C/2)}{}^2 \rangle^{1/2}$	- .0013	- .0036	1.7
$\bar{C}_D$	.0598	.0604	1.0
$\langle C_D{}^2 \rangle^{1/2}$	.0045	.0164	26.1

VI. CONCLUSIONS

The mean values of sectional aerodynamic characteristics for a typical CC Airfoil with steady and oscillating blowing have been determined by direct integration of surface pressure data. In the oscillatory blowing case, selected amounts of unsteady pressure data have been obtained but integration of pressures to obtain aerodynamic transfer functions has not yet been obtained. The oscillatory blowing was produced by a variable area rotating cam in the injection supply line which yielded sinusoidal mass flow rate fluctuation with blowing amplification ratios from 0 to 0.65. Flow in the near-wake was monitored by a constant temperature hotwire anemometer which could be traversed 72 degrees around the trailing edge at a constant distance 0.025 to 2.0 inches from the surface. The velocity profile data were compared with surface pressure data to devise a means of locating the Coanda jet separation point.

From the results the following conclusions may be drawn:

1. Mass flow modulation produced no evident increase of mean or average lift augmentation over that produced by steady injection for oscillation amplitudes as high as 65 percent of C_μ, as shown in Table III.

2. Oscillatory blowing induced oscillatory entrainment which in turn was the main contributor in transmitting pressure waves to the forward stagnation point.

3. The peak turbulence intensity in the wake, as indicated by a hotwire survey, is an accurate means of locating the point of separation and is in agreement with surface pressure measurements.

4. Because of the occurrence of the flow anomaly discussed in Section V, no simple separation point predictive criteria could be formulated.

APPENDIX A

SURFACE PRESSURE TAP LOCATIONS

Tap No.	x (in.)	x/c	y (in.)	y/c
1	0.0	0.0	0.0	0.0
2	0.012	0.0012	0.084	0.0083
3	0.060	0.0059	0.173	0.0170
4	0.119	0.0117	0.247	0.0242
5	0.213	0.0209	0.335	0.0328
6	0.314	0.0308	0.406	0.0398
7	0.517	0.0507	0.528	0.0517
8	0.949	0.0930	0.728	0.0713
9	1.431	0.1402	0.897	0.0879
10	1.929	0.1890	1.038	0.1017
11	2.433	0.2384	1.149	0.1126
12	2.848	0.2791	1.224	0.1199
13	3.954	0.3874	1.357	0.1329
14	5.093	0.4990	1.396	0.1368
15	6.098	0.5975	1.347	0.1320
16	7.130	0.6986	1.226	0.1201
17	7.635	0.7481	1.134	0.1111
18	8.021	0.7859	1.053	0.1031
19	8.670	0.8459	0.881	0.0863
20	9.191	0.9005	0.713	0.0698
21	9.400	0.9210	0.635	0.0622
22	9.598	0.9404	0.560	0.0549
23	9.801	0.9603	0.482	0.0472
24	9.949	0.9748	0.410	0.0402
25	10.053	0.9850	0.339	0.0332
26	10.135	0.9930	0.245	0.0240
27	10.182	0.9976	0.145	0.0142
28	10.193	0.9987	0.090	0.0088
29	10.206	1.0000	0.0	0.0
30	10.194	0.9988	-0.118	-0.0115
31	10.052	0.9947	-0.223	-0.0219
32	10.109	0.9905	-0.307	-0.0301
33	10.040	0.9837	-0.349	-0.0342
34	9.919	0.9719	-0.448	-0.0439
35	9.769	0.9572	-0.524	-0.0514
36	9.590	0.9396	-0.580	-0.0569
37	8.552	0.8379	-0.695	-0.0681
38	7.946	0.7786	-0.740	-0.0725
39	7.562	0.7409	-0.758	-0.0742
40	7.042	0.6900	-0.775	-0.0759
41	6.023	0.5901	-0.786	-0.0770
42	5.101	0.4998	-0.788	-0.0772
43	4.005	0.3924	-0.772	-0.0756
44	2.885	0.2827	-0.736	-0.0721

Tap No.	x (in.)	x/c	y (in.)	y/c
45	2.480	0.2430	-0.708	-0.06944
46	1.969	0.1929	-0.658	-0.0645
47	1.471	0.1441	-0.594	-0.0582
48	0.953	0.0934	-0.517	-0.0506
49	0.515	0.0505	-0.416	-0.0408
50	0.345	0.0338	-0.349	-0.0342
51	0.229	0.0224	-0.285	-0.0280
52	0.119	0.0117	-0.214	-0.0210
53	0.053	0.0052	-0.145	-0.0142
54	0.009	0.0009	-0.070	-0.0069

Uppr. surf. spcl. tubes

55	5.108	0.5004	6.0	inches	
56	5.093	0.4990	9.0	"	Distance
57	5.095	0.4992	10.5	"	Stb'd.
58	7.631	0.7477	6.0	inches	from
59	7.631	0.7477	9.0	"	center

APPENDIX B

SPANWISE PRESSURE DISTRIBUTION

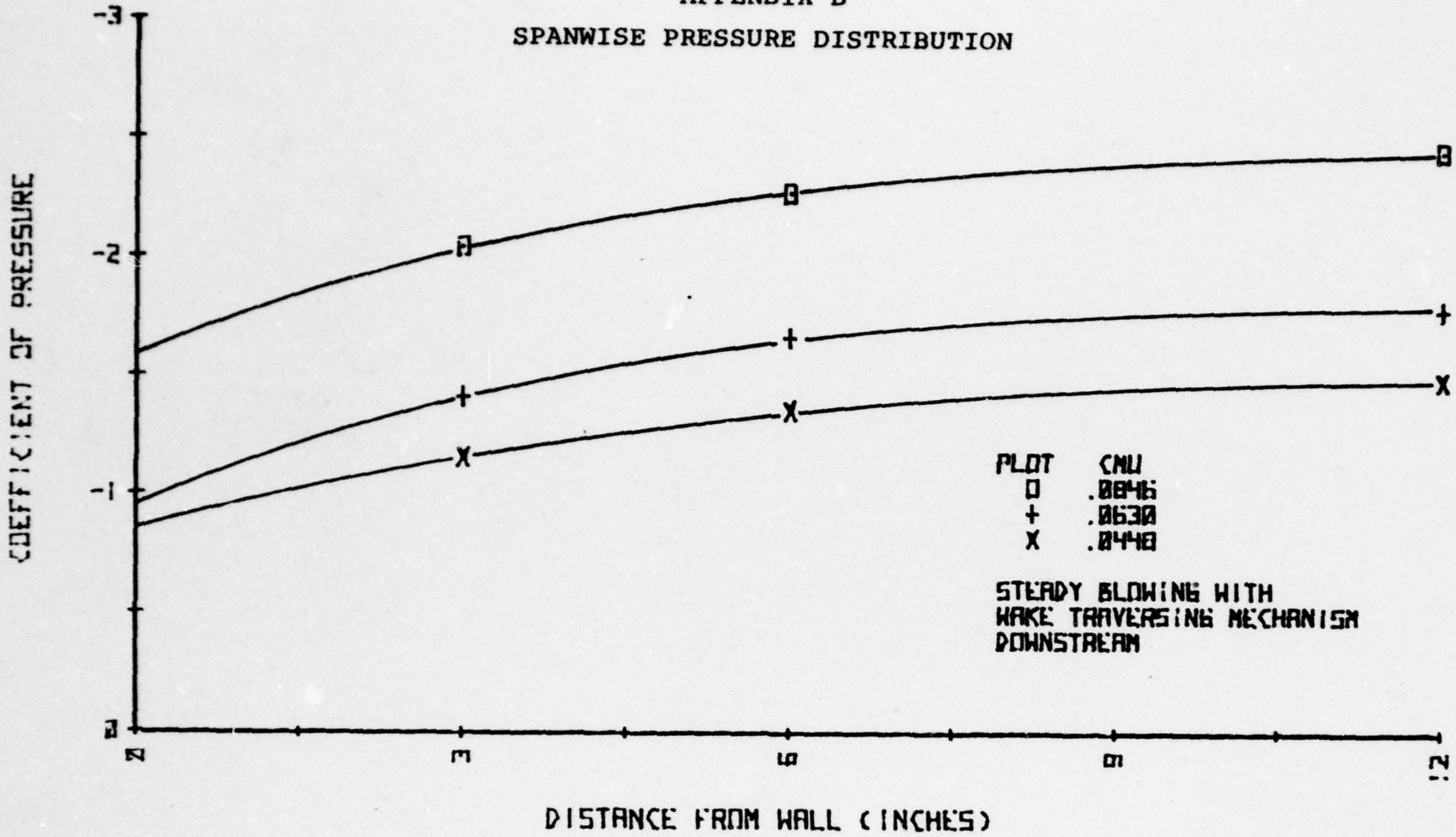

FIGURE B1

COEFFICIENT OF PRESSURE VS DISTANCE FROM WALL

ALONG 0.75*(X/C) FOR ALPHA = -5

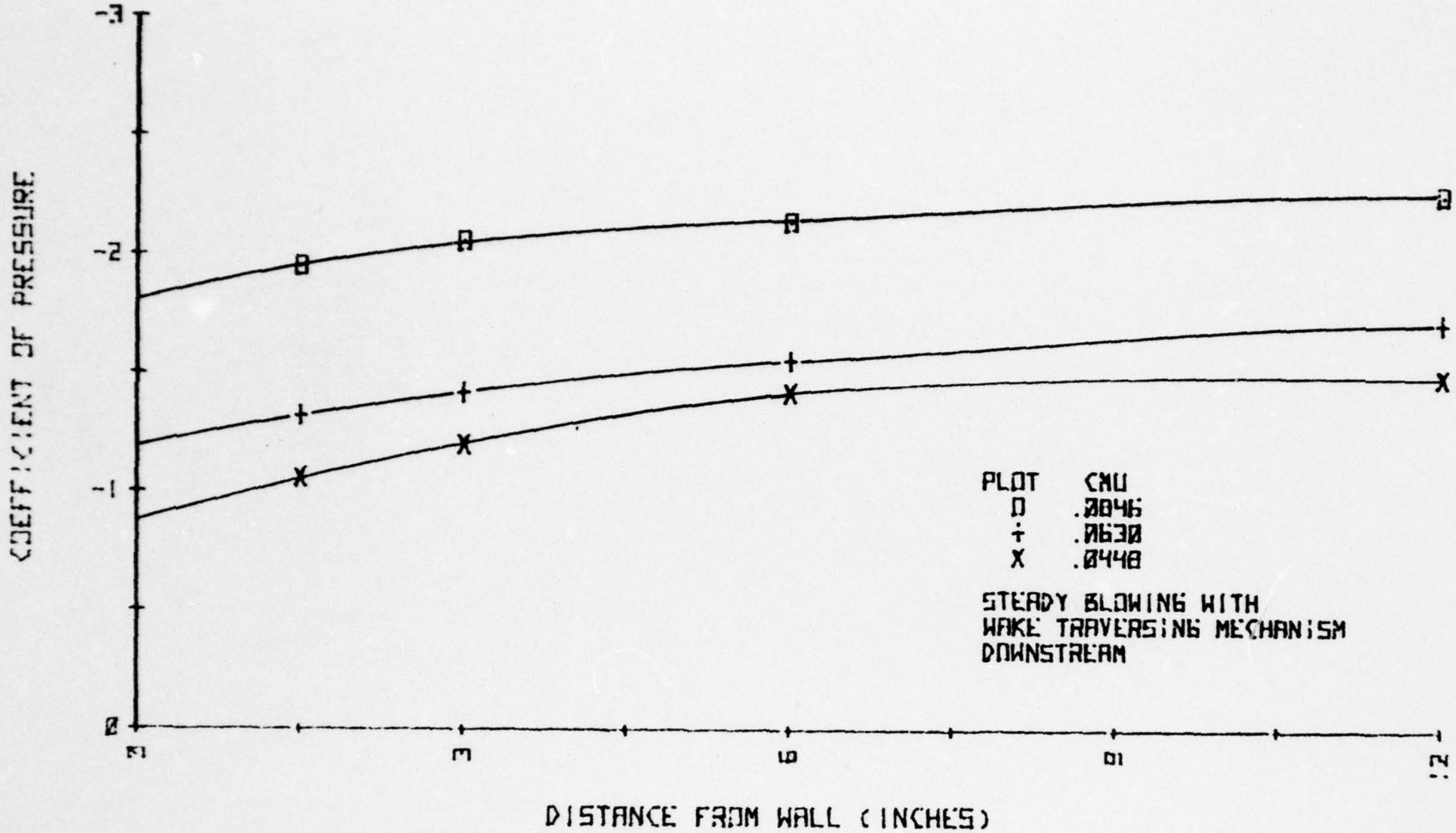

FIGURE B2

COEFFICIENT OF PRESSURE VS DISTANCE FROM WALL

ALONG 0.50*(X/C) FOR ALPHA = -5

APPENDIX C

Hotwire Data for Near-Wake Mapping at $C_{\mu} = 0.0451$

RUN NUMBER 51701 DISTANCE FROM SURFACE (IN.) 1.75

POINT	THETA(CHORD)	MEAN VEL	RMS VEL
1	17	1.195	6.50000E-03
2	15	1.187	6.80000E-03
3	10	1.16	7.50000E-03
4	5	1.16	8.50000E-03
5	0	1.125	0.0108
6	-5	1.12	0.0155
7	-10	1.11	0.035
8	-15.1	1.1	0.067
9	-19.9	1.15	0.115
10	-24.9	1.2	0.15
11	-27.4	1.205	0.163
12	-30	1.185	0.165
13	-32.4	1.135	0.153
14	-35	1.05	0.117
15	-37.6	1.035	0.068
16	-40.1	1.008	0.034
17	-45	1	0.031
18	-49.9	1.03	0.012
19	-55	1.03	7.00000E-03

RUN NUMBER 51702 DISTANCE FROM SURFACE (IN.) 0.025

POINT	THETA(CHORD)	MEAN VEL	RMS VEL
1	17	2.035	0.15
2	14.9	1.935	0.155
3	12.4	1.88	0.165
4	9.9	1.75	0.195
5	7.5	1.64	0.25
6	5	1.36	0.31
7	2.5	1.1	0.34
8	0	0.83	0.315
9	-2.6	0.55	0.24
10	-5.1	0.41	0.19
11	-7.6	0.35	0.155
12	-10	0.288	0.114
13	-15	0.245	0.088
14	-20	0.213	0.082
15	-24.9	0.165	0.074
16	-30	0.12	0.058
17	-35.1	0.12	0.051
18	-40	0.13	0.052
19	-44.9	0.1	0.053
20	-50	0.095	0.047
21	-55	0.085	0.043

RUN NUMBER 51703 DISTANCE FROM SURFACE (IN.) 0.05

POINT	THETA(CHORD)	MEAN VEL	RMS VEL
1	17.1	1.96	0.157
2	15	1.945	0.151
3	12.5	1.88	0.154
4	10	1.84	0.16
5	7.5	1.78	0.18
6	5	1.65	0.235
7	2.5	1.43	0.31
8	0	1.1	0.35
9	-2.5	0.86	0.34
10	-5.1	0.65	0.3
11	-7.4	0.46	0.23
12	-10.1	0.35	0.18
13	-12.5	0.3	0.13
14	-15	0.26	0.103
15	-20	0.25	0.097
16	-25	0.2	0.095
17	-29.9	0.14	0.078
18	-34.9	0.108	0.051
19	-40	0.097	0.038
20	-45	0.1	0.048
21	-50	0.12	0.058
22	-55	0.16	0.068

RUN NUMBER 51704   DISTANCE FROM SURFACE (IN.) 0.1

POINT	THETA(CHORD)	MEAN VEL	RMS VEL
1	17.1	1.6	0.17
2	15.1	1.61	0.195
3	12.5	1.66	0.21
4	10	1.75	0.21
5	7.4	1.82	0.19
6	4.9	1.82	0.175
7	2.6	1.82	0.165
8	0	1.78	0.175
9	-4.9	1.56	0.3
10	-7.5	1.3	0.37
11	-9.9	1.05	0.38
12	-12.5	0.825	0.35
13	-15	0.62	0.31
14	-17.5	0.42	0.23
15	-20	0.335	0.17
16	-24.9	0.308	0.11
17	-30.1	0.28	0.115
18	-35	0.185	0.095
19	-39.9	0.13	0.07
20	-44.9	0.175	0.08
21	-50.1	0.256	0.11
22	-55	0.375	0.135

RUN NUMBER 51705   DISTANCE FROM SURFACE (IN.) 0.25

POINT	THETA(CHORD)	MEAN VEL	RMS VEL
1	17.1	1.385	0.025
2	12.7	1.34	0.021
3	10	1.29	0.021
4	4.9	1.24	0.041
5	2.5	1.225	0.07
6	0	1.23	0.13
7	-2.7	1.36	0.21
8	-5.1	1.46	0.22
9	-7.6	1.55	0.21
10	-9.9	1.63	0.22
11	-12.6	1.62	0.28
12	-15	1.47	0.35
13	-17.5	1.28	0.41
14	-20.1	1.02	0.42
15	-22.5	0.78	0.38
16	-25	0.6	0.33
17	-29.9	0.39	0.16
18	-34.9	0.325	0.12
19	-39.9	0.35	0.13
20	-44.8	0.48	0.14
21	-50.2	0.66	0.13
22	-55	0.31	0.1

RUN NUMBER 51706   DISTANCE FROM SURFACE (IN.) 0.375

POINT	THETA(CHORD)	MEAN VEL	RMS VEL
1	17	1.39	0.018
2	12.9	1.345	0.016
3	10.1	1.325	0.016
4	5.1	1.235	0.018
5	0	1.16	0.029
6	-5	1.14	0.07
7	-7.6	1.2	0.13
8	-10	1.35	0.21
9	-12.3	1.47	0.23
10	-15.3	1.55	0.26
11	-17.7	1.55	0.3
12	-20	1.38	0.35
13	-25	1	0.44
14	-27.8	0.78	0.4
15	-30.1	0.58	0.33
16	-32.5	0.41	0.2
17	-35	0.41	0.16
18	-40.1	0.58	0.14
19	-44.8	0.78	0.11
20	-49.8	0.87	0.08
21	-55	0.97	0.045

RUN NUMBER 51707   DISTANCE FROM SURFACE (IN.) 0.5

POINT	THETA(CHORD)	MEAN VEL	RMS VEL
1	17.1	1.42	0.013
2	10.2	1.35	0.017
3	5	1.285	0.02
4	0	1.23	0.025
5	-5.1	1.17	0.035
6	-10.2	1.14	0.08
7	-12.5	1.19	0.14
8	-14.9	1.37	0.22
9	-17.8	1.44	0.24
10	-19.9	1.515	0.27
11	-22.7	1.39	0.38
12	-25	1.25	0.42
13	-27.7	1.08	0.42
14	-30.2	0.82	0.37
15	-32.4	0.7	0.34
16	-35	0.57	0.24
17	-37.7	0.61	0.16
18	-40.1	0.68	0.12
19	-45	0.86	0.058
20	-50.1	0.9	0.03
21	-55	0.968	0.021

RUN NUMBER 51708 DISTANCE FROM SURFACE (IN.) 0.75

POINT	THETA(CHORD)	MEAN VEL	RMS VEL
1	17.1	1.39	0.013
2	10.1	1.31	0.012
3	5.1	1.27	0.014
4	0	1.227	0.018
5	-5.1	1.16	0.022
6	-10.2	1.11	0.047
7	-12.3	1.11	0.055
8	-15	1.13	0.11
9	-20.1	1.3	0.21
10	-25.2	1.39	0.3
11	-29.9	1.23	0.34
12	-32.4	1.08	0.34
13	-35	0.89	0.23
14	-40.2	0.845	0.1
15	-42.3	0.89	0.052
16	-45	0.91	0.04
17	-50.1	0.98	0.023
18	-55	1.02	0.019

RUN NUMBER 51709 DISTANCE FROM SURFACE (IN.) 1.25

POINT	THETA(CHORD)	MEAN VEL	RMS VEL
1	17.1	1.38	0.012
2	10	1.355	0.012
3	4.9	1.3	0.013
4	0	1.265	0.014
5	-5.1	1.235	0.021
6	-10.1	1.22	0.042
7	-15.1	1.194	0.075
8	-17.6	1.205	0.11
9	-19.9	1.23	0.14
10	-23.4	1.33	0.175
11	-25.1	1.35	0.19
12	-30	1.34	0.23
13	-32.3	1.27	0.23
14	-35	1.18	0.175
15	-37.8	1.085	0.1
16	-39.9	1.081	0.048
17	-44.9	1.085	0.021
18	-49.8	1.11	0.0135
19	-55	1.11	0.01

APPENDIX D

Unsteady Flow Pressure Data

The midspan pressure distributions and upper surface spanwise pressure data for the oscillatory blowing tests and for the oscillating freestream test are presented by run number. The corresponding steady, unsteady and RMS are indicated in Table D1.

TABLE D1

Unsteady Flow Data Key

RUN NUMBER	C_L	C_μ	REMARKS
51002	1.2088	.0438	steady flow for 51003.1
51003.1	1.1836	.0438	9 Hz oscillatory blowing
51003.2	.0521	.0438	RMS data for 51003.1
51301	1.2560	.0441	9 Hz oscillatory blowing
51301.1	.0067	.0441	RMS data for 51301
52001	2.7322	.0856	steady flow for 52002
52002	2.6563	.0856	9 Hz oscillatory blowing
50002.1	.0765	.0856	RMS data for 52002
52601	1.3785	.0457	steady flow for 52602 and 52603
52601.1	.0107	.0457	RMS data for 52601
52602	1.3531	.0457	9 Hz oscillatory freestream
52602.1	.0575	.0457	RMS data for 52602
52603	1.3103	.0457	9 Hz oscillatory blowing
52603.1	.0650	.0457	RMS data for 52603
52604	1.8370	.0645	steady flow for 52605
52604.1	.0090	.0645	RMS data for 52604
52605	1.9903	.0645	9 Hz oscillatory blowing
52605.1	.0536	.0645	RMS data for 52605

RUN NUMBER 51002
MIDSPAN PRESSURE DISTRIBUTION

N	UPPER CP	N	LOWER CP
1	1.003	29	0.134
2	0.760	30	0.323
3	0.560	31	0.425
4	0.413	32	0.464
5	-0.012	33	0.449
6	-0.171	34	0.449
7	-0.372	35	0.419
8	-0.584	36	0.365
9	-0.709	37	0.125
10	-0.820	38	0.090
11	-0.983	39	0.064
12	-0.958	40	0.017
13	-1.177	41	-0.029
14	-1.323	42	-0.070
15	-1.362	43	-0.145
16	-1.416	44	-0.227
17	-1.471	45	-0.250
18	-1.488	46	-0.230
19	-1.468	47	-0.241
20	-1.474	48	-0.294
21	-1.494	49	-0.422
22	-1.500	50	-0.273
23	-2.869	51	-0.137
24	-4.488	52	0.058
25	-4.451	53	0.416
26	-3.535	54	0.860
27	-0.782		
28	-0.503		
29	0.134		

UPPER SURFACE SPANWISE PRESSURE

DFW(IN)	0.5*(X/C)	0.75*(X/C)
12	-1.3234	-1.4709
6	-1.1308	-1.3023
3	-1.0581	-1.1017
1.5	-0.9680	

RUN NUMBER 51003.1
MIDSPAN PRESSURE DISTRIBUTION

N	UPPER CP	N	LOWER CP
1	1.003	29	0.165
2	0.917	30	0.353
3	0.615	31	0.435
4	0.355	32	0.459
5	0.234	33	0.441
6	-0.101	34	0.429
7	-0.219	35	0.405
8	-0.524	36	0.346
9	-0.627	37	0.165
10	-0.805	38	0.115
11	-0.905	39	0.073
12	-0.982	40	0.031
13	-1.178	41	-0.008
14	-1.302	42	-0.039
15	-1.349	43	-0.120
16	-1.402	44	-0.207
17	-1.403	45	-0.230
18	-1.462	46	-0.207
19	-1.395	47	-0.221
20	-1.401	48	-0.311
21	-1.415	49	-0.356
22	-1.451	50	-0.303
23	-2.768	51	-0.003
24	-4.305	52	0.081
25	-4.249	53	0.356
26	-3.277	54	0.835
27	-0.745		
28	-0.367		
29	0.165		

UPPER SURFACE SPANWISE PRESSURE

DFW(IN)	0.5*(X/C)	0.75*(X/C)
12	-1.3018	-1.4034
6	-1.1064	-1.2269
3	-0.9776	-1.0476
1.5	-0.9244	

RUN NUMBER 51003.2
MIDSPAN PRESSURE DISTRIBUTION

N	UPPER CP	N	LOWER CP
1	0.074	29	0.148
2	0.080	30	0.098
3	0.098	31	0.071
4	0.112	32	0.077
5	0.118	33	0.065
6	0.104	34	0.080
7	0.101	35	0.083
8	0.101	36	0.083
9	0.098	37	0.084
10	0.104	38	0.078
11	0.101	39	0.070
12	0.104	40	0.070
13	0.104	41	0.070
14	0.104	42	0.078
15	0.104	43	0.073
16	0.121	44	0.076
17	0.123	45	0.078
18	0.121	46	0.070
19	0.123	47	0.076
20	0.134	48	0.073
21	0.148	49	0.101
22	0.154	50	0.115
23	0.345	51	0.112
24	0.513	52	0.123
25	0.560	53	0.126
26	0.630	54	0.084
27	0.504		
28	0.406		
29	0.148		

UPPER SURFACE SPANWISE PRESSURE

DFW(IN)	0.5*(X/C)	0.75*(X/C)
12	0.1036	0.1232
6	0.0980	0.1120
3	0.0924	0.1036
1.5	0.0924	

RUN NUMBER 51301
MIDSPAN PRESSURE DISTRIBUTION

N	UPPER CP	N	LOWER CP
1	1.003	29	0.221
2	0.896	30	0.363
3	0.371	31	0.475
4	0.478	32	0.487
5	0.096	33	0.467
6	-0.035	34	0.464
7	-0.266	35	0.420
8	-0.597	36	0.377
9	-0.694	37	0.164
10	-0.829	38	0.108
11	-1.003	39	0.065
12	-1.012	40	0.040
13	-1.209	41	-0.011
14	-1.296	42	-0.028
15	-1.330	43	-0.091
16	-1.383	44	-0.147
17	-1.456	45	-0.173
18	-1.449	46	-0.164
19	-1.433	47	-0.085
20	-1.462	48	-0.142
21	-1.467	49	-0.167
22	-1.564	50	-0.028
23	-2.867	51	0.142
24	-4.334	52	0.323
25	-4.116	53	0.700
26	-3.238	54	0.975
27	-0.830		
28	-0.198		
29	0.221		

UPPER SURFACE SPANWISE PRESSURE

DFW(IN)	0.5*(X/C)	0.75*(X/C)
12	-1.2957	-1.4561
6	-1.4193	-1.4929
3	-1.3173	-1.3343
1.5	-1.2266	

BEST AVAILABLE COPY

RUN NUMBER 51301.1
MIDSPAN PRESSURE DISTRIBUTION

N	UPPER CP	N	LOWER CP
1	0.072	29	0.127
2	0.078	30	0.099
3	0.087	31	0.070
4	0.087	32	0.067
5	0.087	33	0.058
6	0.078	34	0.064
7	0.079	35	0.058
8	0.078	36	0.435
9	0.071	37	0.065
10	0.081	38	0.065
11	0.079	39	0.065
12	0.078	40	0.068
13	0.081	41	0.062
14	0.078	42	0.065
15	0.087	43	0.065
16	0.087	44	0.057
17	0.085	45	0.062
18	0.078	46	0.065
19	0.085	47	0.065
20	0.099	48	0.071
21	0.108	49	0.071
22	0.105	50	0.071
23	0.198	51	0.071
24	0.269	52	0.071
25	0.340	53	0.071
26	0.368	54	0.071
27	0.368		
28	0.283		
29	0.127		

UPPER SURFACE SPANWISE PRESSURE

DFW(IN)	0.5*(X/C)	0.75*(X/C)
12	0.0783	0.0850
6	0.0850	0.0850
3	0.0850	0.0850
1.5	0.0793	

RUN NUMBER 52001
MIDSPAN PRESSURE DISTRIBUTION

N	UPPER CP	N	LOWER CP
1	0.291	29	-0.399
2	-0.114	30	-0.040
3	-0.997	31	0.598
4	-0.943	32	0.643
5	-0.886	33	0.682
6	-1.387	34	0.676
7	-1.436	35	0.652
8	-1.613	36	0.613
9	-1.584	37	0.484
10	-1.736	38	0.396
11	-1.920	39	0.342
12	-1.916	40	0.328
13	-2.141	41	0.288
14	-2.258	42	0.276
15	-2.324	43	0.234
16	-2.375	44	0.211
17	-2.447	45	0.188
18	-2.535	46	0.239
19	-2.490	47	0.293
20	-2.553	48	0.333
21	-2.664	49	0.462
22	-2.838	50	0.607
23	-5.729	51	0.769
24	-7.712	52	0.940
25	-8.712	53	1.009
26	-7.821	54	0.863
27	-5.345		
28	-4.179		
29	-0.399		

UPPER SURFACE SPANWISE PRESSURE

DFW(IN)	0.5*(X/C)	0.75*(X/C)
12	-2.2583	-2.4473
6	-2.1425	-2.2678
3	-2.0570	-2.0399
1.5	-1.9516	

RUN NUMBER 52002

MIDSPAN PRESSURE DISTRIBUTION

N	UPPER CP	N	LOWER CP
1	0.582	29	-1.453
2	-0.269	30	-0.020
3	-0.760	31	0.599
4	-0.868	32	0.635
5	-1.076	33	0.673
6	-1.216	34	0.655
7	-1.475	35	0.629
8	-1.427	36	0.611
9	-1.453	37	0.472
10	-1.751	38	0.383
11	-1.721	39	0.383
12	-1.915	40	0.316
13	-2.067	41	0.271
14	-2.243	42	0.263
15	-2.325	43	0.212
16	-2.371	44	0.156
17	-2.327	45	0.148
18	-2.503	46	0.165
19	-2.411	47	0.237
20	-2.570	48	0.274
21	-2.634	49	0.374
22	-2.765	50	0.436
23	-5.553	51	0.668
24	-7.844	52	0.813
25	-8.913	53	1.000
26	-8.098	54	0.330
27	-4.939		
28	-3.679		
29	-1.453		

UPPER SURFACE SPANWISE PRESSURE

DFW(IN)	0.5*(X/C)	0.75*(X/C)
12	-2.2427	-2.3268
6	-2.1369	-2.2458
3	-1.9581	-2.0587
1.5	-1.9246	

RUN NUMBER 52002.1
MIDSPAN PRESSURE DISTRIBUTION

N	UPPER CP	N	LOWER CP
1	0.111	29	0.838
2	0.161	30	0.307
3	0.196	31	0.094
4	0.175	32	0.082
5	0.146	33	0.073
6	0.146	34	0.073
7	0.126	35	0.073
8	0.117	36	0.073
9	0.112	37	0.067
10	0.117	38	0.070
11	0.115	39	0.073
12	0.108	40	0.073
13	0.108	41	0.070
14	0.111	42	0.070
15	0.117	43	0.073
16	0.123	44	0.073
17	0.126	45	0.073
18	0.137	46	0.070
19	0.140	47	0.070
20	0.156	48	0.075
21	0.173	49	0.084
22	0.196	50	0.089
23	0.419	51	0.084
24	0.531	52	0.084
25	0.698	53	0.070
26	0.726	54	0.070
27	1.006		
28	0.866		
29	0.838		

UPPER SURFACE SPANWISE PRESSURE

DFW(IN)	0.5*(X/C)	0.75*(X/C)
12	0.1111	0.1257
6	0.1034	0.1117
3	0.0894	0.1034
1.5	0.0978	

BEST AVAILABLE COPY

RUN NUMBER 52601

MIDSPAN PRESSURE DISTRIBUTION

N	UPPER CP	N	LOWER CP
1	1.018	29	0.192
2	0.762	30	0.393
3	0.194	31	0.501
4	0.032	32	0.475
5	-0.106	33	0.446
6	-0.358	34	0.493
7	-0.209	35	0.440
8	-0.692	36	0.361
9	-0.657	37	0.212
10	-0.971	38	0.156
11	-0.933	39	0.125
12	-1.229	40	0.081
13	-1.390	41	0.008
14	-1.490	42	-0.006
15	-1.540	43	-0.103
16	-1.575	44	-0.167
17	-1.482	45	-0.195
18	-1.604	46	-0.170
19	-1.468	47	-0.203
20	-1.476	48	-0.248
21	-1.462	49	-0.337
22	-1.585	50	-0.220
23	-2.997	51	-0.042
24	-4.724	52	0.209
25	-4.521	53	0.462
26	-3.713	54	0.944
27	-1.086		
28	-0.599		
29	0.192		

UPPER SURFACE SPANWISE PRESSURE

DFW(IN)	0.5*(X/C)	0.75*(X/C)
12	-1.4897	-1.4819
6	-1.4206	-1.3538
3	-1.2006	-1.1532
1.5	-1.0585	

BEST AVAILABLE COPY

RUN NUMBER 52601.1
MIDSPAN PRESSURE DISTRIBUTION

N	UPPER CP	N	LOWER CP
1	0.065	29	0.028
2	0.067	30	0.097
3	0.065	31	0.067
4	0.073	32	0.073
5	0.073	33	0.070
6	0.065	34	0.067
7	0.070	35	0.067
8	0.059	36	0.065
9	0.064	37	0.061
10	0.073	38	0.056
11	0.064	39	0.061
12	0.073	40	0.064
13	0.073	41	0.061
14	0.076	42	0.061
15	0.070	43	0.061
16	0.065	44	0.061
17	0.067	45	0.056
18	0.067	46	0.064
19	0.067	47	0.064
20	0.064	48	0.056
21	0.067	49	0.067
22	0.070	50	0.067
23	0.111	51	0.070
24	0.097	52	0.072
25	0.125	53	0.072
26	0.181	54	0.064
27	0.334		
28	0.251		
29	0.028		

UPPER SURFACE SPANWISE PRESSURE

DFW(IN)	0.5*(X/C)	0.75*(X/C)
12	0.0762	0.0669
6	0.0696	0.0641
3	0.0613	0.0641
1.5	0.0613	

RUN NUMBER 52602
MIDSPAN PRESSURE DISTRIBUTION

N	UPPER CP	N	LOWER CP
1	0.945	29	0.206
2	0.905	30	0.436
3	0.052	31	0.473
4	0.254	32	0.597
5	-0.046	33	0.556
6	-0.334	34	0.441
7	-0.398	35	0.588
8	-0.666	36	0.519
9	-0.837	37	0.270
10	-0.856	38	0.064
11	-1.140	39	0.049
12	-1.049	40	0.081
13	-1.242	41	0.073
14	-1.571	42	-0.116
15	-1.524	43	-0.169
16	-1.553	44	-0.279
17	-1.477	45	-0.247
18	-1.501	46	-0.166
19	-1.459	47	-0.299
20	-1.526	48	-0.302
21	-1.622	49	-0.340
22	-1.500	50	-0.366
23	-3.209	51	0.055
24	-4.619	52	0.416
25	-4.703	53	0.924
26	-3.703	54	0.971
27	-0.945		
28	-0.552		
29	0.206		

UPPER SURFACE SPANWISE PRESSURE

DFW(IN)	0.5*(X/C)	0.75*(X/C)
12	-1.5706	-1.4767
6	-1.4331	-1.3692
3	-1.2267	-1.2616
1.5	-1.0203	

BEST AVAILABLE COPY

RUN NUMBER 52602.1
MIDSPAN PRESSURE DISTRIBUTION

N	UPPER CP	N	LOWER CP
1	0.692	29	0.799
2	0.720	30	0.756
3	0.720	31	0.720
4	0.720	32	0.720
5	0.735	33	0.720
6	0.735	34	0.720
7	0.756	35	0.720
8	0.735	36	0.720
9	0.741	37	0.756
10	0.735	38	0.741
11	0.770	39	0.741
12	0.735	40	0.741
13	0.749	41	0.727
14	0.749	42	0.727
15	0.764	43	0.712
16	0.764	44	0.712
17	0.799	45	0.698
18	0.778	46	0.698
19	0.799	47	0.669
20	0.814	48	0.683
21	0.814	49	0.669
22	0.828	50	0.654
23	0.901	51	0.640
24	0.988	52	0.654
25	1.017	53	0.669
26	1.017	54	0.683
27	1.017		
28	0.959		
29	0.799		

UPPER SURFACE SPANWISE PRESSURE

DFW(IN)	0.5*(X/C)	0.75*(X/C)
12	0.7493	0.7994
6	0.7413	0.7413
3	0.7122	0.7267
1.5	0.7413	

RUN NUMBER 52603
MIDSPAN PRESSURE DISTRIBUTION

N	UPPER CP	N	LOWER CP
1	0.985	29	0.104
2	0.786	30	0.335
3	0.669	31	0.446
4	0.311	32	0.457
5	0.185	33	0.475
6	-0.079	34	0.443
7	-0.442	35	0.425
8	-0.522	36	0.355
9	-0.775	37	0.211
10	-0.845	38	0.076
11	-1.107	39	0.099
12	-0.953	40	0.070
13	-1.164	41	0.042
14	-1.311	42	0.017
15	-1.381	43	-0.076
16	-1.411	44	-0.124
17	-1.470	45	-0.149
18	-1.455	46	-0.146
19	-1.499	47	-0.079
20	-1.417	48	-0.034
21	-1.490	49	-0.115
22	-1.577	50	0.135
23	-2.961	51	0.237
24	-4.479	52	0.304
25	-4.282	53	0.780
26	-3.631	54	0.997
27	-1.155		
28	-0.594		
29	0.104		

UPPER SURFACE SPANWISE PRESSURE

DFW(IN)	0.5*(X/C)	0.75*(X/C)
12	-1.3109	-1.4704
6	-1.4141	-1.4451
3	-1.2563	-1.1465
1.5	-1.2000	

RUN NUMBER 52603.1

MIDSPAN PRESSURE DISTRIBUTION

N	UPPER CP	N	LOWER CP
1	0.103	29	0.254
2	0.117	30	0.099
3	0.176	31	0.117
4	0.176	32	0.117
5	0.161	33	0.132
6	0.161	34	0.132
7	0.155	35	0.132
8	0.147	36	0.161
9	0.141	37	0.155
10	0.132	38	0.141
11	0.141	39	0.141
12	0.132	40	0.141
13	0.132	41	0.127
14	0.147	42	0.127
15	0.147	43	0.127
16	0.176	44	0.127
17	0.183	45	0.127
18	0.191	46	0.127
19	0.211	47	0.141
20	0.225	48	0.155
21	0.259	49	0.197
22	0.296	50	0.197
23	0.676	51	0.197
24	1.042	52	0.211
25	1.211	53	0.183
26	1.338	54	0.099
27	0.986		
28	0.704		
29	0.254		

UPPER SURFACE SPANWISE PRESSURE

DFW(IN)	0.5*(X/C)	0.75*(X/C)
12	0.1466	0.1831
6	0.1549	0.1690
3	0.1408	0.1549
1.5	0.1408	

RUN NUMBER 52604
MIDSPAN PRESSURE DISTRIBUTION

N	UPPER CP	N	LOWER CP
1	0.931	29	-0.273
2	0.631	30	0.355
3	0.000	31	0.571
4	0.014	32	0.614
5	-0.337	33	0.620
6	-0.437	34	0.591
7	-0.806	35	0.549
8	-0.889	36	0.494
9	-1.008	37	0.336
10	-1.191	38	0.265
11	-1.210	39	0.224
12	-1.389	40	0.175
13	-1.603	41	0.115
14	-1.717	42	0.066
15	-1.740	43	0.033
16	-1.803	44	-0.071
17	-1.779	45	-0.057
18	-1.903	46	-0.019
19	-1.803	47	0.003
20	-1.861	48	-0.049
21	-1.918	49	-0.014
22	-2.033	50	0.169
23	-4.011	51	0.459
24	-6.055	52	0.661
25	-6.262	53	0.872
26	-5.445	54	0.981
27	-2.413		
28	-1.915		
29	-0.273		

UPPER SURFACE SPANWISE PRESSURE

DFW(IN)	0.5*(X/C)	0.75*(X/C)
12	-1.7171	-1.7787
6	-1.5574	-1.6612
3	-1.4209	-1.4098
1.5	-1.3224	

RUN NUMBER 52604.1
MIDSPAN PRESSURE DISTRIBUTION

N	UPPER CP	N	LOWER CP
1	0.086	29	0.273
2	0.094	30	0.096
3	0.094	31	0.086
4	0.086	32	0.080
5	0.086	33	0.086
6	0.086	34	0.080
7	0.082	35	0.086
8	0.080	36	0.086
9	0.082	37	0.082
10	0.091	38	0.082
11	0.082	39	0.082
12	0.086	40	0.082
13	0.086	41	0.082
14	0.094	42	0.082
15	0.086	43	0.077
16	0.086	44	0.082
17	0.082	45	0.082
18	0.086	46	0.082
19	0.082	47	0.082
20	0.082	48	0.082
21	0.082	49	0.082
22	0.082	50	0.082
23	0.137	51	0.082
24	0.137	52	0.090
25	0.137	53	0.082
26	0.178	54	0.082
27	0.546		
28	0.464		
29	0.273		

UPPER SURFACE SPANWISE PRESSURE

DFW(IN)	0.5*(X/C)	0.75*(X/C)
12	0.0943	0.0820
6	0.0820	0.0820
3	0.0765	0.0820
1.5	0.0874	

RUN NUMBER 52605
MIDSPAN PRESSURE DISTRIBUTION

N	UPPER CP	N	LOWER CP
1	0.818	29	-0.356
2	0.131	30	0.328
3	0.012	31	0.573
4	-0.230	32	0.600
5	-0.699	33	0.627
6	-0.797	34	0.600
7	-0.694	35	0.558
8	-1.313	36	0.487
9	-1.119	37	0.328
10	-1.367	38	0.256
11	-1.331	39	0.211
12	-1.642	40	0.181
13	-1.797	41	0.122
14	-1.884	42	0.075
15	-1.916	43	0.025
16	-1.961	44	-0.008
17	-1.864	45	0.000
18	-1.976	46	-0.008
19	-1.844	47	0.064
20	-1.906	48	0.014
21	-1.936	49	-0.136
22	-2.056	50	0.197
23	-4.011	51	0.406
24	-5.972	52	0.672
25	-6.428	53	0.903
26	-5.331	54	0.978
27	-2.458		
28	-1.861		
29	-0.356		

UPPER SURFACE SPANWISE PRESSURE

DFW(IN)	0.5*(X/C)	0.75*(X/C)
12	-1.8836	-1.8639
6	-1.6028	-1.7056
3	-1.4556	-1.4889
1.5	-1.3750	

RUN NUMBER 52605.1
MIDSPAN PRESSURE DISTRIBUTION

N	UPPER CP	N	LOWER CP
1	0.119	29	0.472
2	0.164	30	0.125
3	0.179	31	0.104
4	0.209	32	0.104
5	0.164	33	0.113
6	0.164	34	0.104
7	0.139	35	0.104
8	0.134	36	0.119
9	0.111	37	0.125
10	0.119	38	0.111
11	0.125	39	0.111
12	0.119	40	0.111
13	0.119	41	0.111
14	0.119	42	0.106
15	0.125	43	0.111
16	0.134	44	0.111
17	0.139	45	0.111
18	0.164	46	0.111
19	0.167	47	0.111
20	0.181	48	0.125
21	0.194	49	0.153
22	0.222	50	0.153
23	0.514	51	0.153
24	0.667	52	0.139
25	0.903	53	0.111
26	0.972	54	0.083
27	1.042		
28	0.889		
29	0.472		

UPPER SURFACE SPANWISE PRESSURE

DFW(IN)	0.5*(X/C)	0.75*(X/C)
12	0.1194	0.1389
6	0.1111	0.1250
3	0.1111	0.1111
1.5	0.1111	

BEST AVAILABLE COPY

APPENDIX E

Unsteady Hotwire Data Corresponding to C_p Run Numbers 52601 through 52605 for 0.025 in. from Surface

STEADY FREESTREAM, STEADY BLOWING
RUN NUMBER 52601   DISTANCE FROM SURFACE (IN.) 0.025

POINT	THETA(CHORD)	MEAN VEL	RMS VEL
1	17.2	1.95	0.335
2	15.1	1.91	0.337
3	12.7	1.86	0.335
4	10	1.78	0.324
5	7.6	1.72	0.324
6	5	1.6	0.35
7	2.5	1.4	0.426
8	1.3	1.25	0.458
9	0.8	1.2	0.466
10	0	1.08	0.476
11	-0.9	0.97	0.475
12	-2.1	0.88	0.462
13	-4.9	0.585	0.381
14	-7.6	0.46	0.32
15	-10	0.33	0.248
16	-12.3	0.255	0.18
17	-15.1	0.214	0.132
18	-17.5	0.196	0.105
19	-20	0.185	0.09
20	-25	0.145	0.081
21	-30.2	0.102	0.064
22	-35	0.08	0.048
23	-40	0.075	0.043
24	-45	0.06	0.045
25	-50	0.07	0.043
26	-55	0.055	0.04

9 HZ OSCILLATING FREESTREAM, STEADY BLOWING
RUN NUMBER 52602   DISTANCE FROM SURFACE (IN.) 0.025

POINT	THETA(CHORD)	MEAN VEL	RMS VEL
1	17.2	1.88	0.328
2	15.1	1.74	0.333
3	12.4	1.76	0.33
4	10.1	1.72	0.328
5	7.6	1.635	0.342
6	5.1	1.54	0.371
7	3.6	1.42	0.415
8	2.6	1.36	0.446
9	1.6	1.2	0.478
10	0	1.05	0.5
11	-1.1	0.93	0.498
12	-2.4	0.8	0.46
13	-5	0.57	0.41
14	-7.6	0.4	0.332
15	-10	0.33	0.25
16	-12.5	0.26	0.19
17	-15	0.22	0.14
18	-17.5	0.195	0.102
19	-20.1	0.185	0.095
20	-25.1	0.15	0.081
21	-30.1	0.1	0.074
22	-35.1	0.07	0.051
23	-39.9	0.07	0.05
24	-45	0.06	0.042
25	-50.1	0.05	0.043
26	-55	0.058	0.04

STEADY FREESTREAM, OSCILLATORY BLOWING
RUN NUMBER 52603   DISTANCE FROM SURFACE (IN.) 0.025

POINT	THETA(CHORD)	MEAN VEL	RMS VEL
1	17.2	2.01	0.53
2	15.1	1.97	0.55
3	12.4	1.914	0.63
4	10.1	1.75	0.66
5	7.6	1.51	0.74
6	5.1	1.45	0.74
7	3.6	1.325	0.76
8	2.6	1.31	0.78
9	1.6	1.21	0.76
10	0	1.22	0.74
11	-1.1	1	0.72
12	-2.4	0.935	0.65
13	-5	0.701	0.56
14	-7.6	0.55	0.47
15	-10	0.41	0.35
16	-12.5	0.36	0.28
17	-15	0.29	0.19
18	-17.5	0.255	0.16
19	-20.1	0.22	0.13
20	-25.1	0.18	0.1
21	-30.1	0.16	0.085
22	-35.1	0.115	0.068
23	-39.9	0.1	0.056
24	-45	0.125	0.056
25	-50.1	0.1	0.055
26	-55	0.09	0.057

STEADY FREESTREAM, STEADY BLOWING
RUN NUMBER 52604 DISTANCE FROM SURFACE (IN.) 0.025

POINT	THETA(CHORD)	MEAN VEL	RMS VEL
1	17.2	2.55	0.37
2	15.1	2.53	0.36
3	12.4	2.48	0.35
4	10.1	2.46	0.35
5	7.6	2.36	0.34
6	5.1	2.27	0.33
7	3.6	2.18	0.33
8	2.6	2.13	0.33
9	1.6	2.02	0.36
10	0	1.93	0.41
11	-1.1	1.86	0.42
12	-2.4	1.66	0.5
13	-5	1.35	0.54
14	-7.6	0.99	0.52
15	-10	0.72	0.43
16	-12.5	0.56	0.37
17	-15	0.4	0.28
18	-17.5	0.34	0.23
19	-20.1	0.27	0.16
20	-25.1	0.24	0.11
21	-30.1	0.2	0.09
22	-35.1	0.14	0.08
23	-39.9	0.09	0.055
24	-45	0.065	0.038
25	-50.1	0.09	0.036
26	-55	0.075	0.047

STEADY FREESTREAM, OSCILLATORY BLOWING
RUN NUMBER 52605 DISTANCE FROM SURFACE (IN.) 0.025

POINT	THETA(CHORD)	MEAN VEL	RMS VEL
1	17.2	2.45	0.42
2	15.1	2.42	0.42
3	12.4	2.38	0.41
4	10.1	2.33	0.4
5	7.6	2.25	0.4
6	5.1	2.18	0.41
7	3.6	2.11	0.45
8	2.6	2.05	0.45
9	1.6	1.98	0.48
10	0	1.8	0.55
11	-1.1	1.72	0.61
12	-2.4	1.58	0.62
13	-5	1.32	0.66
14	-7.6	1.12	0.63
15	-10	0.82	0.56
16	-12.5	0.62	0.46
17	-15	0.46	0.36
18	-17.5	0.385	0.28
19	-20.1	0.315	0.22
20	-25.1	0.245	0.13
21	-30.1	0.195	0.1
22	-35.1	0.145	0.088
23	-39.9	0.11	0.062
24	-45	0.085	0.05
25	-50.1	0.065	0.052
26	-55	0.08	0.05

LIST OF REFERENCES

1. Griswold, R. W., Circulatory Jet Airfoils, United States Patent 2,885,160, 5 May 1959.

2. Davidson, I.M., Airfoil Boundary Layer Control Systems, British Patent No. 913754, 1960.

3. Dunham, J., A Tentative Theory of Circulation Control Applied to a Circular Cylinder, ARC 27 170, 1965.

4. Cheeseman, I. C., and Seed, A. R., "The Application of Circulation Control by Blowing to Helicopter Rotors," Journal of the Royal Aeronautical Society, Vol. 71, July 1967.

5. Cheeseman, I. C., and Seed, A. R., "The Application of Circulation Control Blowing to Helicopter Rotors," Journal of the Royal Aeronautical Society, Vol. 70, February and July 1966.

6. Kind, R. J., A Proposed Method of Circulation Control, Ph.D. Thesis, Cambridge University, 1967.

7. Williams, R. M., and Howe, H. J., Two Dimensional Subsonic Wind Tunnel Tests on a 20 Percent Thick, 5 Percent Cambered Circulation Control Airfoil, Naval Ship Research and Development Center, TN AL-176, 1972.

8. Englar, R. J., Two-Dimensional Subsonic Wind Tunnel Tests of Two 15-percent Thick Circulation Control Airfoils, NSRDC TN AL-211, August 1971.

9. Englar, R. J., Test Techniques for High Lift Two-Dimensional Airfoils with Boundary Layer and Circulation Control for Application to Rotary Wing Aircraft, NRSDC paper, May 1972.

10. Harness, G. S., An Experimental Investigation of a Circulation Controlled Cambered Elliptical Airfoil, Master's Thesis, West Virginia University, 1970.

11. Oyler, T. E., and Palmer, W. E., Exploratory Investigation of Pulse Blowing for Boundary Layer Control, Columbus Aircraft Division/North American Rockwell Corporation Report NR72H-12, January 1972.

12. Williams, J. R., et al., Analysis of a Pulsing Wall Jet, Report NR72H-325, Columbus Aircraft Division/ North American Rockwell, October 1972.

13. Walters, R. E., Myer, D. P., and Holt, D. J., Circulation Control by Steady and Pulsed Blowing for a Cambered Elliptical Airfoil, West Virginia University Department of Engineering Technical Report 32, July 1972.

14. Englar, R. J., Subsonic Two-Dimensional Wind Tunnel Investigation of the High Lift Capability of Circulation Control Wing Sections, DTNSRDC Report ASED-274, Naval Ship Research and Development Center, Bethesda, Maryland, April 1975.

15. Kaman Aerospace Corporation Report R-1036-2, Contract N00019-73-C-0429, Design Study of a Flight Worthy Circulation Control Rotor System, July 1974.

16. Lockheed Aircraft Corporation Report LR26417, Contract N00019-73-C-0435, Design Study of a Helicopter with a Circulation Control Rotor (CCR), May 1974.

17. Reader, K. R., and Wilkerson, J. B., Circulation Control Applied to a High Speed Helicopter Rotor, Reprint no. 1003, 32nd Annual National V/STOL Forum, American Helicopter Society, Washington, D. C., May 1976.

18. Kind, R. J., "A Calculation Method for Circulation Control by Tangential Blowing Around a Bluff Trailing Edge," The Aeronautical Quarterly, Vol. XIX, August 1968, pp. 170-182.

19. Levinsky, E. S., and Yeh, A. C., Analytical and Experimental Investigation of Circulation Control by Means of a Turbulent Coanda Jet, NASA CR-2114, September 1972.

20. Gibbs, E. H., and Ness, N., Analysis of Circulation Controlled Airfoils, West Virginia University Department of Aerospace Engineering TR 43, June 1975.

21. Englar, R. J., Experimental Investigation of the High Velocity Coanda Wall Jet Applied to Bluff Trailing Edge Circulation Control Airfoils, Naval Ship Research and Development Center RN 4708, September 1975.

22. Cebeci, T., and Smith, A. M. O., Analysis of Turbulent Boundary Layers, Academic Press, 1974.

23. Sandborn, V. A., and Liu, C. Y., "On Turbulent Boundary-Layer Separation," Journal of Fluid Mechanics, Vol. 32, 1968, pp. 293-304.

24. Despard, R. A., and Miller, J. A., "Separation in Oscillating Laminar Boundary Layer Flows," Journal of Fluid Mechanics, Vol. 47, 1971, pp. 21-31.

25. Tsahalis, D. Th., and Telionis, D. P., "Oscillating Laminar Boundary Layers and Unsteady Separation," AIAA Journal, Vol. 12, 1974, pp. 1469-76.

26. Karlsson, S. F., An Unsteady Turbulent Boundary Layer, Ph.D. Thesis, Johns Hopkins University, 1958.

27. Miller, J. A., Transition in Oscillating Blasius Flow, Ph.D. Thesis, Illinois Institute of Technology, 1963.

28. Despard, R. A., Laminar Boundary Layer Separation in Oscillating Flow, Ph.D. Thesis, United States Naval Postgraduate School, 1969.

29. Bauman, J. L., Development of a Control Valve to Induce an Oscillatory Blowing Coefficient in a Circulation Control Rotor, Master's Thesis, United States Naval Postgraduate School, 1976.

30. Bergh, H., A New Method for Measuring the Pressure Distribution on Harmonically Oscillating Wings, Proceedings of the 4th ICAS Congress, Paris, 1964.

31. Bergh, H., and Tijdman, H., Theoretical and Experimental Results for the Dynamic Response of Pressure Measuring Systems, National Aeronautics and Astronautics Research Institute NRL-TRF 238, Amsterdam, 1965.

32. Johnson, R. B., A Technique for Measuring Unsteady Pressures, A. E. Thesis, United States Naval Postgraduate School, 1969.

33. Banning, M. R., The Unsteady Normal Force on an Airfoil in Oscillating Flow, A. E. Thesis, United States Naval Postgraduate School, 1969.

34. Lancaster, E. J., Initial Unsteady Aerodynamic Measurements of a Circulation Controlled Airfoil and an Oscillating Flow Wind Tunnel, Master's Thesis, United States Naval Postgraduate School, 1977.

35. Englehardt, D., Design of a Microprocessor System for Analysis of Unsteady Circulation Control Airfoil Aerodynamic Characteristics, Master's Thesis, United States Naval Postgraduate School, to be published August, 1977.

36. Pickelsimer, B. M., Data Reduction for the Unsteady Aerodynamics on a Circulation Control Airfoil, Master's Thesis, United States Naval Postgraduate School, 1977.

37. Kind, R. J., and Maull, D. J., "An Experimental Investigation of a Low-Speed Circulation Controlled Airfoil," The Aeronautical Quarterly, Vol. XIX, May 1968, pp. 170-182.

38. Collins, M. A., and Simpson, R. L., Flowfield Prediction for Separating Turbulent Boundary Layers, Technical Report WT-4, Department of Civil and Mechanical Engineering, Southern Methodist University, February 1976.

INITIAL DISTRIBUTION LIST

		No. Copies
1.	Defense Documentation Center Cameron Station Alexandria, Virginia 22314	2
2.	Library, Code 0142 Naval Postgraduate School Monterey, California 93940	2
3.	Department Chairman, Code 67 Department of Aeronautics Naval Postgraduate School Monterey, California 93940	1
4.	Professor J. A. Miller, Code 67Mo Department of Aeronautics Naval Postgraduate School Monterey, California 93940	10
5.	Professor L. V. Schmidt, Code 67Sx Department of Aeronautics Naval Postgraduate School Monterey, California 93940	1
6.	Commanding Officer Attn: Mr. R. F. Siewert, AIR-320D Naval Air Systems Command Washington, D. C. 20361	1
7.	Commanding Officer Attn: Dr. H. Chaplin, Code AESD Mr. J. Wilkerson, Code AESD David W. Taylor Naval Ship Research and Development Center Bethesda, Maryland 20084	2
8.	LT Karl Aurel Kail, IV, USN 14243 Minorca Cove Del Mar, California 92014	1